Modeling and Experiments for a Class of Robotic Endoscopes

Thesis by
Andrew Brett Slatkin

In Partial Fulfillment of the Requirements
for the Degree of
Doctor of Philosophy

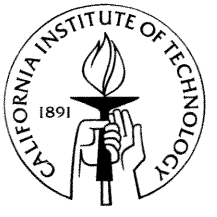

California Institute of Technology
Pasadena, California

1999

(Defended January 6, 1998)

Acknowledgements

This dissertation would not exist if not for the support, guidance and love of a special group of people who will always have my deepest appreciation.

Professor Joel Burdick, my academic advisor, liberally offered his technical, financial and emotional support. I have been extremely fortunate for the opportunity to have worked with this generous man. Whether he realizes it or not, his actions and reactions helped to guide me from "wandering the desert."

Warren Grundfest, M.D., the Director of the Laser Laboratory at Cedars-Sinai Medical Center, has been my advisor within the medical field as well as a member of my Thesis Committee. Without his active support of this work, it would never have proceeded. Warren has always demonstrated a tremendous capacity to envision new medical technology, and his boundless energy and enthusiasm are contagious.

I also wish to recognize the other members of my Thesis Committee. Professors Richard Murray and Erik Antonsson dramatically improved the quality of this dissertation with their reviews of early drafts. And I cannot thank Professor James Knowles enough for his consistent support during my stay at Caltech. I consider myself extremely lucky that Jim Knowles was there: at my "mini orals," during five terms of coursework, at my Candidacy Exams, as a reviewer of my thesis work, and whenever I dropped in on him with a question or problem. He has always shown genuine concern for me (and for all of his students).

My Caltech lab group has been like a family. Thanks to: Hans Hoeg, with whom the Generation Five robot was successfully assembled (his overwhelming confidence in my design was inspiring); Jim Ostrowski, Howie Choset and Jim Radford who performed the thankless job of computer system administration for the Robotics Lab; and Qiao Lin for his truly timely assistance during the typesetting of this manuscript. No recognition of my Caltech "family" would be complete without thanking John Van Deusen and Rodney Rojas of the Mechanical Engineering Ma-

chine Shop. I will always look back happily on the time (years) I spent in their shop. Also, they are consistently valuable design and manufacturing consultants, and other Caltech experimenters should take full advantage of their expertise.

I wish to thank the Cedars-Sinai Medical Center staff and researchers: Carol Ruppe, Thanassis Papaioannou, Ramez Shehada, Laurie Zelby, Linda Whisenhunt and Evelyn Berkowitz. I would not have enjoyed the process or results of my animal experiments without their technical and administrative efforts (and their big hearts).

My love and appreciation of my family and friends must also be voiced. I cannot find words strong enough to express my feelings of appreciation for my parents. Fortunately, they already know how I feel. To Denise, without whom my work at Caltech would never have begun, I know that the pursuit of this degree has been very hard on her. And I wish her peace, love, and happiness, always. To Carol, who has supplied unlimited practical, moral and psychological support. To my daughter, Alexandra, who has been amazingly patient. She puts my life in focus and gives it meaning. To my grandparents, Naomi and David, who have always supported and challenged me to stretch toward goals that appeared out of reach. To Bob, Linda and Mel, I couldn't have asked for better in-laws during these trying times. To Renny, Lisa, Andy, and Kelly who knew better than to ask when I'd be done (but were always dying to), their loving thoughts and actions will always be remembered. And to the rest of my family and old friends whose love and empathy have made all my struggles easier to bear (they should expect to see a lot more of me from now on).

My thanks and love to Anna (I cannot count the ways in which she helped make this thesis a reality) and to Richard Weintraub (his insights over recent years have shaped my life and work – none of this would exist without him).

And finally to Gary Furman, M.D., who insisted that my medical device ideas be conveyed to Warren Grundfest; his actions got this big ball rolling.

Modeling and Experiments for a Class of Robotic Endoscopes

by

Andrew Brett Slatkin

In Partial Fulfillment of the
Requirements for the Degree of
Doctor of Philosophy

Abstract

Current developments in minimally invasive medical practice motivated this study of self-propelled, robotic endoscopes for deep penetration into curved physiological lumens. The conceptual design of such devices is applicable to endoscopy within a variety of lumens in the human body, e.g., blood vessels, but the initial objective of this technology is to provide access to the interior of the entire small intestine without surgical incisions. The small intestine presents several challenges to endoscopic penetration: it is extremely compliant to applied loading, internally lubricated, easily injured, and contains many tight curves along its length of approximately eighteen feet.

This thesis reports the basic design and locomotion concepts for one class of endoscopic robots that are intended to provide safe and reliable traversal of the small intestine via worm-like actuation. Five generations of proof-of-concept prototype robots have been built to validate the fundamental concepts. Furthermore, these miniaturized robots have incorporated the following features: redundant actuation with computer control, tool-free modular assembly, and on-board videoimaging capability. The prototypes have been tested in rubber

tubing, the small intestines of deceased pigs, and in the small intestines of live, anaesthetized pigs.

At the onset of this research, little regarding the elastic properties of small intestine existed in the biomechanics literature that would be applicable to the design of these mechanisms. However, accurate prediction of the small intestine's response to robotic loadings would dramatically improve the research and development process of these machines. Thus, an investigation of the elastic behavior of the small intestine commenced. Finite deformation, nonlinear, anisotropic, incompressible, viscoelastic behavior of the small intestine was studied. This soft tissue biomechanical analysis and experimentation (on living and dissected intestinal specimens) culminated with a numerical model that simulates intestinal response to the actions of a prototypical robotic component. Experiments on *living* specimens were performed to determine the levels of applied loadings and internal stresses that are likely to injure these fragile tissues, and the biomechanics computer modeling incorporates three distinct measures for injury potential.

Contents

List of Figures

Chapter 1

Introduction

1.1 Motivation for Robotic Endoscopy

This dissertation considers issues that are essential to the development of a *gastrointestinal robot* or *robotic endoscope* for traversing the human gastrointestinal system. Such a device could provide minimally invasive access to large sections of the gastrointestinal system which are currently accessible only through invasive methods. *Minimally invasive* medical practice utilizes slender instruments inserted through naturally occurring or surgically produced orifices into interior body cavities for the visualization, diagnosis, and therapeutic intervention of injury and disease. These techniques are aimed at reducing the amount of peripheral tissue which must be damaged in order to reach the surgical site. Minimizing such collateral damage can reduce patient recovery time and postoperative discomfort. Furthermore, potential for deleterious side effects, e.g., keloid development, can be diminished.

Because of these potential advantages, one of the biggest trends in medical surgery in the 1990s is the shift to minimally invasive alternatives from

traditional *open* surgery (i.e., invasive procedures) [59]. Arthroscopic joint surgery, colonoscopic polypectomy (removal of growths from the colon), and laparoscopic gall bladder removal are widely recognized examples of this trend. In addition to improvements in patient care, there are tremendous economic incentives for the adoption of these techniques. As reported by the Wilkerson Group in 1992, approximately 21 million surgical procedures are performed each year in the United States [59] with approximately 1 million performed in a minimally invasive manner. They further estimated that potentially 8 of the 21 million surgeries could have been performed in a minimally invasive manner. Since minimally invasive approaches tend to reduce the duration of postoperative hospitalization, increased use of these techniques would be expected to result in dramatic savings in hospital residency costs and lost patient wages [59]. A major technological impediment to increasing usage of minimally invasive approaches is lack of minimally invasive access to interior body cavities. While the primary focus of this thesis is to provide minimally invasive access to the gastrointestinal system, we hope that successful deployment of this technology will pave the way for other applications of robotic technology to minimally invasive medicine.

Conventional endoscopes provide minimally invasive visualization of interior ducts and cavities, such as the stomach, colon, urinary tract and respiratory tract. The term *endoscope* literally means "inner scope;" thus, an endoscope is merely a tool which provides visual access to the body's interior. Flexible endoscopes use fiber optic bundles or distal CCD chip cameras to transmit an optical image from within the body. Fiber optic bundles can also act as a conduit for laser surgery, i.e., cutting, cauterizing, and/or vaporizing tissue with laser beams. Typically, larger diameter endoscopes contain devices

for steering their distal tips, and their larger size can permit the deployment of simple surgical instruments for manipulation and dissection of tissue. These instruments are currently inserted without incisions into a variety of physiological lumens (tube-like structures) and cavities such as: the esophagus, stomach, colon, urinary tract, respiratory tract, nasal sinuses, seminal ducts, tear ducts, etc. Additionally, with surgical incisions, several other lumens and cavities can be accessed, e.g. the small intestine, the bile ducts, the cranium, and blood vessels.

Gastrointestinal endoscopy focuses on the diagnosis and treatment of diseases of the alimentary canal (mouth, esophagus, stomach, small intestine, colon, rectum, and anus) by the use of flexible endoscopes. *Gastroscopes* are used to visualize the inner surfaces of the stomach and *colonoscopes* provide visualization of the large intestine, or colon. Together, these two ends of the alimentary canal represent only thirty percent of the length of the gastrointestinal tract. The remaining seventy percent, also known as the small intestine, cannot be reached using current endoscopic technology without abdominal incisions. Since the small intestine repeatedly traverses the abdominal cavity, locating a specific disease site within it can require open surgery (laparotomy). Recent estimates from the Journal of Clinical Gastroenterology (1992) indicate that diseases of the small intestine, such as Crohn's disease, ulcerative colitis, and intestinal blockage, afflict approximately 430,000 people annually in the United States. At present, the diagnosis of diseases of the small intestine is done either by assessing the "external" symptoms, often with radiological substantiation (e.g., via barium ingestion, MRI, or ultrasound imaging), or by invasive surgical exploration. In many instances, the current therapy requires extensive surgery with a prolonged recovery period.

1.2 A Brief Synopsis of this Thesis

This dissertation reports efforts to develop a robotic endoscope that can directly access and visualize, without incisions, the entire gastrointestinal tract. The long term goals of these efforts are to produce a physician-guided robot that can be inserted though the mouth or anus, positioned at an entrance to the small intestine using a modified, conventional endoscope, and then commanded to locomote through the small bowel to perform medical diagnostic procedures. Such a device would provide an alternative to the highly invasive diagnostic methods described above. A follow-on goal is to supply therapeutic intervention when possible. For example, the robot may assist in the removal of blockages, excise diseased tissue and perform biopsies, or precisely deliver anti-inflammatory drugs for non-invasive treatment of Crohn's disease. In order to satisfy medical needs such as these, the first step is to develop a robotic endoscope that can dependably travel through the small intestine. Hence, the first half of this dissertation develops a robotic locomotion concept and describes its prototype implementations and subsystems. Additionally, it was recognized early that a thorough understanding of the geometry, elastic behavior, surface texture and lubricity of the small intestine would be critical to the success of this endeavor. To that end, qualitative and quantitative surgical experiments were performed on anesthetized pigs. The quantitative investigation into the elasticity of pigs' small intestines *in vivo* was repeated for excised specimens *in vitro*. From the experimental data, a simplified model for the mechanical behavior of small intestines was created to be a design tool for future robotic endoscopy efforts.

Chapter 2 addresses many new applications of robotics to medicine. The

current state of the art in endoscopy is introduced, and limitations of the existing technology are discussed. Lastly, this chapter touches on a variety of advancing developments in surgical technology that have resulted from the application of robotics and computers.

Chapter 3 proposes a robotic endoscope design concept intended to overcome current endoscopic limitations that prohibit complete access to the small intestine without surgical incisions. Conceptual locomotion modalities for these devices are then presented. And in order to evaluate these concepts, five generations of proof-of-concept prototype endoscopic robots have been designed, built and tested. After a general overview of the proposed robotic system, complete with descriptions of the various subcomponents and their evolution, the final, fifth generation prototype is introduced. For historical purposes, this chapter ends with an overview of the evolution of the five generations of prototype systems. In this concluding section, the salient features and functional performance of these robots are compared and contrasted.

Chapter 4 reports on efforts to accelerate the design process for these medical instruments via investigation into modeling of the mechanical behavior of the small intestine. This chapter opens with an introductory section covering basic concepts of solid mechanics and mathematical elasticity. The next two sections address the specific problems and issues of soft tissue biomechanics. The balance of the chapter reflects original analytical, experimental and numerical research into modeling the elastic behavior of the small intestine.

Chapter 5, in conclusion, revisits: the medical motivation for the endoscopic access of the small intestine without surgical incisions; the robotic system design and implementations; and the biomechanical modeling of the small intestine. This chapter also provides suggestions for future work toward the

viable locomotion of robotic endoscopes for the small intestine.

When this research commenced, little relevant "prior work" existed in the literature. The novelty of this technology has justified the issuance of two United States Patents 5337732 and 5662587 [25, 26]. Forging into uncharted territory, this research path has been circuitous. Many initial forays into a forest of previously unasked questions, unanticipated design problems and modeling issues ended abruptly before yielding useful and reportable results. Continuing with this metaphor, it is hoped that this thesis can serve as a preliminary "trail map" for future endeavors into self-propelled endoscopy.

The original contributions of this work are highlighted below.

- Fundamental design concepts and morphologies of a self-propelled endoscope that could overcome the limitations of current medical technology were investigated.
- An original locomotion methodology was developed, and five generations of endoscopic robot prototypes were designed, fabricated and tested.
- Biomechanics experiments were performed to study the biaxial, "whole organ" behavior of the small intestine; this approach is in contrast to the typically reported uniaxial tensile tests of dissected strips of excised tissue. The experimental apparatus was developed for use on tubular segments of both living and dead small intestines.
- The biomechanics experiments compare the material behavior of both living and dissected intestine in order to determine if and when the dead tissue provides useful data. Since experiments on dissected tissues are substantially less expensive and complicated (the experiments on living intestines require surgical incisions into animials that are fully anaesthetized), these results may be used to plan future experimental investigations.

- The experimental study of the biaxial elastic behavior of living intestine was crucial in identifying the loads and stresses that would potentially cause injury to the fragile intestinal tissues. A study of excised tissues cannot determine the loading (or stressing) that corresponds to the onset of injury of living specimens.
- With experimentally gathered data, a model of small intestinal behavior was developed to act as a tool for future endoscopic robot design efforts. Additionally, this modeling may assist in the design and analysis of other gastrointestinal surgical instruments as well, e.g., innerluminal intestinal staplers that radially load the intestine during anastomosis.
- The biomechanics model was incorporated into a numerical simulation that predicts the imposed loading, internal stress, and "injury potential" that result from actions of a prototypical robotic component.

Chapter 2

Medical Technology

After describing the current state of relevant medical technology, this chapter illustrates engineering efforts to introduce advanced technologies into the practice of health care.

2.1 Endoscopy Primer and Current Practice

As previously mentioned, *endoscopy* refers to the use of medical instruments to view the interior of the human body. There are innumerable anatomical sites for which such visualization is desired; one could argue that almost all medical subspecialties could benefit from devices which provide minimally invasive visualization. Currently, each of the following specializations benefit from endoscopy: Otolaryngology, Orthopaedics, Cardiology/Cardiac Surgery, Pulmonary surgery, Oncology, General Surgery, Neurology/Neurosurgery, Proctology, Gastroenterology, Urology and Gynecology. In order to look into each of these different regions of the body, highly specialized devices and procedures are typically developed. Additionally, if possible, these instruments should be able to provide a platform for therapy as well. Hence, the term *endoscope* can

refer to devices that are vastly different in function and appearance. Examples of endoscopes include: rigid sigmoidoscopes that are merely stainless steel tubes (with lenses) that provide a view of the sigmoid colon (roughly, the last ten centimeters of the colon), arthroscopes which are more sophisticated optical relay systems with rigid tubes through which bone and soft tissues can be manipulated and cut, and bronchoscopes which are thin, flexible instruments which are threaded through the bronchial passages into the lungs. Clearly, each has been uniquely designed for its intended application.

Endoscopes are divided into two major classes of instruments: *rigid* and *flexible*. Rigid endoscopes are especially useful when inserted into large or irregularly shaped cavities within the body. In these cases, the local anatomy does not support the lateral surfaces of the device, and, thus, the endoscope must be rigid. In contrast, flexible endoscopes are typically used in anatomical *tubes* or *lumens* in the body. Such a tube may support the lateral surface of the flexible endoscope as it is threaded into the body. Often these endoscopes are comprised of optical fiber bundles which transmit light into and images out of the lumen. If the lumen into which a flexible endoscope is inserted is sufficiently straight and/or structurally supportive, no steering of the endoscope is necessary to advance it into the body. It will simply follow the contours of the surrounding tube. In cases where the lumen is excessively curved or flexible to provide the necessary guidance for an endoscope, the distal end of the endoscope must be steered manually by the endoscopic surgeon. Endoscopes with this type of bending actuation are very common, but control of their shape is limited to steering of their distal ends.

In cases where access into either a straight lumen or an irregular cavity is desired, a rigid endoscope can be employed. Such devices include tools that

can be inserted into the skull, joints, the abdomen and the sigmoid colon. Each instrument is designed carefully for its intended purpose. For example, in endoscopic gall bladder removal, a laparoscope is inserted into the abdomen through a small incision near the patient's navel (*laparo* is derived from the Greek word *lapara* meaning "the flank" or the abdomen). This device consists of a thin stainless steel tube that protects its internal optical components: an optical fiber bundle that transmits light into the abdomenm and a rod lens that provides visualization for the surgeons. Additional, slender instruments for cutting, grasping, cauterizing, etc., are inserted through other small incisions through the abdominal wall. A videocamera mounted to the laparoscope provides imaging of these additional surgical tools. In contrast, other rigid endoscopes incorporate internal lumens, called *working channels*, that permit direct deployment of surgical tools through the endoscope. In these cases, a variety of simple tools such as snares and grasping forceps can be employed, although typically one at a time. Early sigmoidoscopes provided such functionality.

Flexible endoscopy is considered to be a mature medical technology with many commercial devices available for the diagnosis and treatment of diseases found within various lumens of the human body. To use a flexible endoscope, the endoscopic surgeon holds the proximal end and moves the distal end by pushing, pulling and twisting the device from outside of the body. As mentioned, larger diameter endoscopes can allow limited active bending at the distal end, but none provide sophisticated control of their overall shape. Ideally, the endoscope would slide smoothly within the tunnel-like lumen, but often this is not the case. Many lumens in human physiology are curved along their length, and so endoscopes designed to traverse them must be sufficiently

flexible in lateral bending. Unfortunately, these devices are advanced in the lumen by pushing from behind; this requires them to be sufficiently stiff to prevent buckling. These two contradictory requirements ensure that flexible endoscopes are design compromises. One might expect the encompassing lumen to laterally support the endoscope along its inserted length and thereby reduce the likelihood of significant buckling, but this is a misconception for two reasons. Firstly, some physiological lumens are significantly less rigid than the flexible endoscope itself. These anatomical structures cannot be expected to provide sufficient resistance to buckling of the encompassed endoscope. Secondly, the distal end of the advancing endoscope often drags along undulations on the inner surface of the lumen. In these instances, the surrounding lumen can actually promote buckling instead of relieving it.

Unfortunately, buckling of flexible endoscopes is a main cause of patient discomfort and is potentially injurious to fragile, diseased tissues. It also limits the maximal depth of endoscopic penetration because it is more likely to occur as the unsupported length of the endoscope increases inside the body. Also, limited lateral compliance (to bending) also prevents these devices from negotiating tight bends which exist in many physiological lumens (specifically, such geometry exists in the small intestine). Thus, endoscopic accessibility is limited, and, even under the best conditions, physicians must possess great skill to position current devices deep within the body.

2.2 Robotic Medical Technology

In the last decade, it has been recognized that robotic technology could significantly impact medical practice. This section reviews efforts to introduce

advanced, electromechanical technology to medicine. One should not consider this section to be a comprehensive overview of robotics in medicine but merely a reflection on three classes of efforts to improve medicine using machines and computers. Firstly, just as improvements in automation can improve the quality of manufactured products, medical robotic mechanisms with computer control can be expected to move more precisely than the human hand. Secondly, there are situations where highly trained surgical assistants, i.e., nurses or other surgeons, are employed to merely hold tools in place (as examples: retraction of surrounding tissues and organs, or aiming the laparoscope at the surgical site during laparoscopy) while the active surgeon performs the critical tasks. In such cases, robots could conceivably be employed to replace extraneous surgical staff thereby reducing the surgical expenses. And lastly, as is the objective of this research, advanced technology devices are being developed to improve minimally invasive access to the interior of the human body.

One major industrial advantage of electromechanical automation is the potential for extremely precise positioning control. In a manufacturing setting, this results in close tolerance parts which are produced in a cost effective manner. Similar thinking has been applied successfully to conventional, invasive surgery. For examples, robots have successfully been used to assist hip replacement surgery (known as RoboDoc) [40] and cranial surgery [52, 49]. In both cases, the robots were used to very precisely position surgical tools. RoboDoc actually performed the cutting operations into the femur (upper leg bone) which resulted in an extremely close fit for the joint implant.

In microsurgery, precision movements of the surgical instrumentation can mean the difference between a successful and unsuccessful result. Microsurgical subspecialties include, but are not limited to, opthalmic, neuro-, and

hand surgery. This is very exacting work, and unfortunately microsurgical specialists often have relatively short careers due to age related increases in undesireable hand tremors. It is very tragic that the most experienced practioners with hard earned surgical judgment become unable to perform in the operating room. The field of robotic teleoperation has been developed to allow human beings to remotely manipulate objects using a robot. Such technology has been applied to produce microsurgery stations. In these systems, the surgeon interacts with an input device often referred to as *the master*, and the output device, known as *the slave* moves the microsurgical instrument. The magnitudes of the movements of the slave can be programmed to be a small fraction of those input at the master. In addition, the minute forces of interaction between the microsurgical tool and the tissue can be magnified when reflected back to the surgeon at the master. This master-slave arrangement with its force reflection and positional scaling have allowed older, highly experienced surgeons to perform even the most physically demanding surgeries [6, 61].

One last example of precise electromechanical control of surgical tools comes from radiological therapy of brain cancer. When irradiating a brain tumor, it is important to supply the diseased tissue with the prescribed dosage of radiation while minimizing the radiation exposure of the surrounding, healthy brain tissue. Again, electromechanical technology has been invoked. Using a CT scan of the patient to provide a three-dimensional model of the afflicted brain, a computer algorithm determines an optimal path for the radiation gun around the patient's head that guarantees the correct dosage to all parts of an irregularly shaped tumor while minimally impacting the surrounding healthy tissue [1].

In an effort to reduce costs of surgery, some researchers and companies have attempted to produce robots to replace unnecessary personnel in the operating room. The targets for these staff reductions are "assistants" whose primary role is to hold a retractor to expose the surgical site. Long before the introduction of robotics into medicine, mechanical *iron assistants* were common, but recently they have gained a new level of sophistication. Robots designed to hold and manipulate laparoscopes have been independently developed by IBM and Computer Motion, Inc. [58, 16]. They were both developed to allow the primary surgeon direct control of the laparoscopic view of the surgical site. Although the impressive IBM (TJ Watson Center) device was not commercialized, Computer Motion, Inc., continues to market their robot assistant, Aesop.

Many have recognized that minimally invasive access could be improved by developing devices with actively controlled electromechanical articulation. For example, Sturges et al. [55] have investigated the use of articulated bead-chain mechanisms as foundations for advanced endoscope designs. Also, Fukuda and coworkers have engineered prototype catheters which can actively bend along their length [14]. And, Ikuta and collaborators have developed hyper-redundant robotic endoscope prototypes [31, 30]. But in all of these cases the devices are advanced into the body by forces produced at their proximal ends, which are located outside of the patient. This type of actively articulated endoscope design inherently limits its overall length and, hence, its ultimate reach into the body.

The robotic endoscope design technology developed in this thesis work is reminiscent of pipe crawling robots that exist for inspection of buried pipes and channels (these machines are often referred to as *pipe pigs*). Fukuda and

coworkers have studied self-propelled robotic systems for inspecting small and medium size pipes [15], and Shishido et al. [53] have been granted a United States patent for such an invention [53]. While the topology of the human intestine is analogous to a pipe, there are many significant differences which prevent a simple adaptation of prior pipe crawling robot principles to this problem. First of all, the diameter of the human intestine can vary significantly along its length. Conventional pipe crawling designs do not handle such variations. And, in addition, the intestine is very flexible, fragile, and slippery, and the traction mechanisms used in many prior pipe crawling devices would likely cause injury to the intestinal lining (provided they could produce sufficient traction at all). Of course, patient safety is of critical importance in the design of any medical device, and this introduces additional design requirements that are not relevant to pipe pigs. Hence, similarities between such industrial robots and these medical devices are purely conceptual.

It was with consideration of this prior work that the robotic endoscopes described herein were conceived. Subsequent to the public dissemination of this work, researchers at MIT and Columbia University Medical School collaborated to create a machine that would crawl through the colon ("large intestine," or "large bowel"), but these efforts seem to have been abandoned without reports of any significant results. Their device was intended to locomote via motor driven, tank-like, treads on its opposing sides. This is a substantially different approach than the worm-like concept espoused in this thesis. Such a machine would have to expand laterally in order to maintain traction against the irregular walls surrounding it. At best, this would be very difficult as the colon's internal geometry changes dramatically along its length. It is the contention of Joel Burdick, Warren Grundfest and the author that be-

cause of the *diverticula* of the colon, the sac-like segmentations along its length, this lumen is a more difficult environment through which to maneuver than the small intestine. Snagging on these internal features must be avoided in all colonoscopic practice (endoscopy of the colon). Conventional endoscopes can be carefully maneuvered to prevent this, but any robotic colonoscopic device must be *designed* to reliably and safely negotiate such a challenging environment (and, specifically, vehicles with short "wheelbases" may have difficulty). In general, the small intestine can manifest changes in effective diameter along its length, but typically they are relatively small and occur gradually. In contrast, the diverticula represent dramatic changes in the width of the colon, and they occur repeatedly over relatively short lengths of the organ.

Chapter 3

The Robotic Endoscope

In Section 1.1, the potential impact of minimally invasive access to the entire gastrointestinal tract was briefly discussed. At present, endoscopes are used in surgical applications in regions from the mouth through the stomach and from the anus through the colon, but no endoscopes are introduced into the center of the small intestine without an incision. Thus, patients with inflammatory bowel disease are often forced to have repeated abdominal surgeries to treat their condition. To help people facing this potential ordeal was the primary motivation for this research. The vast length of the small intestine requires a shift in endoscopic paradigms; this work represents one possible approach to this problem. Furthermore, this paradigm may spawn endoscopic designs for other lumens (nongastrointestinal) in the human body; thus, the short term objective of helping patients with inflammatory bowel disease may potentially yield a family of advanced technology robotic endoscopes.

As discussed in the previous chapter, a fundamental limitation of current endoscopic devices is that they are advanced into the body by manipulations at their proximal end. In contrast, the robotic endoscope concept proposed in this research pulls itself along the lumen, obviating any propulsive require-

ments from outside the body. For any device that moves autonomously inside of a human (by any definition of autonomous), patient safety is paramount. This goal will impact almost all aspects of the design of such medical instruments. This chapter introduces mechanical and electronic design concepts for a class of self-propelled, robotic endoscopes in light of patient safety and mechanical/system dependability requirements. Design issues that have been considered include, but are not limited to: the choice of actuation technology, mechanical component redundancy, and control software that can adapt to changing circumstances. Two U.S. patents have issued [25, 26] that describe the locomotion concepts discussed in Section 3.2 as well as a variety of mechanisms that could manifest them. Sections 3.3 and 3.4 describe conceptually the designs of the robotic components and systems investigated. Finally, Sections 3.6 and 3.7 provide discussions of the development and evaluation of five generations of robotic prototypes.

The organization of this chapter may seem awkward at first perusal, i.e., discussion of the later generations of the proof of concept prototype robots precedes that of the earlier generations. This presentation of the design, fabrication, and testing of the experimental robotic systems was chosen because the most valuable and reportable results arose from the fourth and penultimate generation. In addition, the design and development of the fifth and latest generation of prototype robot called upon all accumulated knowledge and insight into the difficulties of locomotion within a living small intestine. Thus, a thorough discussion of these two generations of the prototype family will provide the reader with a deep understanding of the pertinent issues in the implementation of gastrointestinal robotic locomotion.

Primarily for historical perspective, an overview of each of the earlier gener-

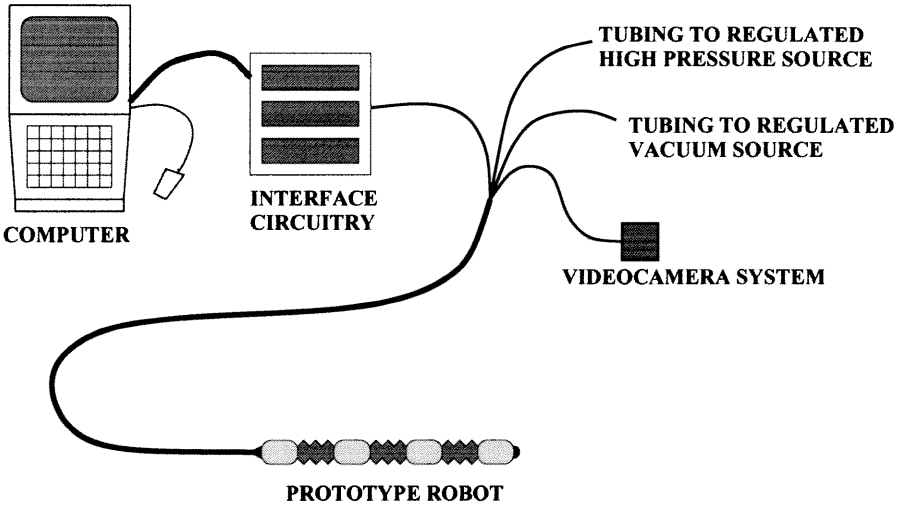

Figure 3.1: Schematic overview of a prototypical robotic endoscope system.

ations of the proof of concept prototypes is provided at the end of this chapter. In these sections, the features and performance of each design will be provided.

3.1 System Overview

A schematic overview of the endoscopic robot system concept is shown in Figure 3.1; the reasoning behind this design will be provided in the following sections. To investigate the various aspects of this technology, five distinct generations of proof of concept prototype robots were designed, built and tested. Common to all of these prototypes is a locomotion system comprised of the robotic mechanism with a trailing tether, an electronic control system, and pneumatic sources and plumbing. Although the earliest robots relied upon hard wired, digital, control electronics, later versions have been controlled by serial signals from a laptop computer. In all these experimental prototype systems, the robots utilize pneumatics for actuation and hence require regu-

lated compressed air and vacuum sources. Additionally, videocamera systems for visualization within the lumen have been incorporated in the design of the later versions.

This subsection will focus on the fundamental concepts that are common to all five generations of experimental prototype robots.

Referring to Figures 3.2 and 3.3, these endoscopes can be considered electromechanical analogs of segmented worms, such as earthworms. These creatures propel themselves by pushing against and stretching through their surrounding environment in a coordinated manner. For this type of locomotion, the robotic endoscope employs mechanisms along its length which can be described as "grippers" and "extensors." The primary purpose of the grippers, or traction devices, is to provide traction against the lumen wall by expanding radially outward. The extensors provide extensibility between the grippers, i.e., they cause the mechanism to locally stretch or shrink in length. Locomotion is the process of generating net displacement of the robotic endoscope inside a lumen by specific sequences of gripping and stretching actions. Such sequences are commanded by an external computer, and thus changes in the selection and control of mechanical movements can be easily accomplished in software. Furthermore, these machines are not limited by their mechanical design to locomote by a particular gripper and extensor sequence. This adaptability may be required for robust locomotion through lumens which exhibit changing geometric or material characteristics along their length (e.g., intestinal curvature or varying cross-sectional diameter). In addition, a large number of similar, or identical, mechanical elements can provide redundancy in the event of an individual component failure; whenever possible, the robot should remain capable of crawling out of the patient if an individual component were to become

Figure 3.2: Photographs of a fourth generation, prototype, robotic endoscope consisting of three grippers and two extensors.

inoperative.

After much consideration of various actuation technologies as well as the requirements of robotic endoscopy of the small intestine, fluid power was determined to be the most viable actuation technology. In contention were numerous alternative approaches including electromagnetic actuation, shape memory alloys, piezoelectric materials, and magnetostrictive materials. But fluid power was chosen for the proof of concept prototypes and is a likely candidate for a viable surgical instrument for the following reasons. Current endoscopic procedures often require carbon dioxide gas, saline solution, and partial vacuum for insufflation (the medical term for inflation of body cavities), irrigation, and suction of gastrointestinal lumens. Consequently, these features must be incorporated into the advanced, robotic endoscopes as well. Thus, these fluidic power sources for mechanical actuation would also be available for the locomotion subsystem of the endoscope. And since large amounts of pneumatic or hydraulic mechanical power can be controlled by small electric signals, this approach could minimize the danger of electric shock to the patient. Hence, fluid power would be a convenient and safe method for generation of substantial actuation forces and displacements in these robotic devices. An additional safety measure of these designs is that the working pressures of the fluid power sources can be kept intentionally small thereby reducing the maximal forces that the actuators can apply. In our prototypes, the high pressure source has been typically maintained at or below 12 psig, while the low pressure has been nominally -14.2 psig (vacuum).

In contrast, each of the competing technologies imposes unique and serious challenges to a robotic endoscope designer. Electromagnetic actuation (electric motors, voice coils, etc.) can produce large mechanical forces and

displacements when driven by relatively large electric currents; unfortunately, such electric signals at work within the body can adversely impact patient safety. Magnetostrictive and piezoelectric materials undergo minute deformations when subjected to large magnetic and electric fields, respectively; thus, devices that utilize these materials must be designed to "amplify" these small mechanical effects. As with electromagnetic actuators, these devices are driven by large electric signals; piezoelectric actuators typically require extremely high driving voltages, and magnetostrictive actuators need large electric currents. Unfortunately, electrical currents as small as 5 milliamps through the heart can cause death. And, finally, shape memory alloys produce mechanical actions when heated, and resistive heating can cause them to rapidly change shape. Unfortunately, rapid cooling of these materials can be very difficult (a sophisticated cooling system may be required). Thus, in applications such as robotic endoscopy, the time response of shape memory actuation may not be sufficiently rapid.

For the aforementioned reasons, the decision to pursue a fluid power design is justified. But selection of pneumatics versus hydraulics remains an unanswered question. The experimental, proof-of-concept prototypes utilize pneumatics for a very practical reason. These machines have many potential modes of failure, including leakage from hoses and actuators. Leakage of air, especially after a catastrophic rupture of an actuator, does not require any "clean up." In conversation, E. Zukoski at Caltech recommended use of the saline source (the surgical irrigation source) for hydraulic actuation as it would likely be a safer fluid power medium in the event of a mechanical rupture of a robotic component. His contention is that the leakage of an incompressible liquid into a patient causes substantially less volumetric distention than air.

Unfortunately, if such a failure occurs, there is the possibility of a high velocity saline jet causing laceration of the fragile intestinal membranes. The momentum flux in a similar pneumatic jet would be considerably lower which could reduce the deleterious cutting effect of a rupture. Clearly, both competing safety issues must be considered carefully before any such device is introduced into a human being. And while the locomotion concepts espoused herein can apply to the design of self-propelled endoscopes that crawl within any biological lumen (such as blood vessels), the detailed design of these mechanisms must reflect the specific needs of their respective applications. In this context, the actuation technologies of the robotic gripper and extensor subcomponents would be chosen for safe and dependable locomotion specifically with regard to the relevant lumen and medical application.

The system described above must be packaged to function within the small intestine. To characterize this environment, mathematical descriptions of both the geometric properties and elastic behavior of the intestine are required. As one example, an estimate of the unstretched diameter of the small intestine is an important parameter to specify the contracted diameter of the endoscopic robot. Based on initial estimates, these robots should have a contracted diameter of less than four-tenths of an inch, or ten millimeters, approximately. To date, the thinnest robotic prototype that has been fabricated was approximately seven-tenths of an inch (eighteen millimeters) in diameter. The curvature of the small intestine imposes additional geometric constraints on the design of these devices. The initial estimate for the minimum radius of curvature for the small intestine is 1.5 inches (38 millimeters). This geometric consideration affects: the maximum length of any rigid segment along the mechanism, the expanded and contracted lengths of the extensors, and the

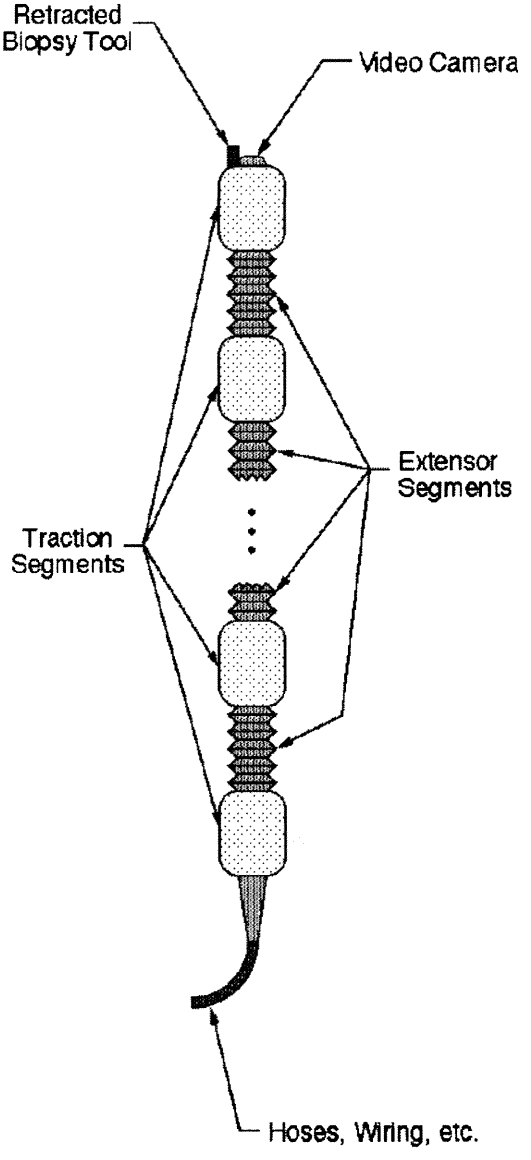

Figure 3.3: Schematic diagram of the robotic endoscope.

minimum radius of curvature that the bendable segments of the robot must achieve.

To date, the prototype design evolution has been dictated by a time consuming "build and test" method where engineering judgment has played a large role. These mechanisms evolved over five generations. With each step of this process, prototype components and systems were built to address specific research issues. Such issues include, but are not limited to, fabrication technologies, locomotion modalities, and system integration (mechanisms, electronics, and software). With each succeeding generation, the intended research objectives grew more ambitious, and the later versions manifested increased sophistication in order to meet their design specifications. Building experimental devices to "explore the design space" without a priori design analysis can be an inefficient approach to developing a viable device. If one could either analytically or numerically "test" each design before its fabrication, then fewer developmental prototypes would likely be required before converging to a viable final design. This motivated the investigation of the biomechanics of the small intestine as reported in Chapter 4. This biomechanics analysis and experimentation provided a foundation for a numerical simulation of the interactions between the robot and the surrounding lumen (highlighted in Section 4.6.3). It is expected that this modeling will be used in the design efforts of future endoscopic robot components.

Lastly, all five generations of these proof of concept prototypes were designed and fabricated solely with the available resources at Caltech. It is anticipated that using common and affordable manufacturing technologies, e.g., injection molding, the necessary size and functionality goals can be met. Unfortunately, most of these industrial tools tend toward cost effectiveness only

as the production volume increases; in other words, they were prohibitively expensive for these experimental research activities.

3.2 Methods for Locomotion

A *gait* is a distinct cycle of changes in the states of the component gripper and extensor segments that leads to a unit of displacement, which we term a *stride*. The displacement that results from one complete gaiting cycle is termed the *stride length*. Repetition of a gait leads to net displacement, or *locomotion*. If the robot is comprised of more than two independently operated gripper segments connected by one extensor segment, it will be capable of locomotion using more than one type of gait.

In Figures 3.4 through 3.8, several gaits are shown for endoscopes which are comprised of two, three and five gripper segments. One can think of these figures as a vertical array of sequential snapshots of a robot as it moves through a tube. For each element of these arrays, the *phase*, or *state*, of the machine is unique. And between the given phases, the conditions of expansion of individual gripper and extensor segments change. Since all phases of these locomotion gaits are aligned vertically in these figures, the stride length of each gait shown can be deduced by comparing the location of the robot in the first and last phases of the gait. While the lumen is represented as a straight tube, the inch-worm type locomotion methods will work if the lumen is curved and has reasonable variations in its cross-sectional shape and diameter. This is possible because the robots are engineered to exhibit passive bending compliance to lateral forces. Of course, *active* control of lateral bending of these machines is mechanically feasible and potentially necessary for at least

the leading segments (although no existing prototype device has incorporated active bending control).

3.2.1 The Gait of a 2-Gripper/1-Extensor Mechanism

For the purposes of illustration, let us first consider a locomotion method for a device consisting of two traction segments and one extensor segment, as depicted in Figure 3.4. This is the simplest design that can generate endoscopic locomotion.

A 2-gripper/1-extensor mechanism can exhibit at most one type of inchworm gait. The sequencing of the gait for forward motion proceeds as follows (in the diagram, forward motion means motion to the right). Let us assume that the sequence begins with the aft traction device expanded to grip the lumen wall (as indicated in the part of the diagram labeled "phase 1"). Meanwhile, the forward gripper and the extensor are in their retracted states. The extensor device is then lengthened (phase 2). While the extensor will typically be expanded to its full length, partial extension is also possible. If the lumen is curved and sufficiently rigid, the lateral compliance of the extensor will cause the expanding extensor to move in the principle direction of the lumen. After the extension is complete, the forward traction device is expanded to grip the lumen wall (phase 3). Once the forward gripper has grown, the rear gripper is retracted (phase 4). The extensor is then retracted (phase 5); typically, the extensor will be retracted to its shortest length, although partial retraction is possible. Subsequently, the rearward gripper is expanded to grip the lumen wall (phase 6). And finally, the forward gripper is retracted. At this point, the device is in the same state as in the beginning of this sequence. However,

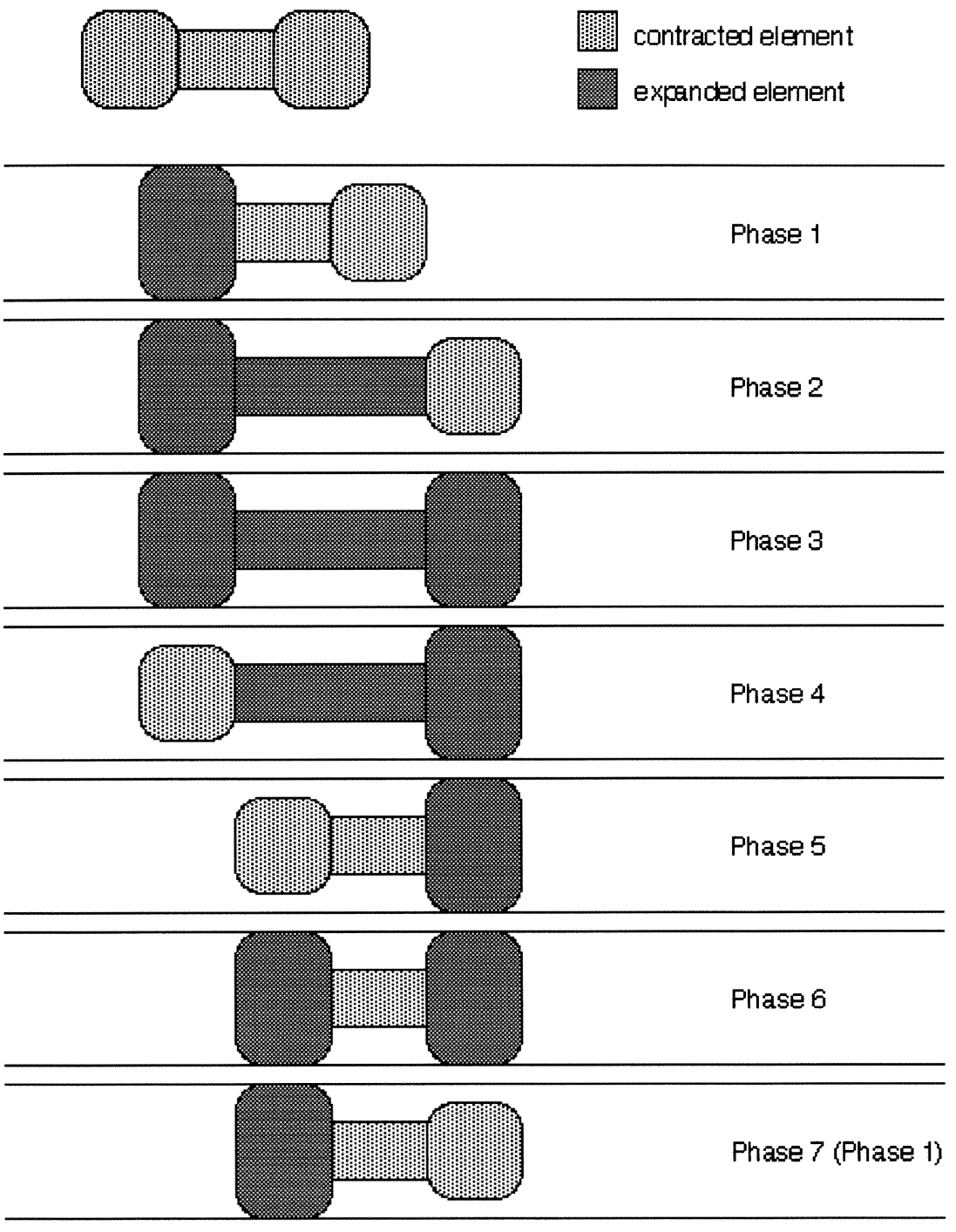

Figure 3.4: Schematic diagram of locomotion for a 2-Gripper/1-Extensor Mechanism.

the robot has moved forward by a one stride length. Assuming no slip, the stride length is the difference between the extended extensor length of phase 2, and the retracted extensor length of phase 5.

These steps comprise a single gait cycle. This cycle can be repeated to provide continual motion. It can also be reversed to implement motion in the rearward (opposite) direction. Loosely speaking, this gait may be termed a "standing wave" gait (using the terminology of Chirikjian and Burdick [7]), since the movement of the extensor can be thought of as a body fixed oscillation.

3.2.2 Some Gaits for a 3-Gripper/2-Extensor Mechanism

Let us now consider means by which a device consisting of 3 grippers and 2 extensors can crawl (e.g., the robot shown in Figure 3.2). This version can manifest locomotion using at least ten distinct gaits. Detailed descriptions of two of these gaits will highlight important characteristics of the device. Also, Figure 3.7 provides self-explanatory schematics of additional gaits.

The first gait which we will characterize is elucidated in Figure 3.5. In phase 1, all of the grippers and extensors are in their expanded states. The rear gripper is retracted in phase 2. Next, the rear extensor is retracted (either partially, or fully) in phase 3. Subsequently, the rear gripper is expanded to make contact with the lumen (phase 4). In phase 5, the middle gripper is retracted. Then, in phase 6, the rear extensor is extended while forward extensor is retracted. In phase 7, the middle gripper is expanded to make contact with the lumen. In phases 8 and 9, the forward gripper is retracted

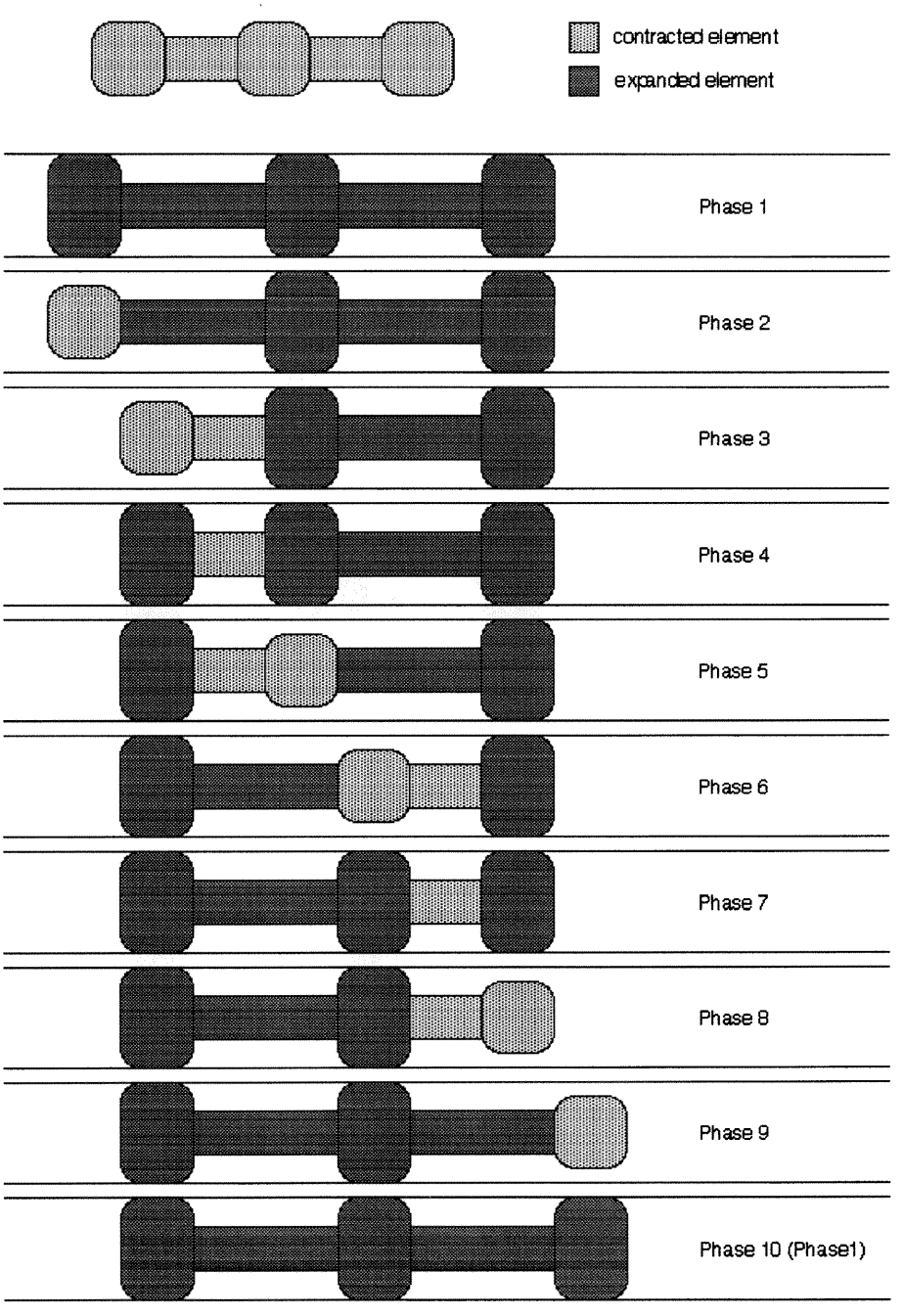

Figure 3.5: Schematic diagram of a traveling wave-like gait for a 3-gripper/2-extensor mechanism.

followed by an extension of the forward extensor. Finally, in phase 10, the forward gripper is again expanded. At this point the mechanism has returned to its original state and has advanced by one stride length. As before, this cycle is repeated for continual forward movement and can be reversed for rearward motion.

From the explanation of this gait sequence, it can be seen that the robot's contact with the lumen wall occurs in a "wave-like" manner. Hence, we can describe this motion sequence as a "traveling wave gait" in much the same manner as those described by Chirikjian and Burdick for hyper-redundant robots [7]. The robot's configuration changes as a body fixed traveling wave of compression; similarly, a traveling expansion wave gait also exists. It should be recounted that lateral compliance of the extensors will enable the mechanism to move in sufficiently rigid, curved lumens as well. Furthermore, it is clear that at any instant, only relatively short segments of the device are being pushed forward through the lumen. This should abate the buckling problems inherent in conventional endoscope designs.

Also noteworthy is that, in this gait, at least two gripping devices make contact with the lumen **at all times**. Consequently, a three gripper robot employing this gait would be able to more robustly grasp the lumen than it would using any gait that provides traction from only one gripper during certain phases of the gait.

Figure 3.6 shows a second example gait for a 3-gripper/2-extensor device. It should be noted that in all phases of this gait, the rear extensor is retracted; this gait functions without operation of the rear extensor. And the same sequence of maneuvers could also be used if the rear extensor were extended. As a consequence, this gait enables this robot to continue crawling even in the

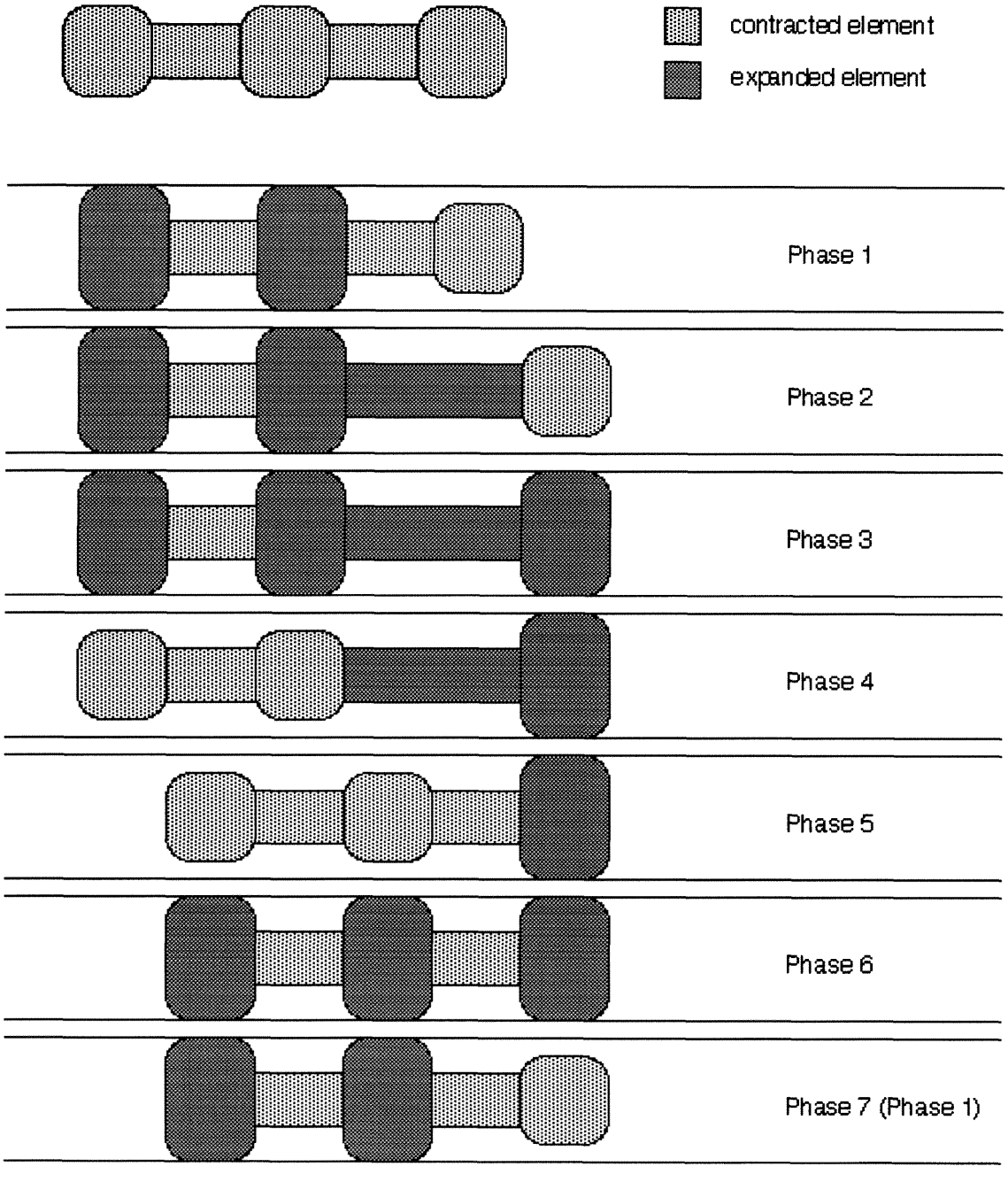

Figure 3.6: Schematic diagram of locomotion for a 3-gripper/2-extensor mechanism.

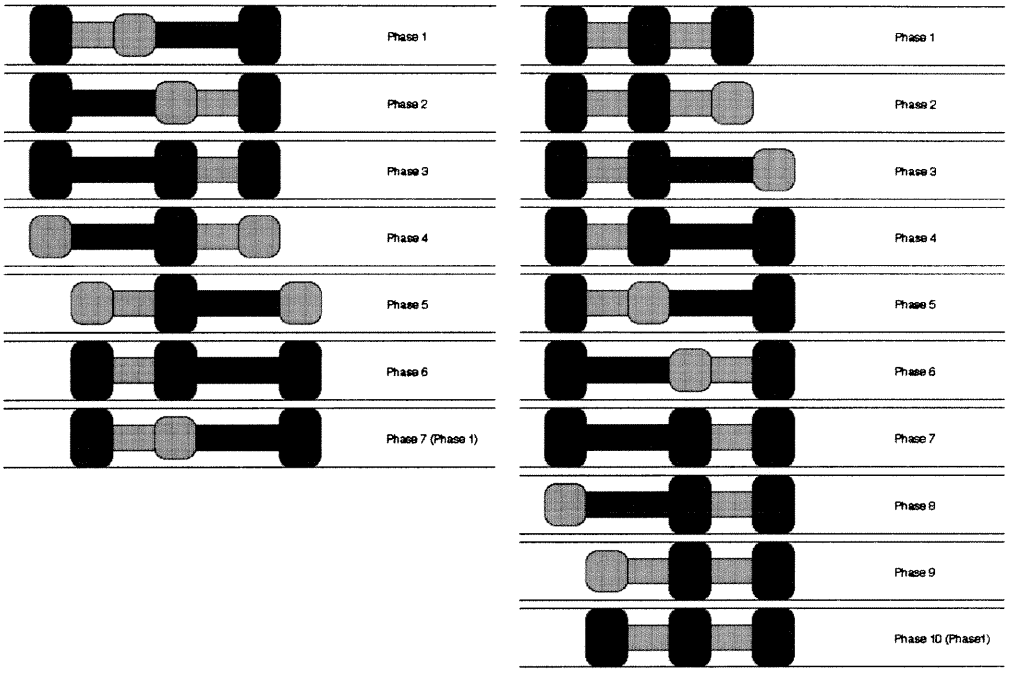

Figure 3.7: Schematic diagrams of additional locomotion gaits for a 3-gripper/2-extensor mechanism.

event of a rear extensor segment failure. Similarly, gaits exist that provide locomotion after **any** single actuator failure (provided that a failed gripper remains in its retracted state). Reiterating, the 3-gripper/2-extensor device can exhibit ten substantially different gaits. Such redundancy could be expected to contribute to increased safety of the overall system.

3.2.3 Gaits for Designs with Numerous Grippers and Extensors

As the number of grippers and extensors in the robotic endoscope design increases, so does the number of possible gaits. For example, Figure 3.8 shows one possible gait for a device consisting of 5 grippers and 4 extensors. One

could systematically develop the sequences for all possible gaits for any such robot using the ideas outlined in the previous subsections.

In general, it is advantageous for an endoscopic robot to be capable of a large number of gaits. Such endoscopes must have many gripper and extensor segments. As shown above, some gaits typically have more grippers in simultaneous contact with the lumen, e.g., traveling wave gaits. These gaits tend to be more stable, though the progress of the device through the lumen will be slower (as measured by the number of required phase changes and the attendant stride lengths). A slower but more robust gait would be useful when the robot moves into region of the lumen where traction is minimal. Furthermore, gaits with more grippers in contact can generate greater traction forces without excessive normal contact loadings; this might be useful for unblocking intestinal blockages/narrowing. Conversely, it may be desirable to select a faster gait when the robot moves into a region of strong traction and vital, healthy tissue. In addition, there exist gaits which are robust to the failure of particular components, as illustrated in Figure 3.6. The ability to switch between gaits as the situation dictates is a key feature of this device.

3.3 Prototype Component Designs

This section conceptually describes mechanisms which can implement the mechanical actions outlined above. As noted in 3.1, these machines consist of a serial chain of grippers and extensors. And the qualitative, experimental results discussed in Section 3.5 suggest that more than two gripper segments (connected by one extensor segment) will be necessary to provide dependable performance.

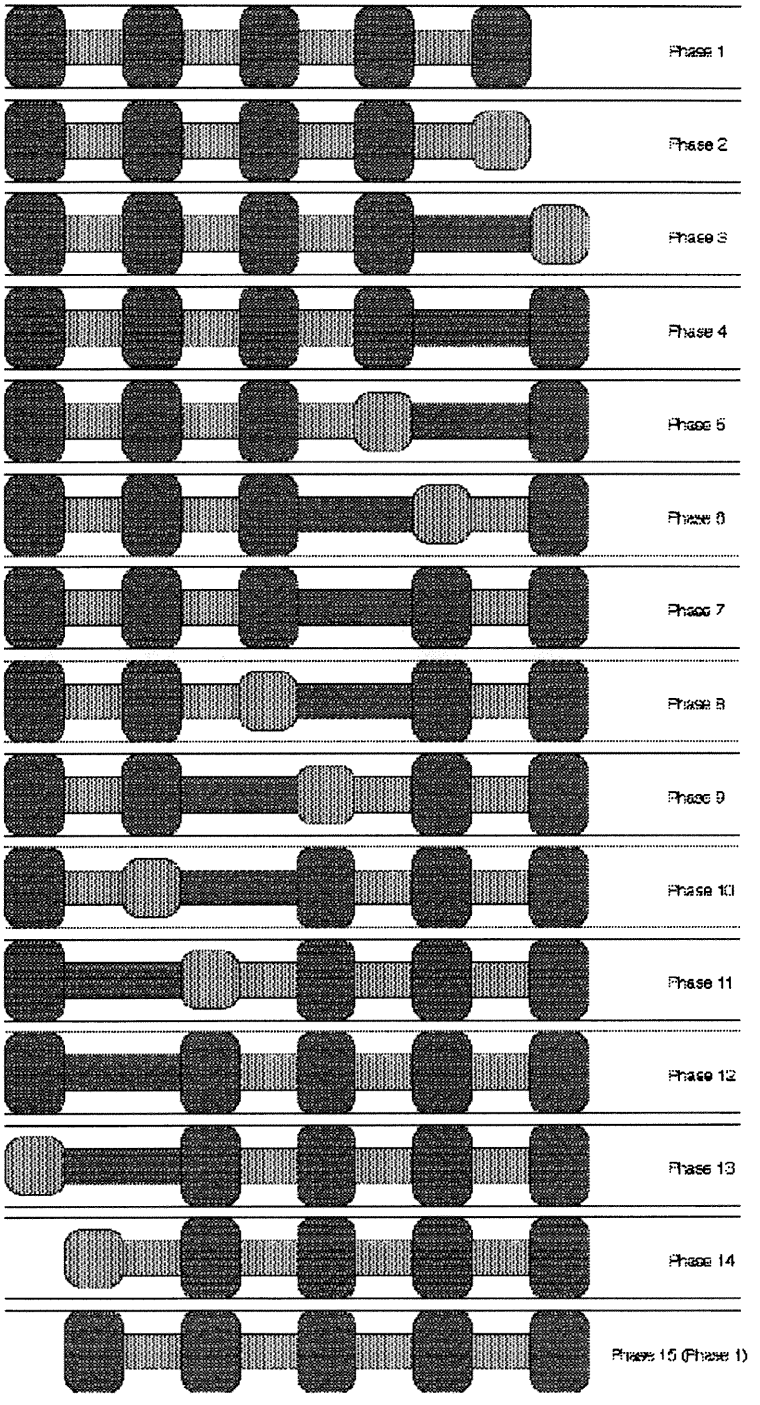

Figure 3.8: Schematic diagram of wave-like locomotion for a 5-gripper/4-extensor mechanism.

3.3.1 Traction Segment Designs

The role of a gripper or traction segment is to grasp the inside surface of the encompassing lumen by locally increasing its effective diameter. In a pneumatically powered design, these cylindrical components are fitted with an external, latex, toroidal balloon. Thus, inflation of this balloon will increase the segment's diameter. Since these segments must gently grasp the inner linings of the lumen so as to minimize the potential for injury to fragile tissues, careful design of the balloons and limits on the operating pressures of the system are needed to reduce the threat of harm to the surrounding intestines. And although all experimental prototypes to date have "balloon" grippers, many other viable mechanisms have also been considered [25, 26].

A schematic of one prototype gripper segment is shown in Figure 3.9. It consists of two, two-way, normally closed solenoid valves for inflation and deflation of the traction balloon. The inflation valve C is opened for a specified duration until the balloon A is sufficiently distended by fluid from the high pressure source line E; this valve is then closed. This design allows the segment to maintain traction without continuous dissipation of power. When traction is no longer required, the deflation valve D is opened which vents the balloon to a partial vacuum line F for a given length of time. This valve is then closed; thus, the traction segment can also remain in its contracted state without continuous expenditure of electrical energy.

Generations One, Four and Five of the gripper segment design evolution share a fundamental manufacturing detail. The toroidal balloons are fabricated from a single, "cylindrical" sheet of latex rubber. This layer of rubber is wrapped around a rigid cylindrical, gripper substructure. The ends of the

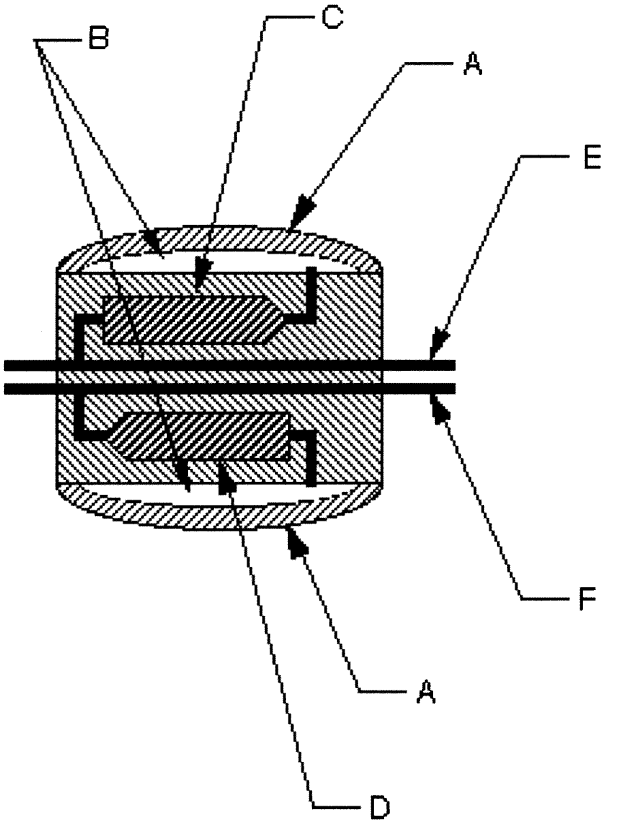

Figure 3.9: Schematic section view of a traction segment.

latex sheeting are adhered circumferentially to each end of the substructure. Then, by porting the valves to the enclosed volume between the adhesive joints, the latex sheet can be inflated radially in its center. The substructures are grooved at each end to hold the cyanoacrylate adhesive at the ends of the gripper segment as the joints cure. This feature prevents the adhesive from flowing freely between the latex and the substructure thereby ruining the assembly. The size of these components is dictated by two criteria: the expected unstressed internal diameter of the small intestines and its own internal packaging requirements (valves, plumbing, wiring, etc.). The relatively large, fourth generation prototype shown in Figure 3.2 is fabricated with aluminum gripper substructures that measure seven-eighths of an inch in diameter, one and one-half inches long with the latex sheeting nearly reaching each end. Given the installation of four solenoid valves (purchased from The Lee Company, Westbrook, CT) within each gripper segment of this device (two for the local gripper, two for an adjacent bellows type extensor segment), the robotic assembly was packaged very tightly. Fortunately, this generation of prototype was sufficiently small to be inserted into the intestine of a relatively large pig (approximately 150 pounds in weight). Within this pig, the robot performed a modicum of crawling. Qualitative, experimental observations of this robot's interaction with the pig's intestine contributed significantly to the design of the fifth generation version of the robot. The design features of that machine will be highlighted in Section 3.6. This latest version utilizes custom, onboard valves, two per gripper segment and two per extensor segment. Using these miniature valves, the gripper substructures are machined to a diameter of 0.700 inches and a length of 1.000 inch overall (including threaded ends for modular assembly). These Generation Five grippers are two-thirds as long

and fourth-fifths as wide as the Generation Four grippers.

3.3.2 Extensor Segment Designs

In the proposed form of locomotion, locally actuated extensibility is required between the gripping actions. *Extensors* provide this axial expansion and contraction. Also, lumens of human physiology are often substantially curved along their length which require endoscopes to bend laterally while advancing. All of the prototype gripper designs to date have been structurally rigid, and so lateral compliance has been incorporated solely in the extensor segment designs. Prototype Generations Two and Three of the design evolution accomplished this with compliant linkages between rigid air cylinder actuators; the first generation design lacked any lateral bending compliance. The extensor design evolved such that Generations Four and Five extensors are fabricated with an external, latex bellows as the primary, flexible structure. This bellows design allows the extensor segments to stretch (and shrink) preferentially in the axial direction under internal inflation (deflation). Within these extensors, internal springs provide the necessary bending, shear and longitudinal stiffness. The presence of these springs also prevents lateral contraction of the soft, latex bellows when the segment is vented to a vacuum. Generation Four and Five robots contain on-board, solenoid valves that control the flow of air in and out of these extensor segments. As in the gripper designs, each extensor actuator is controlled by two two-way valves; thus, the state of inflation of each extensor is maintained without wasting electrical power. To demonstrate the basic structure of an extensor segment, a schematic assembly drawing for the fifth generation prototype is provided in Figure 3.10.

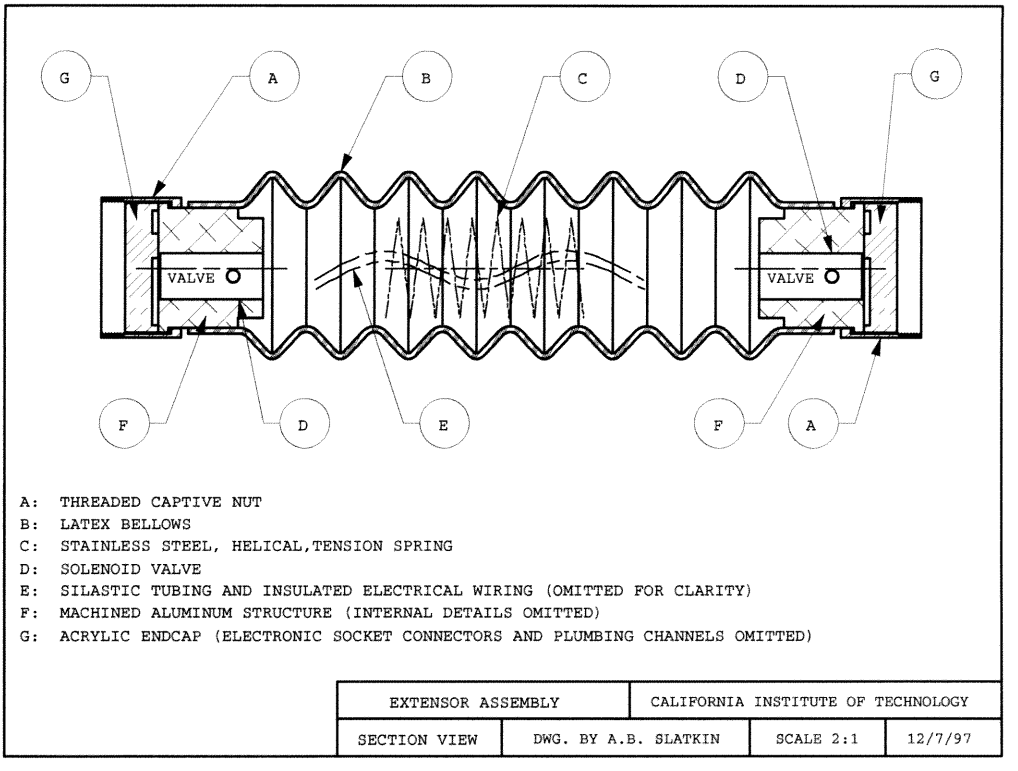

Figure 3.10: Schematic section view of a Generation Five extensor segment assembly.

3.3.3 Valve Designs

This endoscopic design concept could be applied to locomotion within a multitude of lumens found in the human body. It was decided early in this research that initial efforts would focus on the development of a device for the diagnosis and therapy of diseases of the small intestine. The small intestine was chosen because it is the largest diameter lumen that is presently inaccessible in a minimally invasive manner. It was therefore assumed that these miniaturization requirements of this technology would be simplified. This assumption was not quite valid. Considering that these machines are expected to crawl for over fifteen feet through an extremely compliant tube, the need to minimize the weight, stiffness, complexity (numbers of wires and hoses internally and externally), and friction of the trailing cabling becomes important. Additionally, the intestines' fragility, compliance and curvature require such a machine to have multiple gripper and traction segments (more so than are required for a straight, thick/stiff walled lumen such as an artery) which substantially affect the complexity of the final design. One consequence of locomotion within the small intestine is that the fluid control valves must be located on-board the robot itself to reduce the numbers of internal and external hoses. Thus, miniature valves are required to keep the overall dimensions of the assembly from outgrowing the small intestine. It is obvious that the size of each internal component has an impact on the overall diameter of the endoscope. But it is likewise important that any rigid, internal component of the assembly be "short" in the longitudinal direction of the endoscope since the length of such rigid parts affect the robot's overall ability to negotiate highly curved lumens.

In order to miniaturize the robotic system, each internal subcomponent

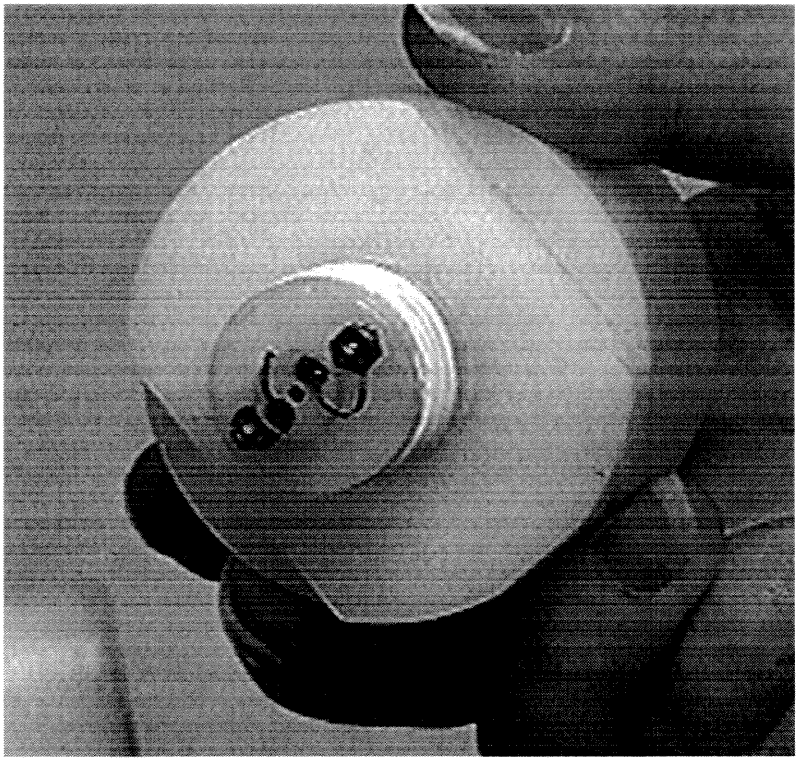

Figure 3.11: A silicon, micromachined valve installed in the test fixture.

should be as small as possible. Toward this end, many commercially available, miniature valves were evaluated, and a comprehensive investigation of advanced valve technologies ensued. Ultimately, two different silicon micromachined, microvalve technologies were studied alongside the smallest available, conventional, solenoid valves. Figure 3.11 depicts one custom, micromachined valve that was evaluated. Ultimately, however, none of the microvalves were able to supply sufficiently high flow rates to the robot's actuators. Thus, conventional, solenoid valves became the only viable solution. Unfortunately, the smallest valves available for purchase, from The Lee Company, Connecticut, are roughly one inch long and .22 inches in diameter. This diameter is suitable for our purposes, but this product's length is excessive if the endoscope is to be able to negotiate tight turning lumens.

Nevertheless, The Lee Company solenoid valves were utilized in the fourth generation prototypes. To minimize the effect of their length on the bending compliance of these robots, no valves were installed in the bellows type extensor segments. Instead, four valves were installed in each gripper in order to control the extension of an adjacent extensor in addition to the gripper itself. This design compromise traded a modest increase in the diameter of each contracted gripper for a vastly improved bending compliance of the robot.

In order to approach a viable experimental prototype for locomotion within the small intestine, a yet smaller solenoid valve was required. Since such a device was not commercially available, it was pursued as part of these research efforts. The resulting valves were incorporated in the fifth generation prototype robots and will be described fully in Subsection 3.6.2.

3.4 Electronic Controls

Regardless of the actuation technologies incorporated in their design, these robots crawl via a coordinated sequence of gripper and extensor actions. Such sequences are generated electronically. As previously mentioned, the movements of the earliest prototypes were commanded by hardwired, electronic circuitry. For these robots, while the speed, direction, and duration of actuation inflation/deflation were all adjustable, they always moved by a fixed sequence of maneuvers of the gripper and extensor segments. Tests confirmed that the robots' locomotion performance and reliability would be improved when provided with an increased gait repetoire. Research in *hyper-redundant*, or snake-like, mechanisms by Chirikjian and Burdick has demonstrated the value of "extra" or *redundant* mechanical components [7]. In the case of robotic endoscopy, such a mechanism could use these *redundant* segments for additional traction when needed in the slippery intestinal environment, around tight bends, or in areas of constriction/obstruction. However, to take advantage of this concept, independent control of each actuator is necessary. This necessitates the use of a computer to command all robotic maneuvers; the robotic control system described below has been applied to both the fourth and fifth generation proof of concept prototypes.

From the first discussions with the physicians, it was determined that these machines would incorporate on-board sensors to measure their interactions with the surrounding tissues. These devices could include, but are not limited to, balloon pressure sensors and tactile/contact loading sensors. Not only would sensor feedback likely improve the robot's overall performance, but it may be crucial to ensure patient safety by permitting the robotic control sys-

tem to limit both the contact forces on and the deformations of the intestine. With a closed loop, feedback controller, each segment's inflation is dictated by its measured impact on the surrounding intestine. Furthermore, sensor information could be used by the locomotion control system to determine autonomously when and/or if a gait change is appropriate. Such autonomy has not been incorporated into any of the initial prototypes, but it is envisioned for future robotic endoscopes.

To date, all robotic prototypes built have operated without sensor feedback, i.e., under open loop control. And their actuation has been strictly digital: *on* or *off*. The degree of inflation of each actuator is dictated by both the pneumatic supply pressures and the durations of the opening of its respective valves, i.e., the valve *dwell*. In other words, if the supply pressures are set to high levels, the actuator's expansion can be held constant by an appropriate reduction in the time that its valves are open; equilibrium of pressure across these valves is never reached. This can allow rapid locomotion through rigid tubing, but it seems to be of much less value for maneuvering within the intestines (this will be discussed in Section 3.5).

Since experiments were conducted at both Caltech and Cedars-Sinai Medical Center, the experimental apparatus had to be portable. And since feedback control has not been incorporated, a standard 80C286 based PC laptop has sufficed to provide motion commands. This basic computer was programmed to emit the requisite, digital commands for locomotion through the standard parallel/printer port. However, in order to "communicate" with the largest number of valves, additional interface circuitry was developed. An abbreviated schematic for this circuit design is given in Figure 3.12. The goal of this interface was to convert the computer's serial commands into parallel signals

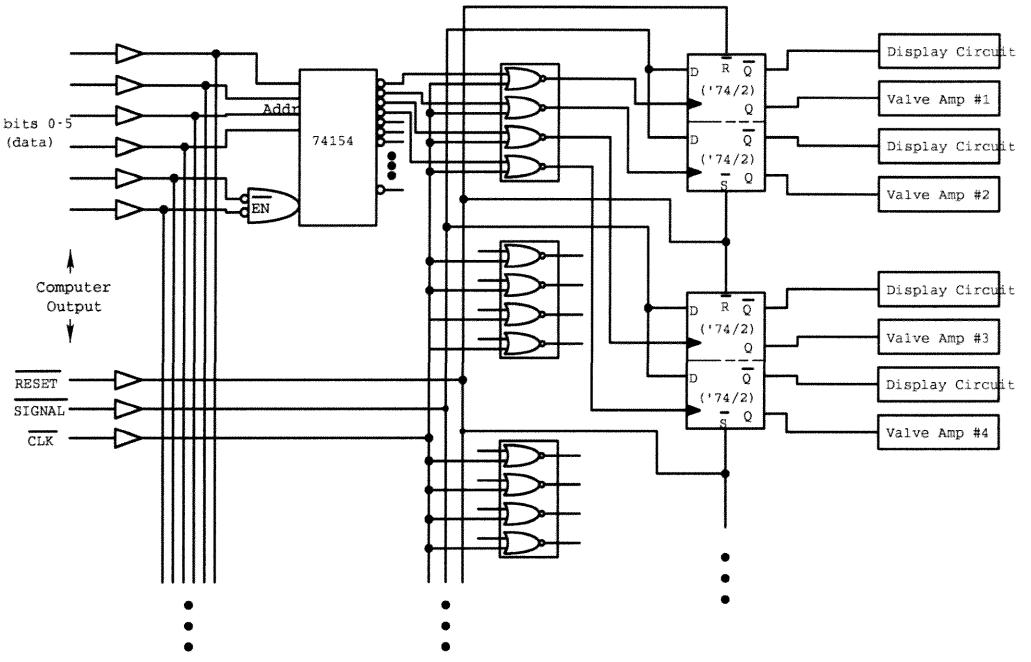

Figure 3.12: Interface circuitry for robotic control.

for output amplifiers that drive the robot's solenoid valves. Since the control computer can output commands at rates several orders of magnitude faster than any mechanical responses of the robot, the minute delays between two serial actuation commands can be negligible. Thus, the robot can be commanded to simulateously inflate and deflate numerous actuators. Using this approach, a parallel (printer) port can control up to sixty-four valves through eight data bits. This is much more capacity than necessary for any practical prototype robot that requires only two valves per segment. In addition to the port's eight "data bits," there are four output "control bits" which have been used for specialized purposes. For example, one bit is used to turn off all inflation valves and open all deflation valves simultaneously. This feature permits rapid extraction of the robot from the lumen. Furthermore, the parallel port

permits bidirectional data flow; the computer can receive up to five bits of data simultaneously. Thus, the interface circuitry can support the transmission of rudimentary sensor information from a robot to the control computer (a potentially necessary feature of future versions of the device).

There are a number of ways to encode the gaiting sequences, but in this implementation, each gait was reduced to an array of valve addresses (stored in a one-dimensional look-up table). Within a particular locomotion gait, generation of both forward and backward movement from each phase requires different sets of valves to be opened and closed. Also, for many gaits, a single step in phase can require the operation of multiple valves simultaneously (traveling wave gaits are examples). Thus, at each phase of the current locomotion gait, the control program must have access to two sets of valve addresses, one for each direction of motion. This allows the operator to select a change in direction at arbitrary times.

Continued locomotion results when the valve commands are sent sequentially to the robot as the program steps through the array (incrementing the array index advances the robot, decrementing it causes the robot to retreat). The speed of locomotion is dictated by the delays between commands to open and close the valves. And, as it was previously mentioned, control of the dwell, i.e., the duration of the valve's open state, will control the amount of inflation of the robot's segments. Lastly, gait changes are accomplished by transitioning from one stored look-up table to another. Smooth transitions between gaits are guaranteed because the robot is programmed to maintain at least one gripper expanded against the intestine at all times.

It is unfortunate that although the computer sends control signals serially to the interface electronics, its output amplifiers are connected to the valves

in a *parallel bus*, electronic architecture. As such, each valve is connected to a common "ground," and one specific signal wire. This means that every electric signal that is carried into the body of the robotic mechanism must pass individually through the robot's tail segment and trailing cable. Limited cross-sectional area within the tail segment therefore dictates the maximum potential number of segments for these machines.

This is a similar problem to one faced in the development of the first, second and third generation prototypes. In these robots, the pneumatic control valves were located "off-board." Thus, each actuator required an individual pneumatic hose to connect it to its control valve. These hoses originated at the valve, traveled through the trailing cable and into the robotic mechanism. In order to allow adequate extensibility, the hoses had to be wrapped helically around each extensor segment. Spatial interference of these hoses with each other as well as with the robots' internal structures limited the potential size of this *parallel fluidic bus*. As a result, assemblies of first, second and third generation prototype robots were limited to three grippers connected by two extensors.

Fortunately, in the case of Generation Four and Five prototypes, the *parallel electronic bus* could be made of wires that were substantially smaller in diameter than the pneumatic hoses used in the first three prototype generations. And since small electric currents can switch large amounts of fluid power, very small wires were used without affecting the robots' overall performance. This cannot be said for the early versions' parallel fluidic design because reducing the diameter of their actuators' hoses would produce significant fluid pressure drops and dramatically affect their actuation performance.

Nevertheless, multiple parallel wires must similarly be routed helically

within or around the extensor segments of robots with this electronic architecture. Such a geometric complication can likewise limit the potential number of gripper and extensor segments of a given robotic design. Ideally, the electronic architecture would be analogous to the pneumatic architecture in the later prototype robotic systems. That is, the drive electronics for each valve would be located within the robotic mechanism itself. With this *serial bus* architecture, at the expense of greatly increased complication in electronic circuitry within the mechanism, the total number of wires routed through the robot would be minimized. Due to the external size constraint of these robotic systems, the required miniature circuitry for serial, control communications and distributed driver electronics necessitates highly specific manufacturing technologies, minimally including surface mounted devices but perhaps requiring ASICs (*application-specific integrated circuits*). This type of development work is only rational in the context of an industrial venture. But this is the technical solution to a known deficiency in the experimental prototypes.

3.5 Prototype Development and Experiments

As previously mentioned, the endoscopic robot design process evolved over five distinct generations. Each stage of development addressed specific issues that include, but are not limited to, the conceptual design, the mechanical design of the componentry, and the electronic/computer control system. The research objectives of the development of the first three generations were quite modest (demonstrate the most basic locomotion concepts, etc.), and the resulting robots, as seen in Figures 3.13 and 3.14, were relatively simple in design and expeditiously fabricated. These generations of the design utilized hardwired,

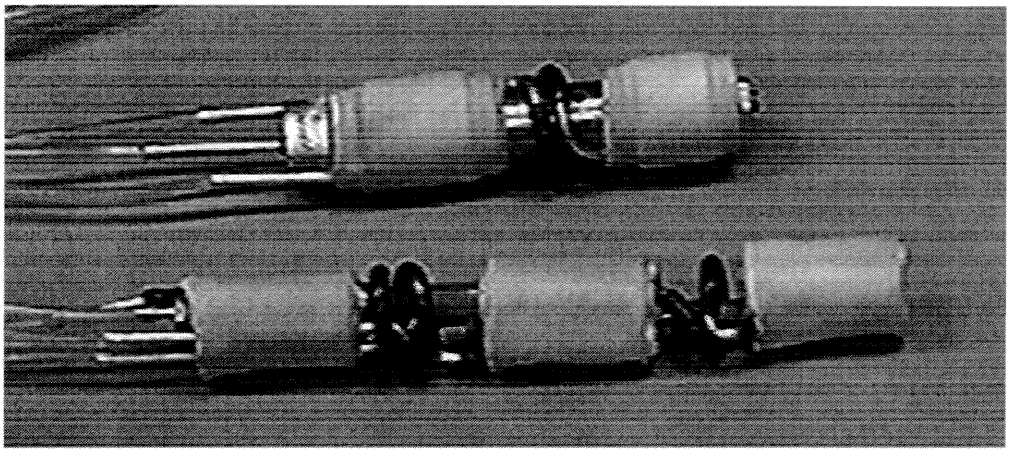

Figure 3.13: A photograph of two prototype robots (Generation One above, Generation Two below).

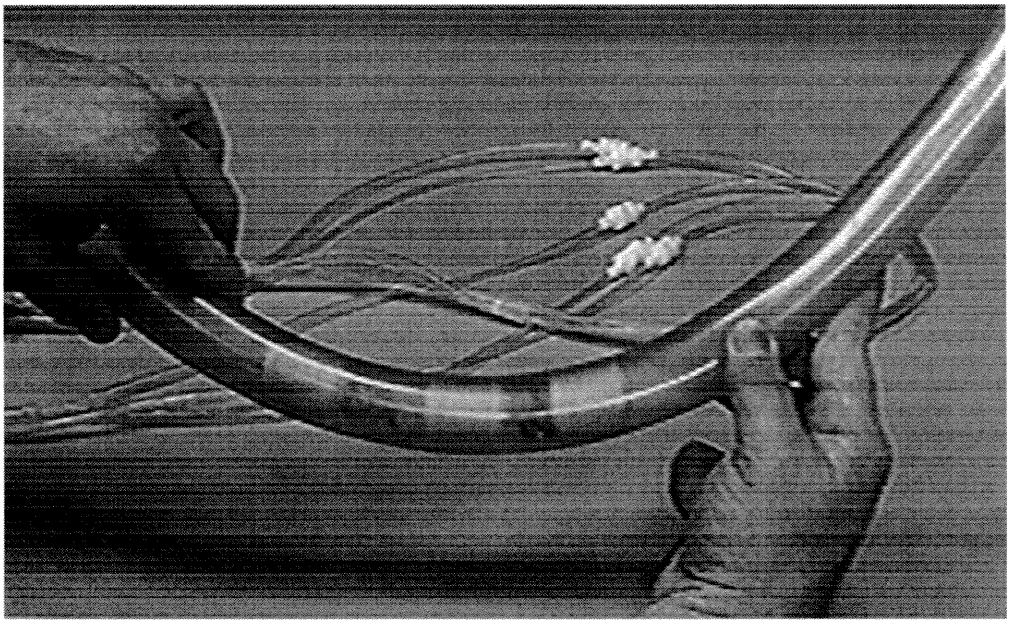

Figure 3.14: A Generation Two prototype crawling through a urethane tube.

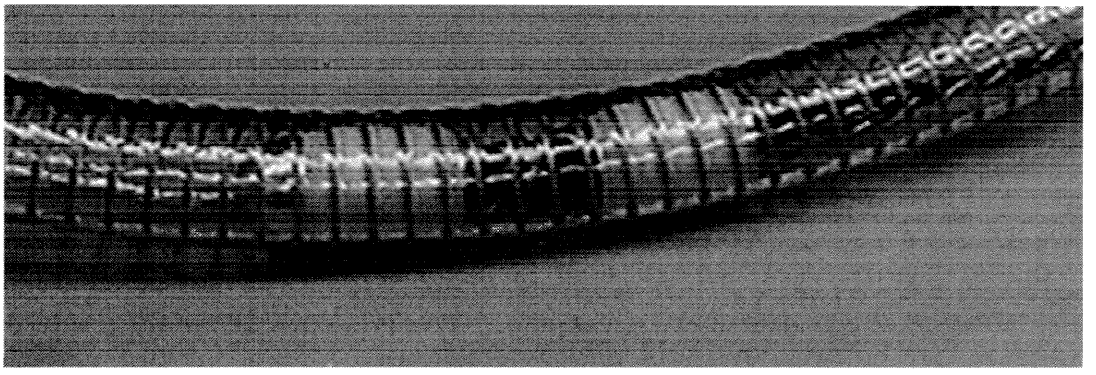

Figure 3.15: A Generation Four device is tested in urethane tubing.

finite state circuitry for locomotion control. And their pneumatic, flow control valves were located adjacent to that external control circuitry, i.e., not within the gripper and extensor components. Thus, each actuator was supplied by an individual hose that was routed throughout the mechanism, into the trailing cable assembly and to the control valve. As mentioned in Section 3.4, these designs were limited in practice to mechanisms containing maximally three gripper segments and two extensor segments in order to accommodate the necessary pneumatic supply hoses within the mechanism. In spite of this limitation, the performance of these machines inspired continued research into this endoscopic locomotion morphology.

Although these early mechanisms were quite simple in design, their successful demonstration of the proposed locomotion concepts led to more sophisticated versions, as seen in Figures 3.15 and 3.16. These later prototypes (Generation 4 devices) utilized commerically available, on-board, solenoid valves and computer controlled operation. The primary goals of these machines were to validate the computer control software and interface electronics, implement

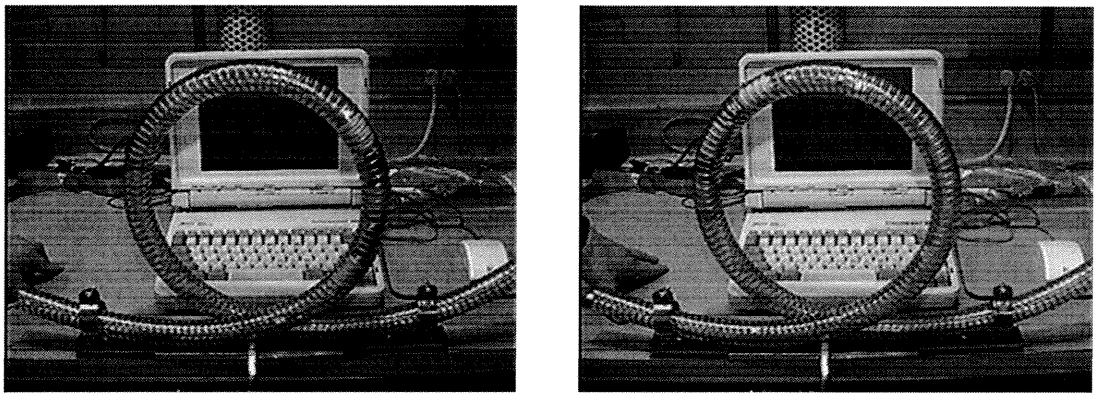

Figure 3.16: A Generation Four, 3-gripper/2-extensor robot negotiates a loop.

intraluminal imaging (via fiberoptic image and illumination bundles), and initiate experimentation within the intestines of pigs. Figure 3.16 was generated during demonstrations of the robot's capacity to alter its speed, gaiting sequence and direction according to the keyboard commands of the computer user. In these demonstrations, the robot would respond to interactive commands of the user.[1] Additionally, these prototypes were introduced into the small intestines of anaesthetized pigs. The crucial insights into intestinal locomotion that these experiments provided will be highlighted in the discussion of the design of the latest prototype robot.

As an additional objective, Generation Four prototype robots were designed to provide visualization from within their environments as well. This was accomplished by incorporating an existing 1.4 millimeter fiberoptic endoscope within the assembly. This endoscope was connected to a xenon light

[1]Direct interaction between the user and the robotic actuation should not be required during surgery using a robotic endoscope. It is anticipated that the surgeon would simply command the speed and direction of the robot's locomotion, and the selection of the locomotion gait would be made autonomously by the robotic control circuitry according to realtime sensor information.

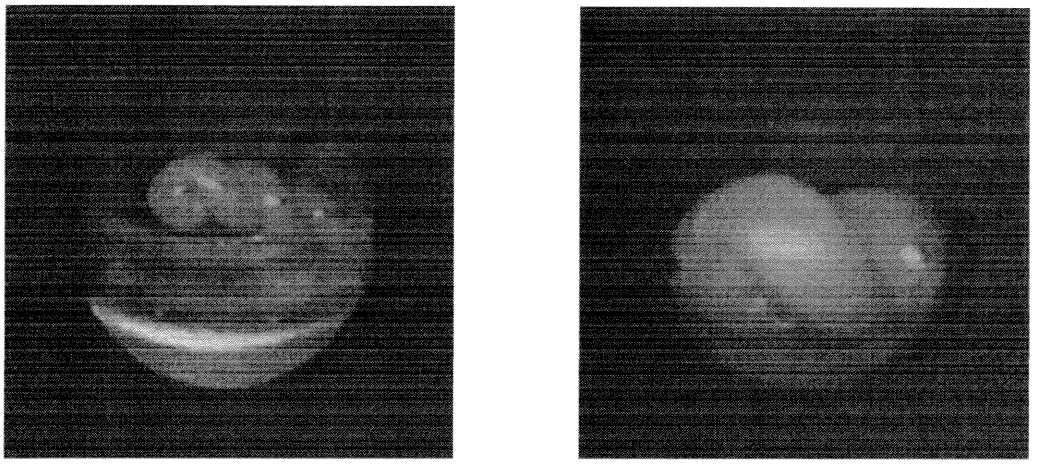

Figure 3.17: A Generation Four prototype robot approaches a simulated polyp within the urethane tube.

source and a CCD videocamera, and thus videotape recordings of these experiments were produced. Although the quality of the videoimaging from the inside of the urethane tubing could be improved, Figure 3.17 demonstrates captured frames from one of these videotapes. From its conception, this fiberoptic imaging design was considered to be an interim solution to the visualization problem for three reasons. Firstly, the robot exhibits local extensibility at every extensor segment. Since optical fibers are inextensible, their routing within or around the robot's segmentation is difficult. Secondly, the robot is ultimately intended to crawl deep within the body, so a trailing optical fiber bundle would add to the weight, stiffness and complication of the trailing cable assembly. And, lastly, the video image quality could be improved by installing a CCD chip in the distal end of the robot itself. Hence, the latest prototype (Generation Five design) has been designed to accept a videocamera "head" segment.

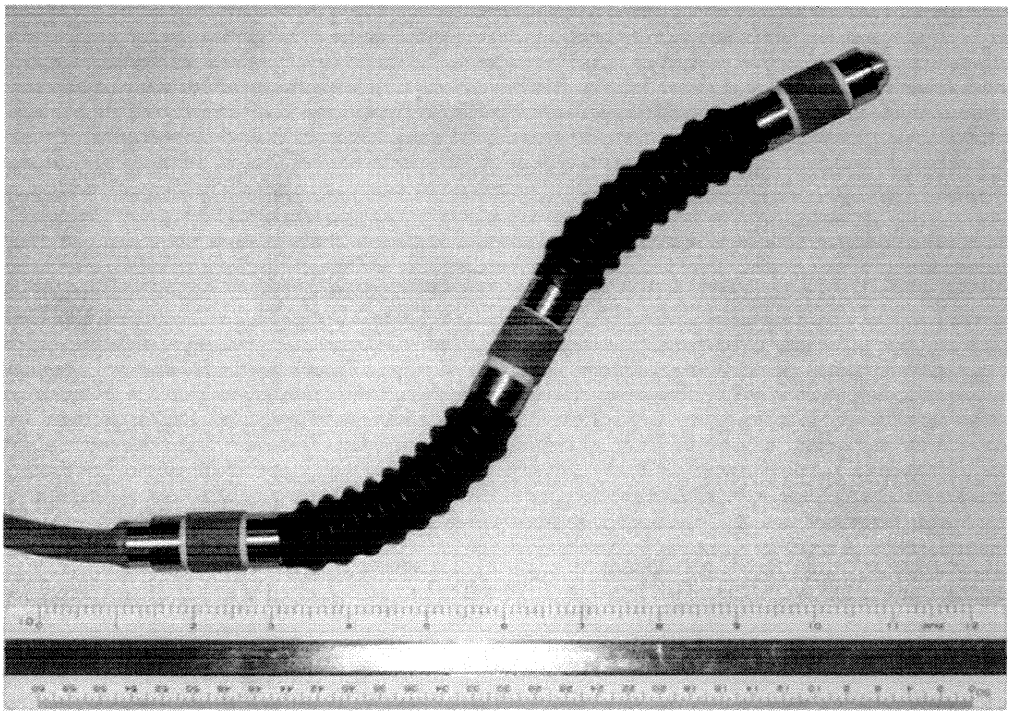

Figure 3.18: The first Generation Five prototype robot.

3.6 The Final Prototype Robot – Generation Five

The first Generation Five robot was assembled in March of 1998, and its experimental evaluation began shortly thereafter. But, as of this writing, only preliminary testing has been completed. To date, the mechanical functioning of the grippers and extensors has been validated; however, locomotion within a pig's intestine has not been reliably demonstrated. This fifth generation prototype was inserted into a single, deceased pig at Cedars-Sinai Medical Center, but that animal had been dead for approximately four hours prior to the testing. These experiments followed the *in vivo*, experimental protocol for

the Generation Four prototypes: a midline incision into the abdomen to expose the intestines, a transection of the small intestine at the desired starting point for the attempted locomotion, and then the insertion of the robot into the intestinal lumen as it is opened by surgical instruments. Once the abdominal incision was completed, several locomotion trials were attempted at different locations along the small intestine. Unfortunately, this pig's small intestine began drying out and shrinking as soon as the animal died. As a result, the robot was squeezed into a narrow, tacky lumen; this was not a reasonable test for the device. Unfortunately, the animal's small intestine was found in this unsuitable condition wherever it was transected. Presently, experimental trials of the Generation Five robot within a living pig are being planned in order to better evaluate its locomotion performance.

As previously mentioned, each successive generation of this robotic concept was built to evaluate specific aspects of endoscopic locomotion. The level of sophistication and capability of the prototypes increased consistently as the designs evolved. This section elucidates the features that were incorporated in the most advanced version, i.e., the Generation Five prototypes.

Features that are found only in this latest family of robots resulted from qualitative observations of the performance of all the earlier generations. But, unlike its predecessors, this design was conceived and built solely to investigate locomotion within the small intestine of a pig. Previous incarnations were intended primarily for locomotion experiments within urethane tubing in the Robotics Laboratory at Caltech; figures presented earlier in this chapter illustrated such endeavors. These experiments were required to study the basic locomotion concepts and validate the control software and interface electronics that would carry over to later versions. The fourth generation was

developed for the initial forays into the bowels of an animal; however, this design's primary objectives were to demonstrate the parallel, plumbing architecture with on-board valves, validate the computer control and its attendant software, provide intraluminal visualization, and test the performance of new, laterally compliant, bellows type extensor segments. These extensors have demonstrated substantial extensibility and lateral compliance (as is evident in Figure 3.2), and so their morphology has carried forth into the fifth generation prototype. And, unless future experiments dictate otherwise, the basic shape and function of both gripper and extensor components are not expected to change dramatically in future generations. Of course, these designs must be refined.

3.6.1 Surgical Experiments Dictated Generation Five Design

The first surgical experiments using Generation Four componentry were conducted in April, 1994, at Cedars-Sinai Medical Center with Warren Grundfest, M.D. These trials qualitatively confirmed that significant traction forces could be generated between smooth surfaced gripper segments and the inner lining of the small intestine of an anesthetized pig. In addition, an assembled Generation Four robot (two grippers, one extensor) was surgically inserted into the pig's small intestine (see Figure 3.19). Because these experiments were conducted through a large abdominal incision, the robot's actions could be studied by observing its effects on surrounding intestine. Figure 3.20 illustrates this; a gripper segment is inflated (the tip of a surgical instrument is included for reference). In these tests, the robot was witnessed to crawl within

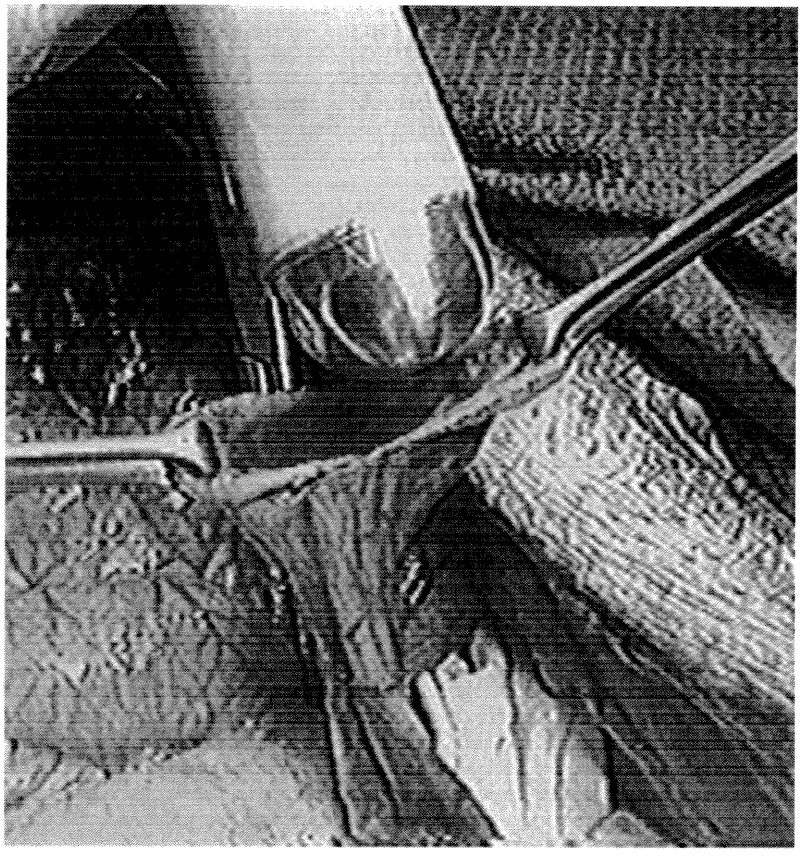

Figure 3.19: A prototype robot (Generation Four) is inserted into the small intestine of a live pig.

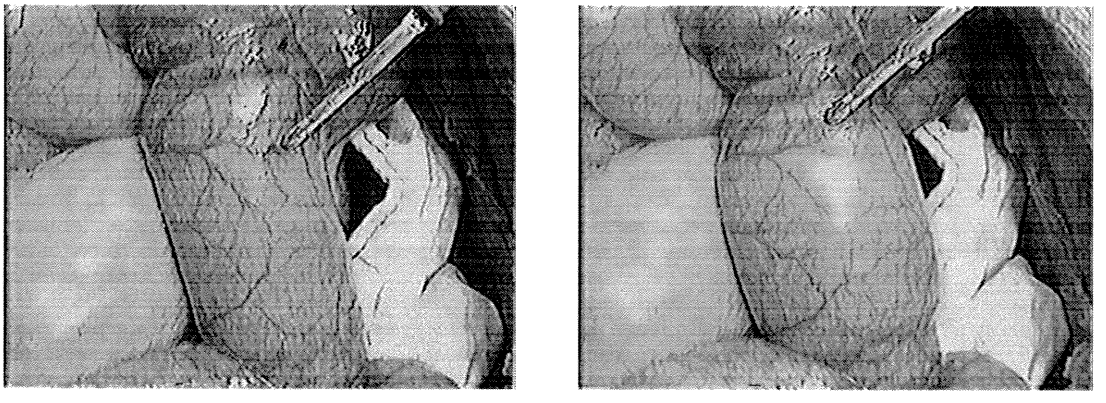

Figure 3.20: One of the robot's gripper segments is inflated (Generation Four).

the lumen, but its performance pointed to necessary improvements in robotic endoscope design (which were incorporated in the fifth generation devices). Since this fourth generation machine was not expressly designed to crawl in intestines, its locomotion was encouraging. But the true value of these *in vivo* experiments were fresh, qualitative insights into intestinal locomotion.

The chief insight was the recognition of fundamental differences between navigating through a solid tube versus a highly flexible one (although topologically they are identical). For the following reasons, a viable, intestinal "pipe crawler" should incorporate features not likely found in the industrial analog. The intestine is a thin membrane with essentially zero bending rigidity, and unless it is distended by internal loading, e.g., internal inflation with air or the presence of an endoscopic robot, this "tube" will collapse under its own weight. Additionally, within the abdominal cavity, the intestine is squeezed by the external hydrostatic pressure that surrounds it. By looking at the surgically dissected end of the intestinal specimen shown in Figure 3.19, one can observe its thin walled, compliant nature. Note the actions of the grasping forceps that are opening the transected intestine, and recognize that from roughly one-half of an inch below the grasped end, the intestine appears to be unstretched. Also, while in situ, the small intestine is loosely supported by a thin membrane called the mesentery. This membrane provides the intestine a supply of blood and maintains its general location within the abdomen. This basic description of the intestine's mechanical behavior gives one cause to reconsider the meaning of "crawling through the small intestine." Generally, locomotion can be viewed as a process in which a body is acted upon by unbalanced forces between it and a rigid environment. Basic mechanics dictates that under such conditions the body will accelerate. To view crawling within

the small intestine this way is inappropriate. A revised "philosophy" for intestinal locomotion is needed. A rigid environment resists forces applied in all directions; in contrast, membranes can only produce reaction forces under conditions of *tension.* This distinction is critical to the design of the endoscopic robot. Such observations (and conclusions) follow.

When the fourth generation prototype was inserted into the intestine, its diameter caused a small amount of stretching of the surrounding membrane, but the ease of insertion led the experimenters to believe that the intestinal stretching was not excessive. (In fact, Dr. Grundfest judged that the diameter of this machine, at seven-eighths of an inch, was nearly small enough for human clinical use.) For the prototype comprised of two grippers and one extensor, the experimental gait sequence began with the rear segment's inflation to gain traction against the intestinal wall. As expected, the extensor was then extended to push the front segment deeper into the intestine. The front segment was then inflated to maintain its station within the lumen. When the front of the robot was anchored, the rear segment was deflated. With this robotic endoscope prototype, the difficulty begins with the next step of the process.

One would hope that the rear segment would slide along the walls of the lumen toward the front segment (thereby providing one stride of advancement for the robot), but unfortunately that is not guaranteed. As mentioned above, the soft walls of the intestine will buckle under small compressive loading. And when the extensor was contracted, frictional drag on the rear gripper caused its surrounding intestine to move forward. The fact that the contracted diameter of these grippers was slightly larger than the effective intestinal diameter exacerbated this problem. Thus, this robotic prototype could not reliably shed

from its ability, with each cycle of the locomotion gait, to reach a little further into the lumen, gather a length of intestine onto its perifery and ultimately eject this excess membrane to its rear. Practically speaking, there could be instances where the robot has completed cycles of its gait, displaced a substantial length of intestine from in front to behind, and nevertheless remained motionless as viewed in an inertial reference frame. Such conditions would not be expected to continue incessantly as the mesentery would eventually be placed into a state of tension once the stationary robot pulls enough intestine past itself. Subsequent biomechanics experiments of the elastic properties of pigs' small intestine inadvertently demonstrated how the mesentery can bear loading applied to the intestines (Section 4.5).

3.6.2 Miniature Solenoid Valve Designs

As mentioned in Section 3.3.3, conventional solenoid valves were used within the bodies of the Generation Four and Five prototypes. The smallest valves currently available for purchase, the two-way LHDA series from The Lee Company of Westbrook, Connecticut, are roughly one inch long and .21 inches in diameter. These subcomponents were installed successfully within the Generation Four robotic mechanisms, but they were considered to be too large for subsequent versions.

The LHDA valves' diameter is suitable for the fifth generation prototypes, but their length was excessive. If the machine was to negotiate highly curved lumens, the fractional length of the robot that is rigid must be minimized. Thus, the length of the internal valves (and any other internal subcomponent) must be reduced as much as possible. It was encouraging, however, that the

LHDA valves' performance was much higher than that required by the robot. Specifically, this design utilizes electromagnetic forces to pull a plunger off the valve seat; these forces oppose the pressure forces from within the valve. The LHDA specifications guarantee operation at 12 Volts DC against a pressure difference of 0-50 psig. 50 psig is substantially higher pressure than these endoscopic robots require. And since the electromagnetic force produced by a solenoid monotonically increases with its length (theoretically linear with the number of turns of wire), one would expect to be able to shorten the length of the valve (specifically, by shortening the length of the internal solenoid) while maintaining adequate electrical/fluidic performance. Unfortunately, The Lee Company was unwilling to miniaturize them further; thus, at Caltech, efforts proceeded to develop yet smaller solenoid valves. The resulting design is illustrated in Figure 3.21.

The dimensions of this valve design are: .500 inches in length, .230 inches in diameter. The internal solenoid was wound with approximately 80 feet of 44 gauge magnet wire (the diameter of which is 0.002 inches including insulation; in comparison, typical white paper is 0.004 inches thick). Each valve was assembled from seven structural parts that were machined conventionally from carbon steel (AISI 1018, cold rolled), stainless steel (AISI 316), aluminum (6061 alloy), and Teflon. As can be seen in this figure, these valves were normally closed with the pressure across the valve and a bias spring holding a conical, Teflon plunger face against an aluminum valve seat. Energizing the solenoid coils with 12 VoltsDC would cause the plunger to open against a pressure differential of 13 psig. Although the stroke of these valves was less than 0.25 mm, the attendant flow rates were sufficient to inflate (and deflate) the actuators in a timely fashion (the requirement was roughly 2 cubic inches

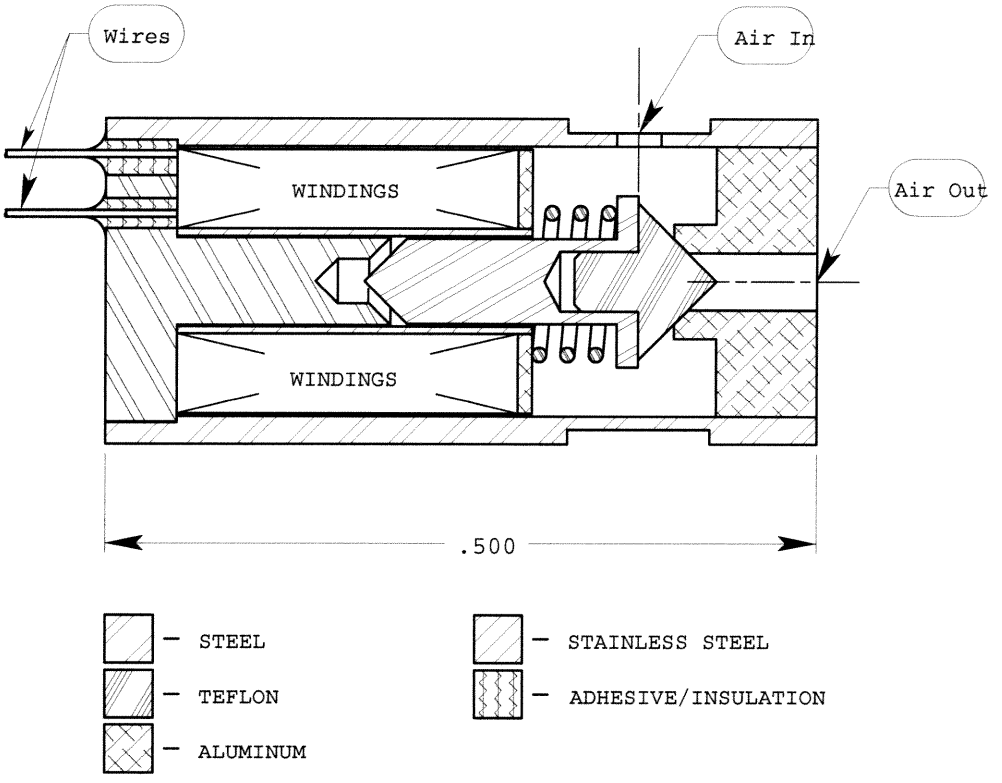

Figure 3.21: Schematic section view of a miniature, normally closed, solenoid valve: the Teflon conical plunger face seals against the chamfered aluminum valve seat.

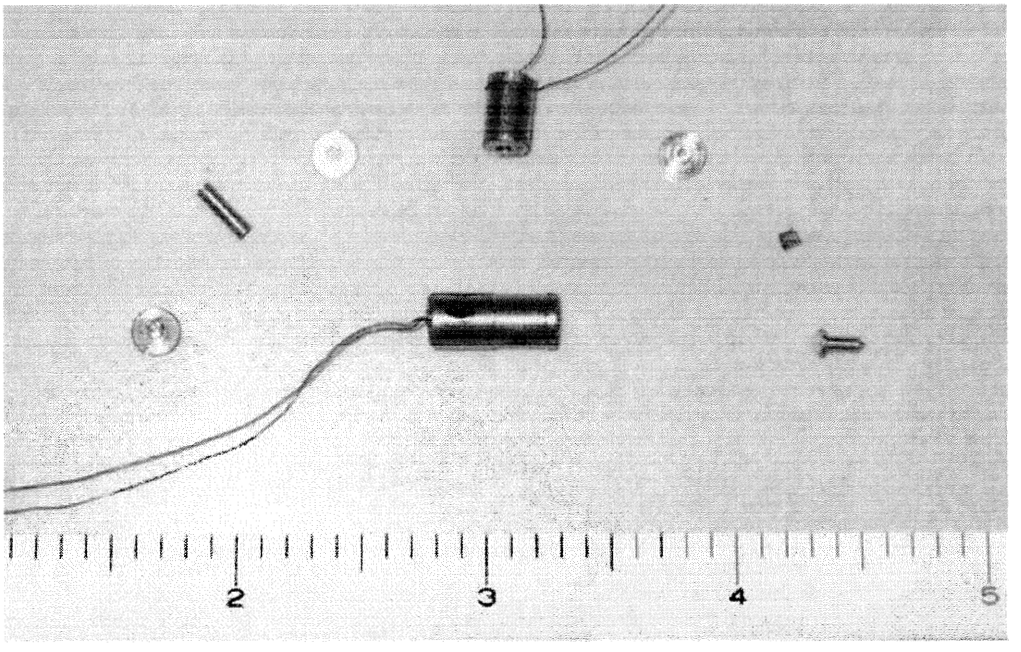

Figure 3.22: Photograph of a completed valve assembly surrounded by various parts and subassemblies.

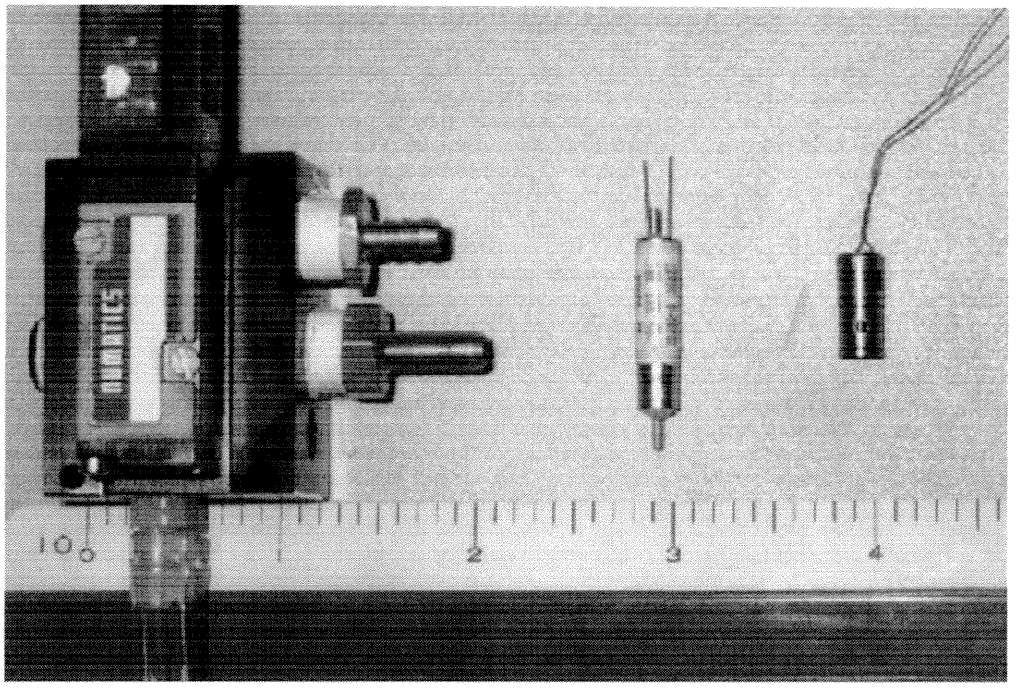

Figure 3.23: Photograph depicting the three solenoid valves used in this project (Left: the off-board valve of Generations One, Two and Three; Center: Generation Four; Right: Generation Five).

of flow per second or 33 cubic centimeters per second).

3.6.3 Bellows Extensors

In an effort to add lateral bending compliance to the endoscopic robot design, the Generation Four prototypes were designed with extensor segments comprised of an external bellows structure over a soft internal spring "skeleton." The resulting extensors were quite compliant to applied transverse loadings (see Figure 3.2). Their inflation and deflation were controlled by solenoid valves (produced by The Lee Company) located within adjacent gripper segments. Conceptually, this extensor design is simple, but to derive the desired

performance, care must be taken in its implementation. The following design and assembly insights improved the relative extensibility, i.e., performance, of these bellows type extensor segments.

A concentrated transverse loading of an unreinforced rubber bellows can deform it in one of two ways. The bellows could bend like a beam or collapse and "shear" catastrophically. A properly designed extensor segment would be immune from shearing deformations. The soft internal spring (whose OD matched the bellows ID) provided sufficient lateral shearing reinforcement to guarantee that the extensor would bend in reaction to transverse loading. Also, latex rubber bellows can be axially compressed substantially from their initially unstressed lengths. But if an unreinforced bellow's length to diameter aspect ratio exceeds a critical limit, it will collapse/buckle laterally instead of longitudinally when subjected to an internal vacuum. When this happens, the change in length of the bellows is negligible. The presence of the internal spring in the extensor design prevented such lateral buckling by bearing radially on the rubber bellows inner diameter. Furthermore, these extensors' contracted lengths were dictated by the "solidified" lengths, i.e., contracted lengths, of their internal springs. This implies that the extensibility of a bellows type extensor increases as the solid length of the internal spring decreases.

Thus, the internal springs were selected to be as short and soft as was practical. To this end, the springs were fabricated from small gauge, stainless steel wire (stainless steel springs are eight-tenths as stiff as those made of standard "music wire"). In both the fourth and fifth generation designs, the internal springs were modified from commercially available tension springs from the Lee Spring Company, Brooklyn, New York (no relation to the valve company). Since these springs were initially produced as tension springs,

it was imperative that each be stretched past its elastic limit before final assembly within the bellows. This provided room within the spring's helix for the extensor to contract before the spring reached solidity. As an additional benefit of this preparatory stretching, the internal spring is softened further as its "initial tension" is removed; thus, the bellows is less inhibited from extending when pressurized.

In multiple respects, the Generation Five prototypes incorporated a number of improvements over the earlier designs. Firstly, these robots utilize the small valves described in Subsection 3.6.2 (Figure 3.21). These subcomponents are less than one half the length of those used in Generation Four. The small size of these valves permitted the fifth generation extensor segments to carry two internally and yet remain sufficiently compliant to bending loads. This change removed two of the four valves from the interior of each gripper (in the Generation Four design). Thus, the fifth generation grippers contain considerably less internal volume occupied by valves. Consequently, with respect to these grippers, the internal cross-sectional area for the electrical and pneumatic buses has been increased while the grippers' external dimensions have been reduced.

As a result of the Generation Four *in vivo* experiments, the fifth generation extensors were designed to have an outer diameter exceeding that of the adjacent, contracted grippers (Section 3.6.1. In addition, for the Generation Five devices, the minimum outer diameter of the bellows (at the end cuffs) was approximately equal to the contracted diameter of the grippers; therefore, the robot's exterior surface was as smooth as possible to minimize its drag against the intestines. And for smoothness considerations, the electrical wiring and pneumatic plumbing was routed completely within the robotic mechanism.

The increased diameter of the extensors provided the necessary room within them for internal electrical wiring and pneumatic plumbing.

Lastly, these extensors were designed to be capable of undergoing large extensibility. Nominally, the contracted length of one of these extensors is 2.85 inches (about 73 millimeters), and its maximally extended length approaches 4.5 inches (approximately 114 millimeters). Of course, by closing an extensor's valve before the pressure equilibrates across it, the deformation of the extensor will be reduced. Thus, this type of extensor module can be used to experimentally study the impact of varying mechanism extensibility on locomotion within a pig's small intestine.

3.6.4 Modularity of the Generation Five Design

The fourth generation of robot prototypes were designed such that once they were assembled, partial disassembly would be difficult. This was due, in part, by the requirement that the mechanism be as small as possible. Thus, 0.020 inch diameter wires were soldered to each valve and then routed back to the rear of the robot (taking helical paths around each extensor segment). Experiments with these machines highlighted two fundamental deficiencies in this prototype generation. Firstly, whenever any internal element of the system failed structurally (primarily wire breakage), "microsurgery" on the robot commenced. Relatively minor breakages often created major repair jobs. At one point during a demonstration at Caltech, one of the robot's two extensor segments developed a visible "aneurism," but, before either the computer or pressure regulator could be reached, it burst. Since this robot was computer controlled and built with *redundant* components, the demonstration could

continue without interruption (the user selected gaits that did not utilize that segment). However, the process of repairing the robot without its complete disassembly required substantial patience, skill and luck. And since experimentation of the fifth generation devices will involve anesthetized animals, their design must allow rapid repairs to be effected.

A fundamental research objective is to evaluate robots built with varying numbers of segments. Due to the complexity of the final assembly of the fourth generation prototypes, the addition of component segments to an existing robot rivals in difficulty the fabrication of an entirely new article. Thus, multiple robots of various numbers of segments would be required to test the relative merits of robots comprised of different numbers of segments.

Surprisingly, these two issues share a common remedy that was incorporated in the fifth generation design: build the robot as an assembly of completely prefabricated modules. Thus, a breakdown of a particular gripper or extensor could be rectified by merely swapping it with an equivalent spare part, and a single robotic system with numerous gripper and extensor modules could effectively investigate the effects of increasing the number of segments on the endoscopic locomotion.

So, this robotic mechanism is comprised of component modules that can be assembled and disassembled without tools. This modular design requirement introduced additional mechanical complexity and physical growth in the dimensions of the fifth generation components (in conflict with the goal of minimizing the size of the system). Threaded fastening provided a reversible, mechanical means of attachment between modules, at the expense of size and ease of the individual component fabrication. Connections are made by squeezing two modules together and locking them together with a surrounding captive

nut containing a 11/16-40 thread. These nuts are carried on each end of the fifth generation extensor modules but represent a negligible increase in their diameter. At the full depth of the threads, the wall thickness of these custom stainless steel components is 0.005 inches (they are easily deformed with finger forces). The small forces applied to these robotic components permit this modular assembly to be accomplished with bare hands.

3.6.5 The Electronic and Pneumatic Bus Designs

The electronic and pneumatic buses must be continuous throughout the fifth generation robots, and design modularity dictates that the electrical and fluidic connections be easily accomplished without additional tools. These goals were accomplished as follows.

To prevent leakage of the pneumatic bus between modules, o-ring face seals are compressed at each interface for the high and low pressure pneumatic supplies. These o-rings nominally have a 1/16 inch inner diameter and a cross-sectional diameter of 0.016 inch (available from Apple Rubber Products, Inc., Lancaster, New York). A 3/32 inch diameter spot face, 0.011 inch deep, is milled to locate the o-rings around each pneumatic channel on the ends of the fifth generation gripper modules. Thus, when the adjacent extensor module is pressed into place, the o-rings are compressed by 0.005 inch to provide the necessary sealing.

Likewise, electronic continuity between gripper and extensor modules is automatically established during the modular assembly. Gold plated, electronic sockets are press fit into the ends of each extensor module. They are located to engage brass pins that emanate from adjacent gripper modules dur-

ing assembly. The resulting electronic bus in the fifth generation prototypes provides for 27 connections across each gripper-extensor interface of the robot. This tight packaging of the electronic bus permits a Generation Five robot to be assembled with seven grippers and six extensors maximally. Although such a robot likely contains more modules than is necessary for most of the anticipated experiments, the large electronics bus was designed for the following two reasons.

In the fourth generation robots, the trailing cable assembly of wires and hoses contained one wire directly soldered to each of the internal solenoid valves. In those devices, there was no superfluous wiring. But, for any fifth generation robot that is assembled with fewer than seven grippers and six extensors, the electrical bus will automatically contain extraneous leads. Consequently, any unused lead of this bus can be employed to support additional electronic subsystems, for example, on-board pressure or tactile sensors.

Generation Four incorporated a fiberoptic videocamera system for visualization from within its environment. This was possible because its electrical wiring and pneumatic plumbing were routed externally around the small diameter extensor segments. In the fourth generation design, the fiberoptic bundles for illumination and imaging ran within the grippers but alongside the extensors. This approach was not viable with the modular construction of the fifth generation design. Alternatively, Generation Five was designed to permit the installation of a distal videocamera system on the end of the robot itself. Currently, two available videocamera technologies have been considered for this assembly; specifically, 1/4 inch CCD videochips and advanced technology, CMOS imaging chips (as small as 1/6 inch), are applicable. A conventional, black and white, CCD chip camera installed in a robotic "nose

module" can transmit intraluminal video images to a monitor via a bus containing at least 3 but at most 13 leads depending on the design and location of the camera's control and signal processing electronics. This number of electrical leads is inclusive for the entire imaging system, e.g., it includes one lead to power for a pair of halogen light bulbs at the distal end for illumination.

If the videoimaging system requires 13 leads of the electronic bus (the worst case), 14 leads of the electronic bus would remain for locomotion control and additional sensors. In other words, in addition to providing a video image from within the lumen, this bus could control a 3-gripper/2-extensor, modular robot **and** operate three additional valves for saline irrigation, carbon dioxide insufflation, and suction of the intestine (insufflation describes the surgical use of gas to distend body cavities and lumens for internal visualization and access). Also, for crawling within the small intestine, the irrigation and insufflation systems could be designed to simultaneously clean debris off of the videocamera lens (it is inevitable that the camera lens will become soiled in this environment).

3.6.6 Design for Ease of Fabrication

Consideration of the manufacturability of these complex systems was critical to successful development of a functioning Generation Five prototype robot. The design of the entire robotic system was dictated by three criteria: minimization of the total and component parts counts, verification that the individual subcomponent parts could be fabricated using available means, and assessment of the final assembly processes of the gripper and extensor modules. Although the "parts count" is an objective measure, the later two issues were evaluated

by engineering/manufacturing judgment and experience.

Such considerations led to gripper modules that were each comprised of a **single**, machined structure, 27 brass rods, 2 solenoid valves, 1 plenum cap, and 1 surrounding sheet of latex rubber. All internal plenums and plumbing channels were machined in place, thereby simplifying the installation of the internal, solenoid valves. Within these gripper modules, the electronic bus was created by embedding 27 brass rods (0.020 inch diameter) into the gripper body which was machined from a dimensionally stable, nonporous, adherable, dielectric material. Ultimately, a machinable, glass-mica ceramic was chosen as this structural material after evaluation of numerous plastic, composite and ceramic candidate substances.

The fifth generation extensor module design was considerably more complex than the associated gripper module design. At each end of an extensor module was 1 stainless steel captive nut, 27 electronic sockets mounted in an acrylic cap structure, and a 6061 alloy aluminum substructure that contained 1 solenoid valve and the subcomponents for the electronic and pneumatic buses. Between the ends of each extensor module was a custom, latex rubber bellows (procured from Latex Products, Hawthorne, New Jersey) surrounding a stainless steel spring that encompassed 27 wires and 2 rubber hoses.

Some details of the fifth generation extensor design are provided below. On each of the extensors, the miniature electronic sockets were press fit into the acrylic end caps and then soldered to 32 AWG stranded wires (the wire's outer diameter is 0.021 inch). These wires were then threaded through the aluminum substructure into the interior of the spring within the outer bellows. These aluminum substructures were adhered to the acrylic caps; the concentricity of the aluminum subtructures with the acrylic end caps was ensured by stainless

steel tubes that fit inside reamed internal, pneumatic passages. These stainless steel tubes serve three additional functions: they sealed the pneumatic bus between the aluminum substructure and the acrylic end caps, they prevented the possible obstruction of the pneumatic bus by adhesives during the assembly process, and they extended a short distance into the inner chamber of the bellows to provide connections for the pneumatic bus through the center of the extensor. Here, they acted as "hose barbs" for two thin, silicone rubber hoses that carried the pneumatic power supplies from one end of the extensor to the other.

In a similar fashion to the gripper design, the pneumatic ports between the high and low pressure supplies and the extensors' control valves were machined into the aluminum substructures. In both designs, the connections between the solenoid valves and their pneumatic sources were created as soon as the valves were adhered in place. Between these aluminum parts of the extensor and within the inner spring, the 27 wires were coiled helically around the rubber tubes to permit extensibility of the module (this rubber tubing was selected because it can undergo tremendous stretching with very little tension; it was also tested for its ability to carry a vacuum – and although it collapsed partially, it did not fully occlude the air flow).

3.7 Overview of the Prototype Evolution

Section 3.1 through Section 3.6 describe the conceptual design of this type robotic endoscope, the methods of locomotion for this concept, and the development of the most advanced versions of the experimental prototype devices. As noted, the process of the prototype development evolved over five distinct

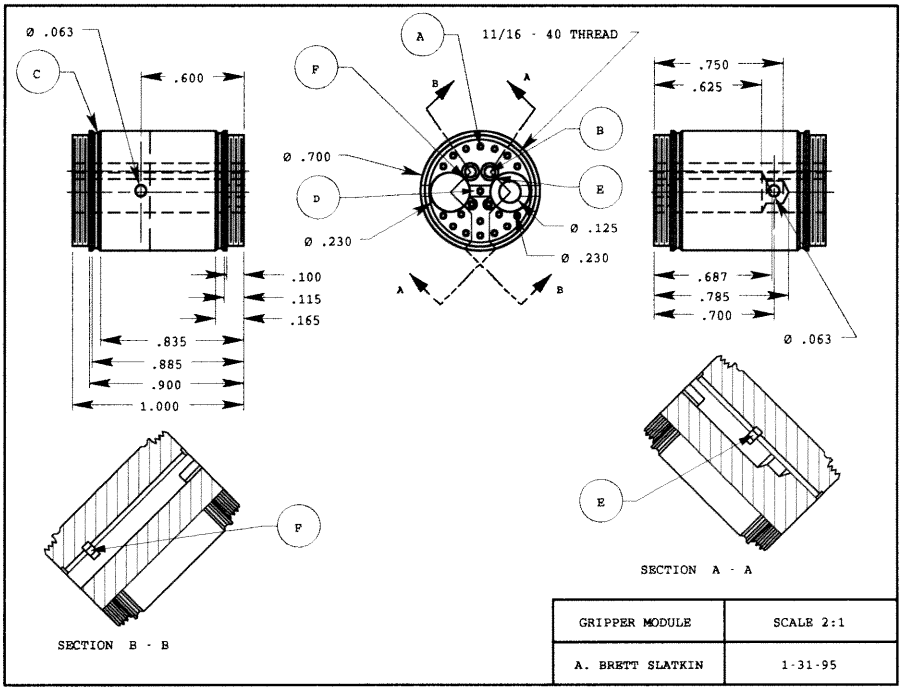

Figure 3.24: The machinable (glass-mica) ceramic substructure for the Generation Five gripper module. This single part serves in place of a complex assembly in Generation Four.

generations. For a historical perspective, a brief discussion of the highlights of the earlier stages in the development is provided below. Since the fifth generation system was discussed at length in the previous section, this section will cover only the first four generations of prototypes.

3.7.1 Generation One

The first prototype, the 2-gripper/1-extensor design shown in Figure 3.13, was created by modifying a 1/2 inch bore, single acting, spring return, air cylinder that had been manufactured by Clippard Minimatic (surplus procurement, no part number was available). From this actuator, all extraneous material was removed to reduce its size. Although these machines are intended to traverse curved lumens, this machine was designed from the start with no lateral bending compliance to curved environments. It was hoped that for sufficiently large diameter lumens (relative to the contracted diameter of the grippers) and for a reasonably short rigid length of the prototype, locomotion could be effected within moderately curved, rigid tubes. The overall length of this device was 3.5 inches (approximately 90 millimeters) with an extensibility of 0.675 inches (approximately 17 millimeters). Its contracted diameter was 0.875 inches (approximately 22 millimeters).

Cylindrical, latex rubber sheets were fixed to aluminum gripper "segments" located on each end of the rigid air cylinder (one was adhered to the rear of the structure, the other was threaded onto the push/pull rod). Since all internal volume was occupied by structure, the three flow control valves were located externally from the robotic mechanism. In this design, the air cylinder and the two balloon grippers were each controlled by their respective pneumatic

hose connected to a three-way, solenoid valve (a spool valve). When "off," these valves ported their corresponding actuator to the ambient air pressure. When the valves are turned "on," compressed air would flow through the hoses into the actuators. This machine crawled reliably without requiring a vacuum source as the air cylinder's internal spring was sufficiently strong to contract the robot while crawling.

In order to demonstrate semiautonomous locomotion of this machine, digital control electronics were produced. This circuitry consisted of: a timing/clocking circuit, a set of output amplifiers to drive the necessary solenoid currents, and a digital, finite state machine that, given each current state (phase) of the machine, simultaneously calculated both the preceding and subsequent phase in the locomotion gait that would result from one step backward or forward, respectively. Thus, with a toggle switch, the human user could command the robot to change directions at any time. This circuitry also permitted the investigator to arbitrarily change the speed of the locomotion via a potentiometer; however, since the gait itself was encoded in hardwired circuitry, the kinematic sequence of crawling actions was fixed (for that 2-gripper/1-extensor design, this was not a liability).

Given its obvious limitations, this robot successfully achieved its intended goals: (a) validate the basic gripper and extensor mechanism in its concept by demonstrating reliable locomotion within slightly curved, urethane tubing, (b) investigate viable materials, designs and fabrication methods for the mechanical componentry, and (c) test the electronic circuitry and solenoid valve system that would, in modified form, control prototype generations two and three. Unfortunately, this machine could not effect locomotion through a lumen that exhibited any significant curvature.

3.7.2 Generation Two

Two significant limitations were addressed in the second evolutionary step in these design efforts. Firstly, the size of the first generation machine was unacceptable for any envisioned animal studies. Thus, the second generation design would have to be significantly smaller than the first. Additionally, the first prototype was only capable of crawling though curved tubes with inner diameters substantially greater than its contracted diameter. To improve on the previous work, this design was: (a) built approximately 20 percent smaller in diameter, (b) assembled with 3 grippers and 2 extensors (utilizing two miniature pneumatic cylinders), and (c) fabricated with elastomeric universal joint connections between the components for lateral bending compliance. To further improve the ability of the second generation prototype to negotiate curved lumens, the body length of its rigid air cylinders, at 1 5/16 inch (about 33 millimeters), were much shorter than the 3 inch (about 76 millimeters) long body of the air cylinder of the first generation. These pneumatic cylinders were manufactured by Clippard Minimatic (part number SM-6). The principal advantage of these subcomponents were their overall dimensions: 1/4 inch bore with a 3/8 inch stroke (less than 10 millimeters) with a contracted length of 1 13/16 inches (46 millimeters). In addition to these modifications, the design of the gripper balloons changed substantially. In this design, self contained, sealed, toroidal balloons were adhered to the perifery of the assemblies containing the pneumatic cylinders. These balloons were fabricated from cylindrical sheets of latex rubber that had been folded back into a torus, sealed with adhesive, and ported with short lengths of vinyl tubing. This design simplified the design of the gripper segments as the sur-

rounding balloons were no longer required to seal against the inner structure. This prototype is shown in Figures 3.13 and 3.14.

The wall thickness of the rubber sheeting used in the grippers was dictated by its availability, not by careful analysis of the anticipated pneumatic loading. As a result, reliable locomotion performance required that two different compressed air pressures be supplied to the robot, one for the grippers and another for the extensors. The small pneumatic cylinders would only supply sufficient axial forces for locomotion at pressures that caused the gripper balloons to burst. In addition, these small pneumatic cylinders' internal, return springs provided insufficient force to pull this robot along. Thus, these extensors would stretch only when their pneumatic cylinders were driven by pressures significantly higher than the safe limits of the grippers and contract only when their internal pressure fell well below atmospheric, i.e., vacuum. Although careful mechanical design allowed the fourth and fifth generations to utilize a single high pressure source, the use of vacuum to contract the actuators has persisted through to the latest generation.

Due to its lateral bending compliance, this type of robot demonstrated reliable locomotion within moderately curved, urethane tubing. Furthermore, the inner diameter of this tubing was less than one inch in diameter when straight and it collapsed significantly when bent. Thus, this design was capable of crawling through rigid, curved lumens with an effective inner diameter approaching that of the small intestine. The fundamental problem with this design was the difficulty of routing the pneumatic hoses around and though the assembly without creating interference with the extensor actions. It appeared as though a practical upper limit for the number of segments used in the assembly of a prototype robot that lacks on-board valving is three grip-

pers and two extensors. Conceivably, the use of extremely small diameter vinyl tubing would permit a builder to exceed this limit; however, from the earliest conceptual designs, internal valves had been envisioned. (Sufficiently miniaturized valve technology was not available when this research commenced, but advancements in this technology has always been anticipated.) A secondary problem with this design was that the fabrication of acceptable toroidal balloons was quite difficult.

3.7.3 Generation Three

This generation of the prototype represents the end of the evolutionary branch for certain aspects of the early development. This robot followed the first and second generation designs as it employed rigid air cylinders for extensor actuation, off-board valves, and a newly developed methodology for the fabrication of the toroidal balloons. In contrast to the prior prototypes, this design used double acting air cylinders instead of single acting ones with spring return. This design change resulted from three important considerations. Firstly, double acting air cylinders typically exhibit a longer pushrod displacement for given cylinder length than do single acting variants. Secondly, unlike single acting air cylinders, they are typically assembled into a "closed system," i.e., no air is pumped around the outside of such actuators; this would be beneficial if the outside of the air cylinder is inside the small intestine of a pig. And, lastly, these actuators can be driven in both directions without resorting to drawing a vacuum on the piston face; this would obviate the requirement of a vacuum pump in the experimental apparatus and improve its portability between the laboratories at Caltech and Cedars-Sinai Hospital.

The second generation version highlighted potential advantages of fabricating the gripper balloons as complete and separate subcomponents. In the development of Generation Three, the predominant share of the work was focused on the molding of liquid latex into gripper balloons. In addition to the machining of several molds, two motor driven drying stands were built to rotate these axisymmetric molds in order to minimize balloon asymmetries due to effects of gravity on the solidifying rubber. Successful toroidal balloons eventually resulted from these efforts, but, ironically, the biggest impact of these manufacturing efforts came from their failures. While working on balloon designs for gripper segments, several attempts were also made to produce rubber latex bellows for an improved extensor segment design. Versions with and without internal fiber reinforcement were attempted, but none performed sufficiently well to replace the rigid, pneumatic cylinders. It was clear, however, that in some future incarnation of the device, such bellows would likely produce the most viable extensor structures.

A breakthrough came shortly thereafter when The Lee Company, Westbrook, CT, announced its commercial introduction of High Density Interface (LHDA) solenoid valves. Thus, before the intermediate, and admittedly inferior, third generation prototype was completed, all the necessary components became available for Generation Four. One Generation Three robot was built, but its performance was not notable. And, by then, the stage was already set for a new prototype that would incorporate many new and desirable features.

3.7.4 Generation Four

As elucidated above, the fourth generation of the prototyping sequence represents a new beginning in the design process. It returns to the first generation by virtue of the gripper segment design. In this version, the gripper balloons are again created by adhering thin, cylindrical sheets of latex rubber to aluminum substructures. But, except for the general concepts, the similarities end there. In these robots: all valves are located within the robotic mechanism; separate extensor segments provide dramatic, lateral bending compliance by their spring reinforced, bellows design; the control system is commanded by a computer allowing "on the fly" changes in the locomotion parameters and gait selection; and the capacity to carry a fiberoptic videosystem with an additional on-board valve for insufflation and aerodynamic lens cleaning. This machine locomoted extensively within urethane lumens demonstrating all of its specific design objectives: crawling through curved lumens, mechanical redundancy, videoimagery from within the lumen, etc.

This version's bellows extensor segments are roughly 1.2 inches (about 31.5 millimeters) when contracted and approximately 2.2 inches when extended (about 56 millimeters). Thus, in addition to the vastly improved lateral compliance (when compared to the rigid, air cylinder designs), these components produced dramatically increased relative extensibility (they stretch roughly 83 percent from their contracted length, versus less than 21 percent for Generation Two extensors, for example). Fourth generation prototypes are shown in Figures 3.15, 3.16 and 3.19.

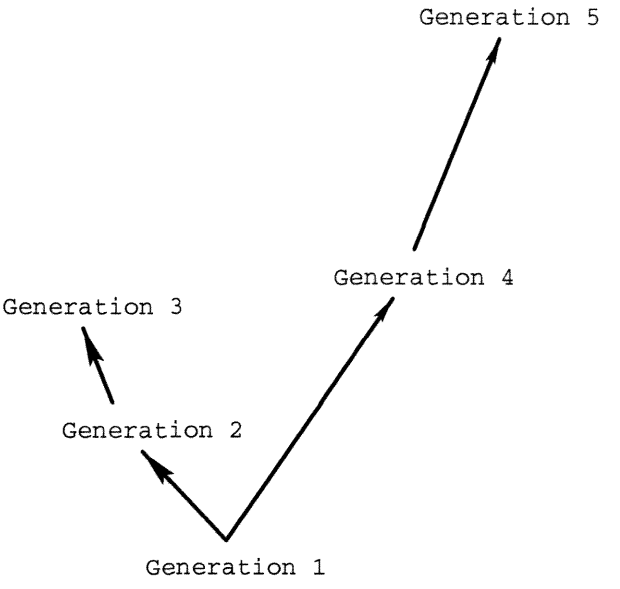

Figure 3.25: Robotic endoscope taxonomy.

3.7.5 Robotic Prototype Taxonomy and Relative Performance

From the first generation prototype, the evolutionary development of subsequent versions branched into two distinct groups of designs. Generations One, Two and Three share their hardwired electronics and solenoid valves (which are connected to their corresponding actuators via trailing hoses). In addition, these initial steps in the design evolution carried a common conceptual feature: that their extensor actuation was accomplished by rigid, pneumatic cylinders and that any bending compliance resulted from the universal joints that connect the mechanism. Furthermore, the second and third generation developments were characterized and shaped by investigations into sophisticated toroidal, gripper balloon fabrication.

The fourth and fifth generation designs represent a break from the evo-

lutionary progress of the first three generations. These devices have at least as much in common with the first prototype generation (the gripper segment designs) as they do with the second or third versions. The conceptual design of the gripper segments of Generations One, Four and Five are fundamentally similar. And, owing to disparate extensor designs, the fourth and fifth generations can be considered to be have undergone a separate development process than the second and third versions. Thus, Figure 3.25 demonstrates such a taxonomic relationship. The relevant features of each design are tabulated in Figure 3.26.

To further describe this evolution, an analysis of the relative speeds of locomotion of these robots was performed. Their locomotion speed is dictated by three parameters: the number of phases within the chosen locomotion gait, the rate at which the actuation commands are given, and the stride length of the gait. Thus, calculation of the crawling speed of these robots is straightforward. Since prototypes have been built with various numbers of gripper and extensor segments, comparisons between speeds of these machines must be based on selection of comparable gaits for all representatives. Every such robot can effect a type of 2 gripper/1 extensor gait, one in which the endmost grippers are actuated and all the extensors function in parallel. When so commanded, each robot will crawl at its fastest speed for a given rate of actuation commands. However, the larger the number of segments with which a prototype has been assembled, the faster it will locomote. In fact, the speed is directly proportional to the number of actuated extensors; given the same gripper and extensor components, a 3 gripper/2 extensor robot will crawl twice as fast one built with two grippers and one extensor.

Perhaps, a more meaningful measure of the relative performance of these

machines is to compare the calculated speeds of two gripper embodiments from each generation crawling at actuation rates that have been demonstrated by the experimental robots. The results of these calculations are included in Figure 3.26, when possible. Since an insufficient evaluation was performed on the third generation (and prototypes were built using air cylinders with three different stroke lengths), no speed measure was tabulated for it. In contrast, a theoretical speed measure has been provided for Generation Five since all extensors will exhibit, within tolerances, equal extensibility and knowing that these machines can operate at comparable command rates to those demonstrated by Generation Four, a "maximum speed" was calculated. This is the value that has been included in Figure 3.26.

It should be noted that these speeds provided do not represent the ultimate performance of these machines in urethane tubes. Since large investments of time and energy were required to build these devices, it would have been unwise to damage them permanently in an attempt to determine their maximum locomotion performance in urethane tubing. In order to increase their speed, one can merely increase the source pressures to the actuators (to ensure that they are inflated and deflated rapidly) which will permit a higher rate of actuation commands. This approach increases the potential for breakage in trade for a faster robotic response, a dubious exchange. Careful observation of the inflation of a robot's components allowed incremental increases in working pressures, but these changes were made slowly (nevertheless, given such care, a number of rubber components did fail after repeated applications of apparently *safe* loadings).

One last thought, the "top speed" of these robots in the laboratory environment, i.e., in rigid tubing, may not be a viable performance criterion.

Generation	Air Cylinders	Bellows Extensors	Toroidal Latex Gripper Balloons	Single Layer Gripper Balloons	"Max" Speed in/s (mm/s)
1	X			X	1.35 (34)
2	X		X		.75 (19)
3	X		X		N/A
4		X		X	1.5 (38)
5		X		X	1.65* (42*)

* Estimated

Figure 3.26: Table of the features of the five generations of prototype robots.

As discussed earlier in this chapter, experiments in the small intestine of pigs created a paradigmatic shift in the approach to endoscopic locomotion. In these experiments, the dissimilarity between the intestines and rigid tubing was glaringly apparent. One must consider the reactions of the intestines when establishing the rates of commanded actuation of a endoscopic robot, and the resulting speed of locomotion would likely be substantially slower than the robot's maximum in a rigid environment. Thus, the value of an analysis of the speeds of locomotion of these devices should be somewhat discounted.

Chapter 4

Tissue Modeling and Experiments

4.1 Mathematical Elasticity Primer

This section is intended to provide a basic understanding of the concepts of solid mechanics. It will only address those principles of elasticity that arise in this investigation of the mechanical properties of small intestines. Thus, it is not a foundation for the general principles of elasticity theory, but the fundamental concepts which are required to understand the analysis herein will be provided. These subsections will also introduce problematic issues of soft tissue biomechanics that are further discussed in Sections 4.2 and 4.3. Problems in solid mechanics tend to fall into two basic categories: (a) given a particular loading on a solid body, find the resulting deformations, and (b) determine the loads which cause a particular body to deform in a given manner. In these two cases, the goal is to investigate the relationship between the forces on and deformations of a given body.

The following subsections introduce the fundamental concepts of solid mechanics: *stress*, *strain*, *constitutive laws*, etc. The *state of stress* is a measure

of the "intensity" of the forces being carried through each point within the body. In general, the *stress state* will vary between points within the body. Because of this, the resulting deformation is also expected to vary between points within the body. Also, any prediction of material deformations or displacement of points fixed to the body must take both the geometry of the body and the applied loadings into consideration. Simply put, experiments could be performed for every object of interest in order to determine: its force-deformation behavior, the forces that cause it to break, etc. But one would rather have tools to predict such behavior from knowledge of the composition of the body and its geometry. Conversely, if one could remove the effects of the geometry from the experimental behavior of a particular body, an understanding of the fundamental material properties of the body's composition would result. This is accomplished in two ways, firstly the effects of the geometry on the force/moment loading on the body are automatically removed when one considers the stress state within the body (instead of the actual applied forces/moments). In addition, the deformations are likewise dependent on the initial geometry of the body. As a simplistic example, imagine a given tension applied to two different pieces of cable. One cable segment is twice as long as the other, but they are both comprised of the same material. In this thought experiment, the longer cable would be expected to stretch by twice the amount of the shorter one. It would be beneficial to be able to "normalize" this behavior in order to predict the stretching of any length cable segment. This is the objective of the next subsection in which the displacement-strain relationships (kinematics) are introduced. The following subsection addresses the force-stress relationships (kinetics). Lastly, the material properties, or the constitutive relationships that describe the stress-strain behavior (independent

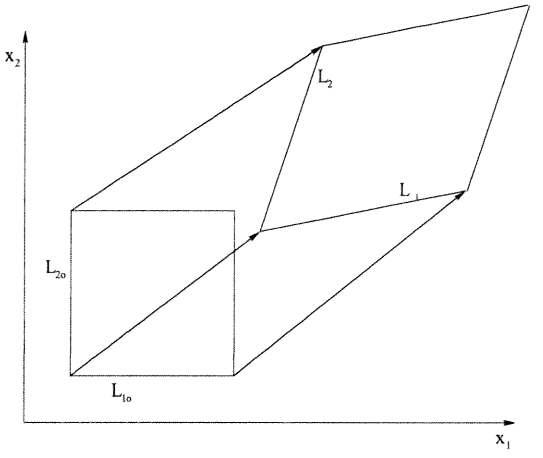

Figure 4.1: General deformation of an element of solid body.

of the body geometry), are introduced in the third elasticity primer subsection.

4.1.1 Material Kinematics

In mechanics, *kinematics* is the mathematical analysis of *motions* of a body without regard to loading applied to it. Similar analytical approaches are taken to study the kinematics of rigid bodies, compliant bodies and even fluids; however, this section will address kinematics of deformable, solid bodies. Such analysis results in *displacement-strain* relationships for a solid body.

Although numerous concepts of kinematics are required for the general study of deformations of solid bodies (for example, rigorous mathematical definitions of configurations of bodies of interest, the deformation gradient tensor, etc.), most will be ignored in this very brief introduction to elasticity. The purpose of this section is to present only those concepts of kinematics that are relevant to this modeling of small intestines. The notion of *strain* is as a normalized measure of the stretching of a body. Conceptually, material kine-

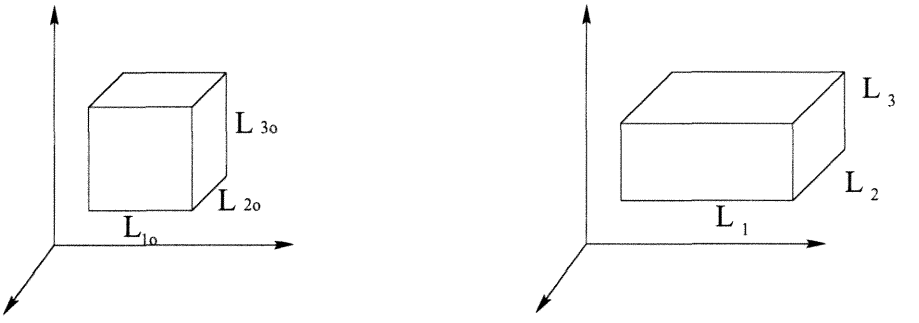

Figure 4.2: Deformation as viewed in principal axes.

matics are illustrated in Figure 4.1, the displacement and deformation of an element of a solid body. The changes in the relative lengths and angles between the edges of this element of the deformed body represent the strains of this element. As one can see, the measure of the strains will be a function of the choice of reference frame applied to the problem, and there is a transformation law to switch between reference frames (this formula is not invoked in this research). Material kinematics can be further refined into *normal* and *shearing* effects. In this context, shearing strains are those which alter the angles between lines fixed on the body. Normal strains are measures of the changes in length of body fixed line segments. When an orthogonal reference frame is applied to the problem such that the shearing strains vanish, the problem is viewed along its *principal axes* (this typically requires the solution of an eigenvalue problem for the deformation gradient tensor). An example of this is seen in Figure 4.2. From this figure, the *principal stretch ratios*, or merely the *principal stretches*, are computed by dividing the length of each

edge of the deformed element by its undeformed length, i.e.,

$$\lambda_1 = L_1/L_{1_0} \ , \quad \lambda_2 = L_2/L_{2_0} \ , \quad \lambda_3 = L_3/L_{3_0} \ . \tag{4.1}$$

(These are the eigenvalues of the deformation gradient tensor.) There are a number of alternative strain measures that can be calculated from these principal stretches [18]. Green and St. Venant calculated principal strains as

$$E_1 = \frac{1}{2}(\lambda_1^2 - 1) \ , \quad E_2 = \frac{1}{2}(\lambda_2^2 - 1) \ , \quad E_3 = \frac{1}{2}(\lambda_3^2 - 1) \ . \tag{4.2}$$

In contrast, Almansi and Hamel preferred to compute principal strains as

$$e_1 = \frac{1}{2}(1 - \frac{1}{\lambda_1^2}) \ , \quad e_2 = \frac{1}{2}(1 - \frac{1}{\lambda_2^2}) \ , \quad e_3 = \frac{1}{2}(1 - \frac{1}{\lambda_3^2}) \ . \tag{4.3}$$

Additionally, some authors prefer to measure "true strain" as $log\lambda$, and the commonly utilized *infinitesimal strains* are calculated as $\varepsilon_i = \frac{L_i - L_{i_0}}{L_{i_0}} = \lambda_i - 1$. So,

$$\varepsilon_1 = \lambda_1 - 1 \ , \quad \varepsilon_2 = \lambda_2 - 1 \ , \quad \varepsilon_3 = \lambda_3 - 1 \ . \tag{4.4}$$

In a general context, the *state of strain* is tensor valued, and important justifications for these different strain definitions exist. But with the simplifying assumptions of this thesis work, all of the analysis is performed using the principal stretches directly, i.e., λ_i, and the only definition of principal strain used henceforth will be $\varepsilon_i = \lambda_i - 1$. This choice of the simplest definition of strain comes from Y.C. Fung [18], "use of any one of these strain measures is sufficient. . . . They are different numerically. . . ." So although finite de-

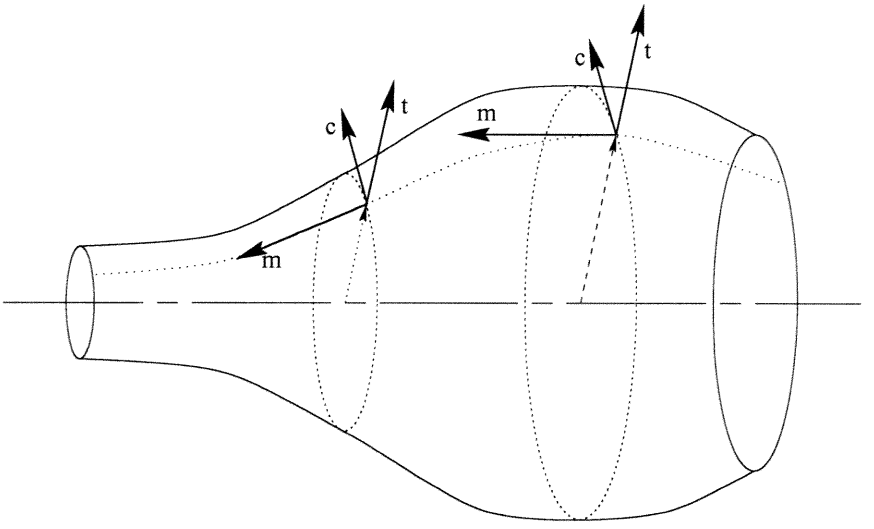

Figure 4.3: Reference frames for analysis of axisymmetric, thin walled bodies.

formation theories of general elasticity typically use Almansi or Green strain tensors (or yet more sophisticated ones, as is common in the geophysics realm), simplicity is to be pursued in these initial attempts at intestinal modeling.

Since the *body* of interest is modeled as a thin walled, axisymmetric membrane under the actions of axisymmetric internal loading (no torsion is admitted), the only admissible deformations are likewise axisymmetric. Symmetry arguments suggest that within the reference frames identified in Figure 4.3 only *normal strains*, i.e., no *shear strains*, are produced. Thus, the natural axes of this analysis are principal axes.

4.1.2 Kinetics

In the context of mechanics, kinetics represents the relationships between forces applied to and stresses within a given medium. These derivations are applications of balance laws of mass, momentum, and angular momentum

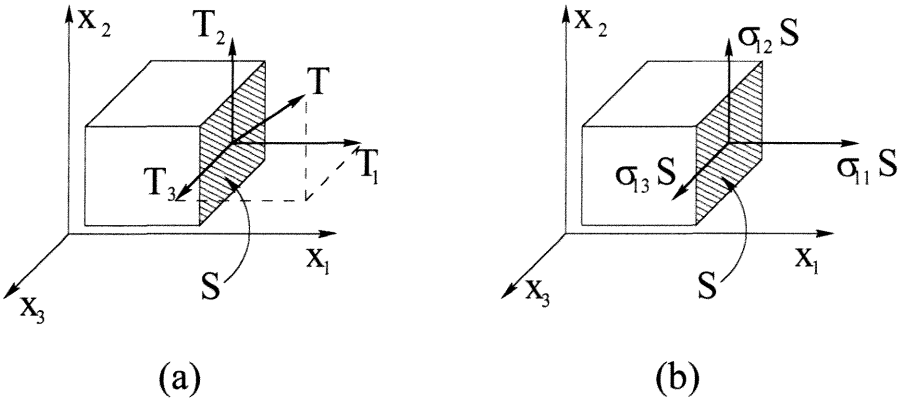

Figure 4.4: Derivation of stresses acting on an element.

to small elements of material within the body of interest. Fundamentally, a small element of the solid body is viewed as a free body upon which external, surface forces, i.e., *tractions*, and internal, body forces, e.g., gravity, act. Forces applied to each side of the element can be resolved into orthogonal components that act parallel to and perpendicular to that surface. Considering Figure 4.4 (a), the force components, T_i, which act on the side facing the positive x_1 direction are illustrated. Dividing this force by the area of the surface on which it acts, S_1, one calculates the *contact force density* or *traction* on that surface. The orthogonal components of this force density are the *normal stress* and *shear stresses* acting across this surface: the normal stress is $\sigma_{11} = T_1/S$, and the shear stresses are $\sigma_{12} = T_2/S$ and $\sigma_{13} = T_3/S$. Thus, in Figure 4.4 (b), the arrows represent the force components applied to the x_1 side. Likewise, the stresses can be determined for the remaining five sides of the parallelepiped. In an analogous manner as the kinematics, the state of stress is a tensor field. Thus, the measures of these components of stress are dependent on the choice of coordinate frames. When a frame is chosen

such that the shear stresses vanish leaving only normal stresses, these stresses are the *principal stresses.* Fortunately, the principal axes for stresses are the same as those for strains. And again, symmetries in this axisymmetric, thin intestinal membrane problem eliminate any shear stresses along the natural axes of the body. And so the natural axes of the biomechanics problem studied in this thesis are convenient ones; no coordinate change of variables formulae are required.

In engineering practice, a common structural mechanics problem is to predict the behavior of given solid bodies when subjected to anticipated loadings. The primary objective of such work is to guarantee that the analyzed structure will not *fail* while in service. Often, several different failure criteria must be applied; these include, but are not limited to, material yielding (inelastic/permanent deformations of the structure), ultimate strength (breakage of the structure), and fatigue (propagation of cracks due to cyclical loading). Each of these phenomena are predicted directly by studying the states of stress within the material.

A brief thought experiment will clarify the difficulties associated with this problem. Imagine a rod of a solid, homogeneous material. Now apply some tension to it, i.e., pull it at both ends with some force. If the rod were perfectly rigid, then the actual state of stress near its middle could be calculated by dividing the applied tension by the rod's unstressed cross-sectional area. But, with the possible exception of highly pathological material behavior, under tensile loading, axial stretching causes an attendant lateral contraction in such a rod. Thus, the actual mean stress in the middle of the rod can only be calculated by dividing the applied tension by the measured cross-sectional area of the loaded specimen.

To measure this lateral contraction as well as the longitudinal loading and stretching provides an additional complication to the experimental material scientist (the experimental apparatus is required to measure both axial and lateral deformations). But the real difficulty is the one facing a solid mechanician who intends to predict the deformation of a given body under loading (using analytical methods). The constitutive law provides the stress-strain behavior for the body's material. But, as described in this thought experiment, the stress due to a constant tensile loading will depend on the deformation of the body under that load. Therefore, in order to predict the deformation due to the stress in the body, the elastician will need to know the deformation *a priori* in order to calculate the stresses which are causing the deformation. This is a cyclical problem! One could use an iterative method to numerically approach this problem, or in particular cases, the analysis could be reduced to a convergent, infinite series which would yield a "closed form" solution.

Fortunately, most engineering problems are solved without any concerns for these issues. This is due to the fact that engineering materials undergo very small deformations even at the critically high levels of stress that cause failure. And since these deformations are small, it is reasonable to measure the stress state from the applied forces acting on the *unloaded geometry* of the body. These stresses are alternatively referred to as the *engineering stresses*, the *nominal stresses* or the *1st Piola-Kirchhoff stresses*. The *true stresses*, also known as the *Cauchy stresses*, are computed as expected by normalizing the internal forces by the actual, *deformed geometry* of the body. It should be obvious that when the deformations are known, the nominal stresses can be calculated from the true stresses and vice versa. Thus, as long as the choice of stress description is identified, either approach is valid. In terms of advan-

tages, the nominal stresses are convenient for the reasons stated above, and the Cauchy stresses are used to develop the analytical balance laws, e.g., the balance laws of momentum (Newton's Second Law). And although the nominal stresses are more commonly used in most problems of solid mechanics, all analysis in this thesis will be developed from studying the mechanical equilibrium of small elements of the stressed/deformed intestinal membrane and so the Cauchy stresses are appropriate.

4.1.3 The Constitutive Relations

The term *constitutive relationship* refers to a mathematical statement that relates the stresses and strains (and even temperatures) of a particular material. Such behavior may or may not depend on the elapsing of time or the loading history of the body. Such material models can also be conservative or dissipative of the energy of stretching.

In the general, linearized theory of elasticity, the constitutive law requires 81 independent parameters for a complete description of the three-dimensional, small deformation behavior of a material. Generally, arguments are made to simplify this mathematical description; such arguments include assumptions of homogeneity, isotropy (material symmetry groups), conservation of angular momentum, etc. Ultimately, only two independent parameters are necessary to fully describe the constitutive relations for the classical, linear elasticity theory of simple, homogeneous, conservative, isotropic materials undergoing isothermal, *infinitesimal deformations*. Unfortunately, none of these simplifying assumptions apply to the modeling of the small intestine performed herein. Typically, accurate modeling of the mechanical behavior of soft bi-

ological tissues is a much more complex undertaking. These materials are often composed of substructures (collagen and elastin fibers, varying cellular functionality, etc.) which have differing elastic behavior; such materials are called *composites* in inanimate engineering applications. Composites are by definition *inhomogeneous*, and in general they are also *anisotropic*, meaning that they exhibit differing behavior when loaded in different directions. Additionally, these biological tissues are considered *soft* because they undergo large deformations when moderately stressed; hence, the classical assumption of infinitesimal deformations is typically inappropriate. And due to the impact of deformations on the kinetics as discussed in the previous subsection, such *finite deformations* dictate a *nonlinear* analysis even under the highly simplifying assumption of a *linear* constitutive relationship. Furthermore, in nonlinear elasticity theory, the constitutive relations must be determined for deformations from an unstressed reference configuration of the body. In contrast, a valid modeling of linearly elastic behavior of a solid body can be performed for any chosen reference configuration of that body.

The nonlinear behavior of biological, soft tissues is evident in the literature, as highlighted in the following sections. As mentioned above, this complication dictates that all deformations be measured from an unstressed reference configuration of the solid body. For soft materials, this alone can be extremely difficult. But unfortunately, the problem is exacerbated by the apparent *memory* of the biological materials. As it will be discussed in Section 4.2, previous researchers have often identified that the mechanical behavior of soft tissues changes over repeated cycles of loading and unloading. They argue that such *preconditioning* causes the constitutive behavior of these materials to converge [38]. They consider this experimental practice essential for increased repeata-

bility of their experiments. Thus, these materials have a *memory* for their loading history. This implies that the unstressed reference configuration is likewise dependent on the loading history. If *residual stresses* are present in the body of interest, then one must make a distinction between an *unloaded* reference configuration and an *unstressed* reference configuration.

4.2 Prior Work in Soft Tissue Biomechanics

A great deal of study of the mechanical properties of soft tissue is represented in the biomechanics literature. Much of this work concentrates on quantifying the healing rates of wounds. In 1929, an investigation by Howes, et al. [29], validated the use of tissue tensile strength, as opposed to wound surface area, to evaluate wound healing. In the intestines, both uniaxial tensile strength and bursting strength (when inflated) are used to measure the relative merits of different surgical techniques, instruments, and medications on healing [4, 36, 41, 46, 3, 39, 50, 51, 10, 27, 28]. In addition, there are several biomechanics researchers who strive to better understand the fundamental behavior of tissue elasticity. Most of this work focuses on other biological structures and tissues, but their analytical and experimental approaches highlight many challenges in tissue modeling. This work is notably represented by Yamada's text [60]; he studied the mechanical properties of biological materials for roughly twenty-five years (between 1938 and 1963, World Wars excepted). And in this text, he has compiled the results from thousands of biomechanics experiments performed by numerous researchers on every region of the human body. Data is provided describing tissue and organ biomechanics for specimens dissected from cadavers of humans that ranged in age from five month

fetuses to octogenarians. Included are the same properties as measured on an innumerable list of other animal species. These comprehensive investigations compare the biological structures, tissues and organs taken from an incredible variety of fauna (weasels, ostriches, humans, carp, cattle, kangaroos, to name a few). But, ironically, no data is given which describes the behavior of pigs' small intestines (the initial environment for the proof of concept, robotic endoscope prototypes). But in order to justify assumptions that must be made in the modeling of the small intestine, an overview of the study of general, large deformation behavior of nonlinear, time dependent, anisotropic, and inhomogeneous materials will be provided.

Firstly, as it has been noted, when attempting to model soft tissue, such materials often undergo very large deformations. In such nonlinear solid mechanics, all material deformations must be measured from an unstressed configuration state of the body. Often, as in this case of extremely compliant intestines, an unstressed configuration is unattainable; it is hoped that appropriate experimental data reduction can provide a reasonable estimate of the unstressed state. In general, nonlinear/finite deformation, solid mechanics analysis is very challenging. There is, however, a form of finite deformation elasticity that is more likely to yield a desirable result: it is known as *rubber elasticity.* In rubber elasticity, the body is assumed to undergo only *isochoric* or *locally volume preserving* deformations, i.e., it acts as an *incompressible* solid (where Poisson's ratio is 0.5). This behavior occurs when a material's "bulk modulus" or resistance to a change of volume under applied pressure is much greater than its normal or shearing stiffness ("Young's modulus" or "shear modulus"). This last sentence is not technically accurate as the intestines in question behave nonlinearly and thus cannot be described by simple

moduli, but nevertheless these concepts of solid mechanics can elucidate the notion of an incompressible material. Very often, investigators of soft tissue biomechanics assume that the materials under observation are incompressible, and this simplification is seldom questioned. Carew and collaborators [5] are an exception; they have shown that this simplifying assumption is quite valid for arterial tissues. In their study, Poisson's ratio for arteries was computed to be 0.4998. One could hope that, since this precedent exists for arteries, the small intestines behave isochorically as well; of course, this should be verified experimentally.

Due to the fact that many biological materials are comprised of connective fibers which are oriented in specific directions, their elastic response is dependent upon the direction that an incident loading is applied, i.e., they are *anisotropic.* Such anisotropy has been detected in a variety of biological structures, from human [22, 48] and rabbit [38] skin to arteries [2]. Specifically to the problem at hand, Fackler, et al. [13], investigated the influence of the microstructure of intestinal tissue (from rats and cattle) on its largely anisotropic behavior. They performed uniaxial tensile tests of specimens cut at various angles from the longitudinal direction and demonstrated that stiffness and ultimate strength are much greater in the axial/longitudinal direction than the circumferential one (although it was noted that the maximal circumferential elongation is greater than the maximal axial elongation). Additionally, they noted that the stiffest and strongest direction was oriented about thirty degrees from the "axis" of the intestine. But their stress-strain plots show the axial behavior to be only slightly less stiff and strong as that at thirty degrees. Nevertheless, they claim that the purpose for this "reduces the tendency of the intestine to buckle where it bends." These experiments and explanation will

be revisited in the next section of this chapter. They further contend that the nonlinear constitutive relationship between stress and strain of intestinal tissue results from the connective fibers stretching and eventually aligning more closely to the applied loading. Likewise, Lanir and Fung [38] argue that, for rabbit skin, tissue "stress-strain relations are nonlinear–the stiffness of the tissue increases with increasing strain." Moreover, they observe that rabbit skin stiffness is slightly dependent on the strain rate as well (this effect seems relatively small in their plots). In this study, a square sheet of skin was placed in a mechanism that provided a variety of quasistatic uniaxial and biaxial loading conditions. Under an assumption that rabbit skin is an *incompressible* material, they studied the stress response for different loading rates, uniaxial and biaxial stress relaxation effects as functions of time and temperature, the effects of preconditioning of the specimens (cyclical uniaxial and biaxial loading of tissue during which the stress response is shown to converge), etc. It must be noted that these investigators carefully studied the anisotropy, hysteresis in the constitutive law, and the time dependence on the material response as well as the uniqueness of the unstressed configuration. They ultimately concluded: that the material properties of rabbit skin are inherently nonlinear (and only slightly dependent on the strain rate), that the biaxial relaxation tests point to nonlinearity in the time dependence, and that the uniaxial relaxation tests were not true relaxation tests as there were considerable changes in the transverse dimensions during the process. But perhaps the most revealing conclusions were:

> Biaxial mechanical tests are an important tool for the investigation of tissues. It was found, however, that in the case of skin

> the results of mechanical tests must be interpreted cautiously, and that the tests must be performed carefully due to special properites of the tissue: Results are not repeatable under certain conditions and are always dispersed; a preconditioning process is necessary; the equilibrium configuration is hardly obtainable during the test procedure and can only be related to the fully relaxed configuration indirectly.

This demonstrates the truly difficult task of accurately characterizing soft biological materials.

The relaxation tests pursued by Lanir and Fung [38] represent one of two distinct time dependent material processes. This stress relaxation within a deformed specimen of biological tissue is analogous to behavior called "creep" in conventional engineering materials. In a biological context, several researchers, e.g., Shuter, et al. [54], Duffy and Shuter [11] Kenedi, et al. [34], have considered this creep effect. In 1967, Fung [21] proposed a "quasilinear" stress decay of the form $A+B\ln(t)$; Duffy and Shuter and their collaborators [11, 54] followed this approach in their research. Although, the aforementioned experiments by Lanir and Fung [38] demonstrate that this mathematical description does not accurately describe the creep of biaxially loaded rabbit skin. In addition to creep, there is another biomechanical process that has been shown to evolve over time. This is the "tissue regeneration or growth" phenomenon (discussed in Shuter, et al. [54]). When a living specimen of biological tissue is subjected to an applied loading, new cells are grown in this region. This is a very interesting effect, but it is irrelevant to our robotic endoscope project because typically it requires several weeks to manifest (this effect is critical

to the success of "tissue expanders" which plastic surgeons use to produce additional tissue for skin grafts).

The previously cited examples of soft tissue biomechanics were presented because they elucidate the complexity of soft tissue behavior in general. In the case of the small intestine, Yamada [60] reproduces the results from Iwasaki [32], Iwasaki and Okamoto [33], Takigawa [56], Ohara [45], Kubo [37], Oda [43], Kimura and Tokuda [35], Yoshida [62], and Yoshikawa, et al. [63]. Additionally, he presents the shear strength studies on dogs' small intestines performed by Ogawa and Narumiya [44]. With relevance to the robot's modeling, Yamada provides the following quantities: tensile breaking loads, ultimate tensile strength, tensile strain at failure, bursting strength, and its associated volumetric change for the ileum, jejunum and the duodenum of humans of various ages (and for a menagerie of animals as well, but ironically pigs were not studied). Unfortunately, the graphs illustrating the anisotropic stress-strain relationships of the three major regions of the human small bowel are not an adequate foundation for the modeling developed in this thesis primarily for the following reasons. Firstly, these investigators do not indicate whether the reported stresses are *true stresses* or *nominal stresses* (a distinction that will be clarified in Section 4.4). And even if one assumes that, as is predominantly the case, these constitutive laws relate the nominal stresses to the Lagrangian strains, the experiments were limited to studies of uniaxial tension in strips of excised intestinal tissue. Several researchers of biomechanics, Carew, et al. [5], Reihsner, et al. [48], Chuong and Fung [8, 9], and Omens and Fung [47] to name a few, have endeavored to study whole organs and structures under applied tractions that better reflect the naturally imposed loading conditions. Both approaches are valuable as they contribute complementary aspects to our un-

derstanding of the mechanical properties of soft, biological tissues. However, all cited studies of biomechanics of the small intestine have utilized dissected test specimens subjected to uniaxial tension or burst strength measurements (where all kinematic behavior is reduced to changes in the internal volume of a tubular specimen with or without constraints).

The endoscopic devices described here are intended to crawl through living intestines. This highlights a particular void in the biomechanics literature; after an extensive literature search, no investigation was identified which characterizes the mechanical behavior of the small intestine *in vivo*. This is not surprising as such experiments could be considered extravagant, requiring surgical facilities, anesthesia equipment with cardiac and pulmonary monitoring, etc. Unfortunately, these complications were necessary for gathering critical information about this organ in situ. For all of the data available for the elastic properties of excised small intestine, no investigator could provide a value of either applied traction or internal stress that can cause injury to the living tissues. Their standard for "failure" of the membrane was the same as the one for an inanimate material: it ripped, tore or ruptured. This is not an acceptable measure of excessive loading or stress for living tissues. It is our contention that serious injury occurs long before this obviously critical event, and, ultimately, this was confirmed by our experiments.

4.3 Issues in Tissue Modeling

It is anticipated that this modeling and analysis will aid the design process of devices which are to be inserted in the human small intestine. So, specifically, the material and geometric properties of living, human, small intestines

are sought. Unfortunately, it is not possible to conduct the necessary experiments on living human tissue, and, as mentioned in the previous section, dissected tissues cannot provide all requisite data. In cases such as this, medical researchers and surgeons in training often use pigs as biological models for human organs and tissues. Surgeons at Cedars-Sinai Hospital describe the organs from adult pigs as being smaller and more delicate than those of human adults. Thus, they believe that adult pigs represent good biological models for juvenile humans [24]. In the case of robotic endoscopy, that would imply that pigs' intestines provide a conservative approximation; being smaller and less rigid, these intestines should be more difficult to navigate than those of adult humans. In addition, one can study pigs' intestines *in vitro* as well as *in vivo*. So it may be possible to make comparisons between deceased and vital pigs' intestines that extend to the case of human intestines. And, if so, one could make inferences about vital human intestines from the results of studies of intestines from human cadavers.

As it was noted in Section 4.2, biological materials often have very complex elastic properties, i.e., nonlinear behavior, anisotropy, and viscoelastic effects. And, of course, these properties can vary significantly from animal to animal. In the case of the six meter long, small bowel of a single pig, material properties also can vary along its length [60]. Because of these complications, a thorough modeling of the small intestine from even a single animal is extremely difficult. Ironically, such an effort would not have much practical value because a reliable gastrointestinal robot must be able to locomote through any intestine it encounters. To design such a machine, experiments on a large statistical ensemble of intestinal segments should be conducted (specimens from different animals as well as different locations along the organ), and the results should

be "averaged."

This research has studied specifically the elastic behavior of intact segments of the small intestine in response to radial and axial forces supplied by internal pressure. Since the endoscopic robots are designed to locomote by pushing radially against the intestinal wall and stretching it axially, this seems to be a logical focus for our study of intestinal behavior. This study will not yield a complete characterization of the mechanical properties of intestines (one that provides the strain response to arbitrary stressing or the stress response to arbitrary straining), but this expedient methodology should form the basis of a model with predictive powers for the design of an endoscopic robot. Initially, this analytical model will be derived by considering the intestine as an axisymmetric, homogeneous, nonlinear, anisotropic, viscoelastic pressure vessel undergoing large deformations due to internal, axisymmetric loading distributions.

Intestines have thin walls which contain blood vessels, smooth muscles, etc. (a variety of internal structures) so the assumption of homogeneity is not appropriate if the "local" or "microscopic" elastic behavior is to be considered. It will be assumed herein that such variations in the mechanical properties that occur at a microscopic scale are likely to "average out" when the intestines are studied macroscopically. The motivation of this work is to predict the macroscopic effects of these robots on the surrounding intestines. Thus, this investigation proceeded under the assumption that these materials could be adequately modeled as homogeneous.

Nonlinear elasticity theory considers finite deformations (as opposed to infinitesimal deformations) of objects from an unstressed reference configuration. But one cannot take measurements of intestines in an unstressed state.

Thus, an attempt will be made to derive an unstressed reference configuration from the available measurements.

As mentioned in Section 4.2, anisotropy is a complication which has been observed in intestinal tissue; hence, all models which are claimed to represent intestinal behavior should include this phenomenon.

Another important feature of biological tissue, as described in Section 4.2, is its time dependent elastic behavior. For a given, constant loading, material deformations will tend to grow or creep. And since these endoscopic robots may be required to maintain positions near disease sites for long periods of time (on the order of minutes), an adequate understanding of this creep/viscoelastic phenomenon is required as well.

Any strain rate dependence on intestinal stiffness, as identified by Lanir and Fung [38] to be a small but not negligible characteristic of rabbit skin, will be ignored in this research since the experimental loading rates will approximate those expected from the robot.

In order to develop a tractable theoretical description of these thin membrane structures, the additional assumption of axial symmetry is initially imposed. This is not always a well justified simplification as regions of the intestines are quite curved, but in each experimental measurement, extra care will be taken to ensure that the specimen is reasonably straight and aligned with the axis of the experimental apparatus.

The assumption of axial symmetry implies that the material properties, the loading and deformations are all considered to be independent of the point of measurement around the circumference of the tubular membrane. In the last section, it was noted that Fackler and collaborators have observed that the stiffest direction for intestinal tissue is oriented roughly thirty degrees

from the longitudinal axis [13]. Their data shows this direction to be slightly stiffer than the longitudinal direction. This does not violate the assumption that the aniostropic material properties are also axisymmetric; in other words, the anisotropy specifically is *orthrotropy* with the principal axes aligned with "natural" axes of the cylinder. Their paper focuses on the microscopic visualization of the collagen and elastin fibers in the membrane. Their use of polarizing light microscopy provides them an explanation for both anisotropy and the observed stiffening of intestinal tissue under loading: the internal, initially "wavy," connective fibers gradually straighten under loading. They observed that these connective fibers are initially oriented at roughly plus and minus thirty degrees from the longitudinal direction. By dissecting narrow strips of tissue for uniaxial tensile testing, they presumed that the stiffest and strongest directions are not parallel to the longitudinal axis of the organ. But this is not necessarily correct. By performing a thought experiment, one can note an inconsistency. Assume that a composite, cylindrical pressure vessel is built with reinforcing fibers oriented helically at plus and minus thirty degrees from the axis of revolution. Because the fibers are wrapped in both directions, the resulting vessel is axisymmetric. Now, section out thin strips of this cylinder for unaxial testing. Because the strength and stiffness come from the reinforcing fibers (primarily), then tensile test specimens with longer fibers will be stronger and stiffer than those with shorter fibers as shorter fibers tend to place more stress (tensile and shearing) on the matrix between them. In this case, the strongest and stiffest directions would be at plus and minus thirty degrees, i.e., the fibers are aligned with the loads applied by the testing machine. And the weakest and softest direction would result from strips taken from the tube at ninety degrees. Interestingly, this is the reported behavior

in the paper by Fackler, et al. [13] Due to the axis symmetry of construction of this vessel, under axisymmetric loading, its deformations should likewise be axisymmetric. Thus, such stretching behavior could be viewed globally as increases in circumference (diameter) and length, and these orthogonal directions are the desired, "natural" axes of the anisotropy. And in this case, the overall behavior of the intestine under an internal, biaxial loading is not directly reflected by the results from such uniaxial tensile testing. Thus, experiments that provide a "whole organ" view of the mechanical properties of the intestine are valuable.

Another simplifying assumption will be made: all admissible deformations of intestinal tissues are isochoric. As identified in the last section, incompressibility is generally assumed by soft tissue biomechanicians. It was proven to be valid for arteries, but it has yet to be proven for intestines. It is reasonable to expect the intestines to deform in this manner as they are composed of a significant volume fraction of water (an "incompressible" fluid). And attempts will be made to justify this assumption.

As mentioned in the elasticity primer, Section 4.1, nonlinear analysis requires that all deformations be measured from an unstressed reference configuration. The work of Fung (described above) demonstrates that biological tissues have *memory* of their loading history. Furthermore, Fung and Liu [20] showed that for arteries, the residual stresses in loaded tissues can be quite significant. This may not be applicable to the intestinal biomechanics problem as arteries are quite stiff, highly loaded, thick walled structures; in contrast, the small intestine is thin walled, generally unstressed, and collapses under its own weight. Thus, the ability of intestines to carry residual stresses is less likely, but as yet unstudied. But in the modeling of these intestinal

tissues, it will be assumed that a derived, unloaded reference configuration is also unstressed. In other words, an attempt to derive the unstressed reference configuration will be made (as is required for a nonlinear analysis). But this derivation will assume that no residual stresses remain in the small intestine once the external loading is removed. Neglecting to *precondition* these intestinal tissues provides a more relevant model for the endoscopic robot as it will encounter intestines that have not been "exercised."

4.4 Elasticity Theory of the Small Intestine

4.4.1 Equation of Equilibrium for a Pressure Vessel

For a thin walled pressure vessel, such as is shown in Figure 4.5, the equation for equilibrium of each element of the vessel is given by:

$$\frac{\sigma_m}{\rho_1} + \frac{\sigma_c}{\rho_2} = \frac{p}{t} \ , \tag{4.5}$$

where, for each element:

σ_m = the normal stress along a meridian

σ_c = the "hoop" or circumferential, normal stress

ρ_1 = the radius of curvature of the meridian of the element

ρ_2 = the radius of curvature normal to the meridian

p = the applied, internal pressure

t = the wall thickness of the pressure vessel

Conceptually, the intestine can be viewed as a long, thin walled membrane

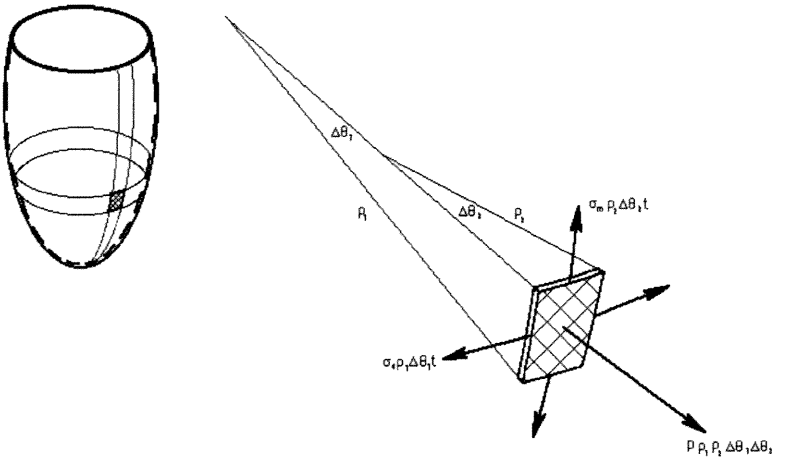

Figure 4.5: Pressure vessel analysis.

which stretches in diameter and length under internal loading. This is quite similar to the behavior of thin walled pressure vessels. Typically, pressure vessels are analyzed for deformations and stresses due to the application of internal, normal tractions only, i.e., internal pressure without any shearing forces. In the case of the robotic endoscope, this is not an adequate model because the robot "crawls" as a result of shearing tractions. However, the pressure vessel analysis is applicable for determining the circumferential and meridional stresses in regions where the locally applied shearing tractions are zero (or negligible). Additionally, the experiments performed to determine the elastic response of the intestines convert short segments of intestine into inflated pressure vessels. This experimental approach minimized the dissection of the intestinal specimens and therefore allowed them to be studied while still living or *vital* as the membrane wall and the mesentery (which supplies blood to the intestine) remained intact. This equation was thereby employed to convert the raw experimental data into the desired constitutive relations (as

discussed in Subsection 4.4.3). Furthermore, Equation 4.5 is also applicable for calculation of the applied normal traction on the membrane when the internal material stresses are known (even in the presence of an applied meridional shearing traction). In the computer simulation of the elastic response of the intestine to an expanding gripper segment (described in Subsection 4.6.3), the circumferential and meridional stresses are specified and the applied normal traction is subsequently calculated using Equation 4.5.

4.4.2 Constraint for Incompressible Materials

As previously mentioned, biomechanics of soft tissues is commonly based on the assumption that the materials are incompressible, that is, they undergo only locally volume preserving deformations. Thus, the assumption is invoked by imposing a constraint on the deformation field: only deformations which preserve the volumes of infinitesimal material elements will be admissible. In this investigation, this assumption will be very important as measurements of the deformations of specimens of the small intestine are difficult. Specifically, the nondestructive, experimental measurement of the thickness of the intestinal wall is a significant challenge. Thus, by assuming that the intestine behaves as an incompressible solid, its deformed wall thickness can be calculated from changes in its measured diameter length.

Since these deformations are restricted to be locally volume preserving, a relationship which binds the geometric variables can be derived. In Figure 4.6, the tubular membrane, or *body*, is deformed from its initial cylindrical configuration to an arbitrary, axisymmetric one. The desired kinematic constraint is described by equating the volume occupied by a ring element in its initial

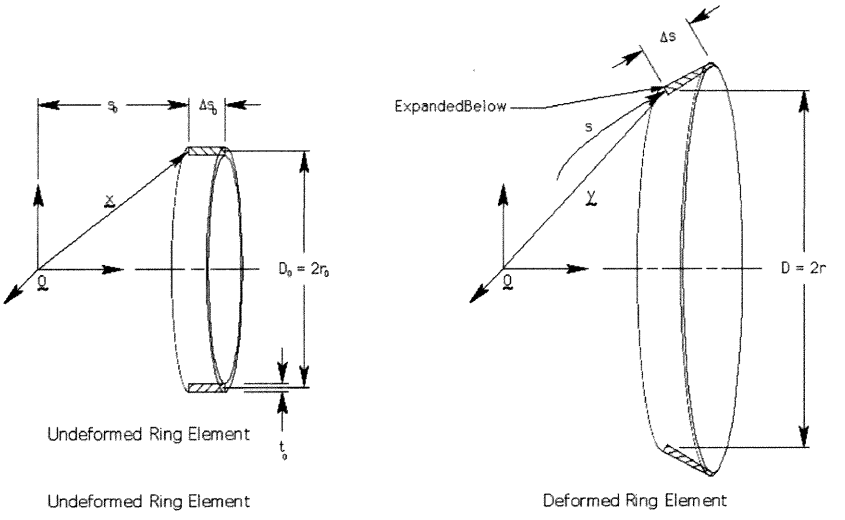

Figure 4.6: Geometry for analysis of the "incompressible" kinematic constraint.

and deformed configurations. The volume of the undeformed ring element of Figure 4.6(a) is $V_0 = 2\pi r_0(\Delta s_0)t_0$. Once deformed, the ring element appears as shown in Figure 4.6(b). The volume of material in the deformed element is given by:

$$\begin{aligned} V &= 2\pi r_{\oplus} \int_A dA^* \qquad (4.6) \\ &= 2\pi r_{\oplus} A \\ &= 2\pi r_{\oplus} \frac{\Delta s}{2} \left[t\Big|_s + (t + \frac{\partial t}{\partial s}\Delta s)\Big|_s \right] \\ V &= \pi r_{\oplus} \Delta s \left(2t\Big|_s + \frac{\partial t}{\partial s}\Big|_s \Delta s \right) \qquad (4.7) \end{aligned}$$

The "centroid radius," $r_{\oplus}$, (i.e., the distance from the axis of symmetry to the centroid of the section of the deformed ring element), approaches r as Δs approaches zero. Neglecting the higher order $(\Delta s)^2$ term, the volume of the deformed ring element becomes:

$$V \rightarrow 2\pi r t \ \Delta s \ , \quad \text{as } \Delta s \rightarrow 0 \qquad (4.8)$$

Finally, by equating the volumes occupied by the deformed and undeformed ring elements, Equations 4.7 and 4.8, the constraint for locally volume preserving deformations (of incompressible materials) is determined.

$$V_0 = V \implies 2\pi r_0(\Delta s_0)t_0 = 2\pi r t(\Delta s) \qquad (4.9)$$

Thus,

$$\frac{t}{t_0} = \frac{r_0}{r}\frac{\Delta s_0}{\Delta s} \ , \qquad (4.10)$$

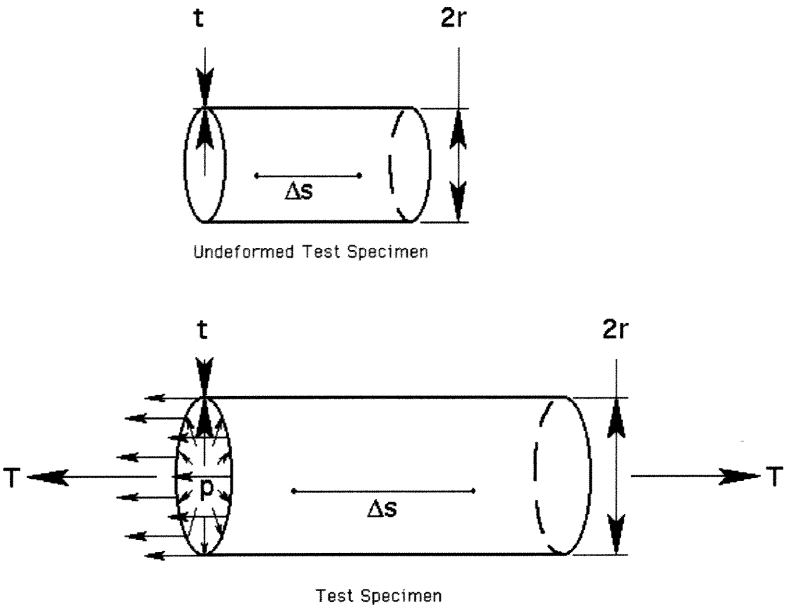

Figure 4.7: The simplified modeling of the experimental specimens.

or

$$\frac{t}{t_0} = \frac{r_0}{r}\frac{ds_0}{ds} . \tag{4.11}$$

These equations form a constraint on *admissible* deformations in our model for the small intestine. (This result can be rewritten as $\lambda_m \lambda_c \lambda_t = 1$. The product of these principal stretches is well known as the *Third Scalar Invariant* or *determinant* of the *Deformation Gradient Tensor* which is unity for deformations that locally preserve volume.)

4.4.3 Generation of the Constitutive Relations

How can experiments be performed to produce the necessary constitutive relationships for the small intestine? These experiments were designed to provide simple boundary conditions and tractions on segments of pig's intestine which

would thereby produce the required stress-strain relationships. Firstly, in this investigation, it was assumed that the experimental segment of undeformed intestine can be modeled as a right, circular cylinder. This is the stress free, undeformed reference configuration for these elastic bodies (membranes). Since this analysis will consider the nonlinear, solid mechanics of intestinal tissue, the only permissible reference configuration is *unstressed.* The membrane is then subjected to an internal pressure traction, and its deformation is measured. The ends of the intestinal segment are sealed with plugs, one of which is allowed to move freely in the axial direction. The deformed membrane is likewise assumed to take the shape of a right, circular cylinder. Thus, the membrane is modeled as shown in Figure 4.7. In light of St. Venant's Principle, the deformations of the test specimens are measured at points "far" from their ends where stress concentrations can be expected.

This modeling of the tissue mechanics permits the following calculations of the mechanical stresses within the intestinal membrane. Under this assumed deformation, the radius of curvature for a meridian is approximately infinite, $\rho_1 \rightarrow \infty$, and the radius of curvature normal to a meridian, ρ_2, is merely r. Also, the assumption of locally volume preserving deformations, Equation 4.10, will allow the circumferential and longitudinal stresses to be calculated without complete measurement of the deformed intestinal segment. These stresses within an experimental specimen will be determined from measurements of the internal pressure, the initial, unstretched membrane thickness, and the deformed diameter and length of the cylindrical segment.

To calculate the circumferential stress, the pressure vessel equilibrium equation, Equation 4.5, is recalled. With these radii of curvature this equation

yields

$$\sigma_c = \frac{pr}{t} . \tag{4.12}$$

And Equation 4.10 permits substitution for the deformed thickness, $t = t_0 \frac{r_0}{r} \frac{\Delta s_0}{\Delta s}$. Therefore, the circumferential stress ("hoop stress") is given by

$$\sigma_c = \frac{r^2}{t_0 r_0} \frac{\Delta s}{\Delta s_0} p . \tag{4.13}$$

Equation 4.5 is not directly applicable for calculation of the axial stress in this cylinder. Simply, this stress is derived by dividing the applied tensile force by the cross-sectional area of the thin intestinal membrane. (In this cylindrical geometry, the axial stress represents the *meridional* stress, hence the subscript "m" on the σ term.) The applied tensile force is generated by the applied internal pressure acting on the internal ends of the cylindrical assembly. This force is calculated to be the internal pressure multiplied by the cross-sectional area enclosed by the intestine, i.e., $T = p \cdot \pi r^2$.

$$\sigma_m = \frac{T}{2\pi r t} \tag{4.14}$$

$$\sigma_m = \frac{p \cdot \pi r^2}{2\pi r t} \tag{4.15}$$

$$\sigma_m = \frac{pr}{2t} \tag{4.16}$$

Again, Equation 4.10 is used to obviate the measurement of the deformed

thickness, t.

$$\sigma_m = \frac{r^2}{2t_0 r_0}\frac{\Delta s}{\Delta s_0}p \tag{4.17}$$

In these experimental trials, the strains of the intestinal segments will be calculated from measurements of the deformations as follows. The meridional strain (axial in the experiments) is given by

$$\varepsilon_m = \frac{\Delta s - \Delta s_0}{\Delta s_0} = \frac{\Delta s}{\Delta s_0} - 1 \; . \tag{4.18}$$

The circumferential strain is calculated from the measured diameter (or radius) of the deformed specimen.

$$\varepsilon_c = \frac{2\pi r - 2\pi r_0}{2\pi r_0} = \frac{r}{r_0} - 1 \; . \tag{4.19}$$

And, similarly, the strain in the thickness direction is given by

$$\varepsilon_t = \frac{t - t_0}{t_0} = \frac{t}{t_0} - 1 \; . \tag{4.20}$$

Again, the constraint for locally volume preserving deformations, Equation 4.10, will be invoked if the deformed thickness measurements are not reliable, i.e., $t = t_0 \frac{r_0}{r}\frac{\Delta s_0}{\Delta s}$. So,

$$\varepsilon_t = \frac{1}{t_0}\left(t_0 \frac{r_0}{r}\frac{\Delta s_0}{\Delta s}\right) - 1 = \frac{r_0}{r}\frac{\Delta s_0}{\Delta s} - 1 \; . \tag{4.21}$$

With these equations from stress and strain, we have a means to gener-

ate curves for stress versus strain from the available experimental data: the internal pressure, the membrane thickness, the intestinal diameter, and the segment length of the specimen. Given these principal biaxial stresses and triaxial strains, two biaxial constitutive laws are proposed:

$$\sigma_c = \sigma_c \left(\varepsilon_c + \nu\varepsilon_m\right) \tag{4.22}$$

and

$$\sigma_m = \sigma_m \left(\varepsilon_m + \nu\varepsilon_c\right) \tag{4.23}$$

or

$$\sigma_c = \sigma_c \left(\varepsilon_c + \nu\varepsilon_m + \nu\varepsilon_t\right) \tag{4.24}$$

and

$$\sigma_m = \sigma_m \left(\varepsilon_m + \nu\varepsilon_c + \nu\varepsilon_t\right) \tag{4.25}$$

where ν is Poisson's ratio for the material, which equals 0.5 for incompressible materials. The former constitutive relations relating these principal stresses to the *in-plane* principal strains, Equations 4.22 and 4.23, was motivated by Y.C. Fung's reporting of such a nonlinear modeling of the cell membrane for red blood cells [19]. Physically, one can interpret these equations in the following way. Each principal stress response is a nonlinear function of the sum of its corresponding strain with a fraction of the transverse strain(s). The scaling of the transverse strain(s) is given by Poisson's Ratio for the material.

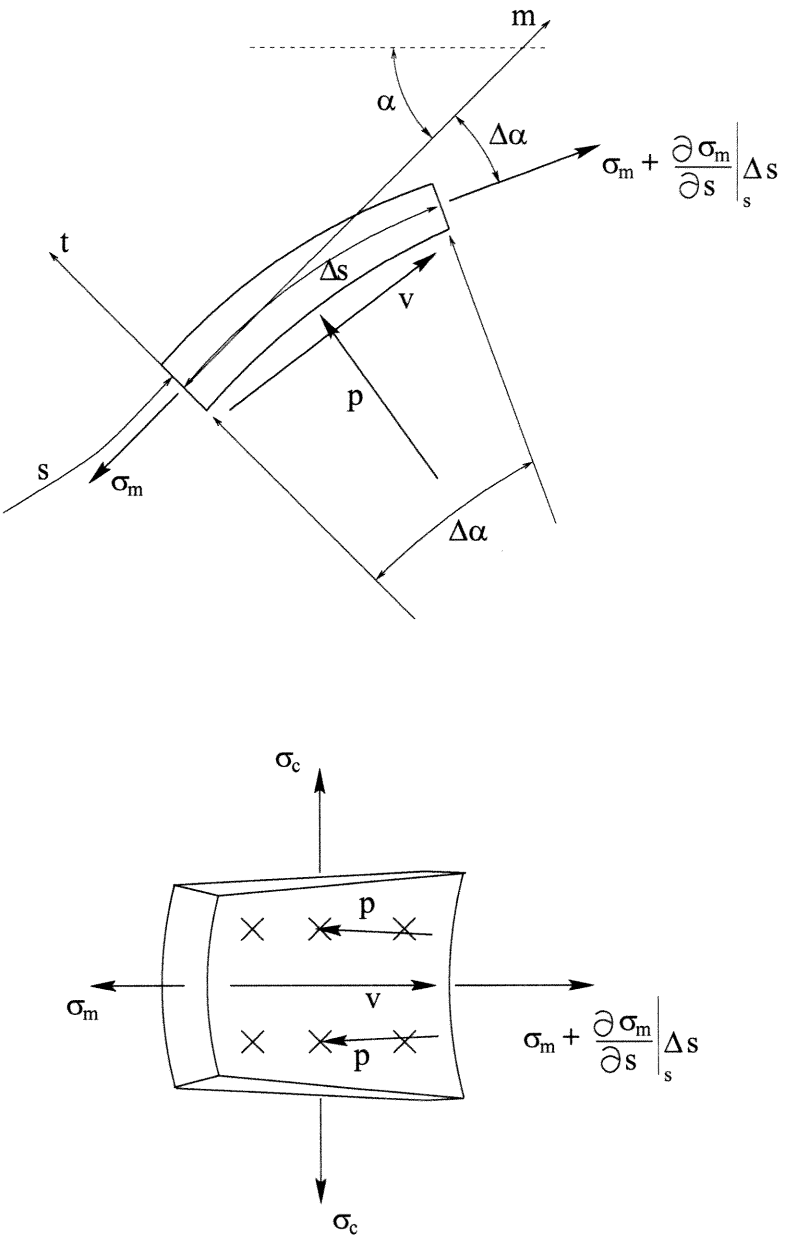

Figure 4.8: A "free body" element for the derivation of the shearing traction distribution.

4.4.4 Calculation of Shearing Traction Distribution

As mentioned previously, the intestinal analysis will presume a deformation field on the membrane. From these assumed deformations, the strains, the stresses and ultimately the applied tractions can be derived. In this section, arbitrary, axisymmetric deformations are allowed; thus, in general, both normal (pressure-like) and shearing tractions will result. Referring to the free body diagram of a small element of membrane shown in Figure 4.8, and utilizing Newton's Second Law ($\vec{F} = m\vec{a}$), equations for the applied tractions are derived. The magnitude of the time rate-of-change of the momentum of these intestinal elements is expected to remain low during all robotic actions (since the membrane is thin and of relatively low density and the actuation accelerations of the robot are anticipated to be relatively small). Thus, a quasistatic analysis should yield a reasonable first model (membrane equilibrium is presumed as opposed to membrane dynamic behavior). Figure 4.8 depicts two views of a free body diagram for a small element of intestinal wall complete with all stresses, tractions and geometric variables. Invoking the equilibrium condition on this body, i.e., the sum of all forces equals zero, will produce the desired relationship between the stresses and tractions. The area, S, of the membrane element is given by $S = \Delta s \cdot \frac{1}{2} r \left[\Delta\theta + (r + \frac{\partial r}{\partial s}\Delta s)\Delta\right]$. The shearing traction, v, is defined as the shearing force per unit area of membrane. Summing the forces in the direction tangent to the meridian at s, i.e., $\Sigma F_m = 0$

gives:

$$
\begin{aligned}
0 \;=\; & -\sigma_m\, r\Delta\theta\, t \\
& + \left(\sigma_m + \frac{\partial\sigma_m}{\partial s}\Delta s\right)\left(r + \frac{\partial r}{\partial s}\Delta s\right)\Delta\theta\left(t + \frac{\partial t}{\partial s}\Delta s\right)\cos(\Delta\alpha) \\
& + v\Delta s \;\cdot\; \frac{1}{2}\left[r\theta \;+\; \left(r + \frac{\partial r}{\partial s}\Delta s\right)\Delta\theta\right] cos\left(\frac{\Delta\alpha}{2}\right) \qquad (4.26)
\end{aligned}
$$

$$
\begin{aligned}
0 \;=\; & \Delta\theta\left\{ -\sigma_m\, rt \;+\; \sigma_m\, rt\cos(\Delta\alpha)\right. \\
& + \left[\;\sigma_m\, r\frac{\partial t}{\partial s}\cos(\Delta\alpha) \;+\; r\frac{\partial\sigma_m}{\partial s}t\cos(\Delta\alpha)\right. \\
& \qquad \left. + \sigma_m\frac{\partial r}{\partial s}t\cos(\Delta\alpha) \;+\; vr\cos(\Delta\alpha)\;\right]\Delta s \\
& + \left[\; r\frac{\partial\sigma_m}{\partial s}\frac{\partial t}{\partial s}\cos(\Delta\alpha) \;+\; \cdots\;\right](\Delta s)^2 \\
& \left. + \;\frac{\partial\sigma_m}{\partial s}\frac{\partial r}{\partial s}\frac{\partial t}{\partial s}\cos(\Delta\alpha)\,(\Delta s)^3\;\right\} \qquad (4.27)
\end{aligned}
$$

In this analysis, the measure of the element in the azimuthal direction, $\Delta\theta$, drops out (this problem is axisymmetric and the forces of interest are normal to that coordinate direction). Now taking the limit as $\Delta s \rightarrow 0$, the higher order terms vanish. Also, for smooth membranes, as $\Delta s \rightarrow 0$, $\rho_1\Delta\alpha \rightarrow \Delta s$. The smoothness implies that ρ_1 is strictly positive (nonzero). Thus, $\Delta s \rightarrow 0$ implies that $\Delta\alpha \rightarrow 0$. Therefore, $\Delta\alpha$ is safely considered to be "small." This implies that $\cos(\Delta\alpha) \longrightarrow 1$ and $\cos\left(\frac{\Delta\alpha}{2}\right) \longrightarrow 1$. Making these substitutions and cancellations yields

$$
0 \;=\; \sigma_m\, r\frac{\partial t}{\partial s} \;+\; r\frac{\partial\sigma_m}{\partial s}\,t \;+\; \sigma_m\frac{\partial r}{\partial s}\,t \;+\; vr\;. \qquad (4.28)
$$

So

$$
v \;=\; -\left[\sigma_m\frac{\partial t}{\partial s} \;+\; \frac{\partial\sigma_m}{\partial s}\,t \;+\; \frac{\sigma_m}{r}\frac{\partial r}{\partial s}\,t\right]\;. \qquad (4.29)
$$

Noting that the multiplication rule for differentiation provides that

$$\frac{\partial}{\partial s}\left(\sigma_m\, t\right) \;=\; \sigma_m \frac{\partial t}{\partial s} \;+\; \frac{\partial \sigma_m}{\partial s}\, t \tag{4.30}$$

yields the simplest form of the shearing traction distribution:

$$v \;=\; -\left[\frac{\partial}{\partial s}(\sigma_m\, t) \;+\; \frac{\sigma_m\, t}{r}\,\frac{\partial r}{\partial s}\right] . \tag{4.31}$$

For the computer simulation of robot-intestine interaction, another form of the shearing traction equation will be utilized. In this case, the applied shear, v, will be calculated as a function of the constitutive laws and the kinematics of the problem (posed only in the variables r and t). Returning to Equation 4.29:

$$v \;=\; -t\left[\frac{\partial \sigma_m}{\partial s} \;+\; \frac{\sigma_m}{r}\,\frac{\partial r}{\partial s}\right] \;-\; \sigma_m \frac{\partial t}{\partial s} . \tag{4.32}$$

Recalling that the constitutive relations for this "plane, biaxial stress state" are modeled by Equations 4.22 and 4.23:

$$\begin{aligned} \sigma_c &= \sigma_c(\varepsilon_c + \nu\varepsilon_m) \\ \sigma_m &= \sigma_m(\varepsilon_m + \nu\varepsilon_c) . \end{aligned}$$

Substitution of Equation 4.23 into Equation 4.32 and applying the Chain Rule for differentiation yields

$$v \;=\; -t\left[\frac{\partial \sigma_m}{\partial(\varepsilon_m + \nu\varepsilon_c)}\,\frac{\partial(\varepsilon_m + \nu\varepsilon_c)}{\partial s} + \frac{\sigma_m}{r}\,\frac{\partial r}{\partial s}\right] - \sigma_m \frac{\partial t}{\partial s} . \tag{4.33}$$

Additionally, $\frac{\partial r}{\partial s} = \sin\alpha$ where α is the angle the tangent to the meridian at s makes with the longitudinal axis of the problem. So,

$$v = -t\left[\frac{\partial\sigma_m}{\partial(\varepsilon_m+\nu\varepsilon_c)}\left(\frac{\partial\varepsilon_m}{\partial s}+\nu\frac{\partial\varepsilon_c}{\partial s}\right)+\frac{\sigma_m}{r}\sin\alpha\right]-\sigma_m\frac{\partial t}{\partial s}\,. \tag{4.34}$$

Using the definitions of strains used herein, the kinematic constraint for incompressible materials, and the differentiation rules, this equation can be rewritten as

$$v = -\left\{t\frac{\partial\sigma_m}{\partial(\varepsilon_m+\nu\varepsilon_c)}\left[\frac{t_0 r_0}{(tr)^2}\left(t\sin\alpha+r\frac{\partial t}{\partial s}\right)+\frac{\nu}{r_0}\sin\alpha\right]+\sigma_m\frac{\partial t}{\partial s}+\frac{\sigma_m t}{r}\sin\alpha\right\}. \tag{4.35}$$

With the exception of the stress term, σ_m, and its derivative, $\frac{\partial\sigma_m}{\partial(\varepsilon_m+\nu\varepsilon_c)}$, this equation is purely kinematical, and σ_m and $\frac{\partial\sigma_m}{\partial(\varepsilon_m+\nu\varepsilon_c)}$ are determined for any strain state by the experimentally generated constitutive law.

This form of the *shear traction distribution* equation is the basis for the numerical simulation of a robotic segment's influence on the intestine that follows in Section 4.6.

4.4.5 Criteria for Excessive Loading of the Intestines

In the biomechanics literature, most of the experiments are conducted on soft tissues that have been dissected from the body. In these cases, ultimate stresses and strains are determined when the experimental specimens break. Unfortunately, in the living organism, injurious loads and deformations may be significantly lower than those which tear or rip the tissue. In the experiments described in the following section, observations were noted of constriction of

blood flow and subsequent hemorrhage at quite modest levels of applied loading. The pressure loading on the inner wall of the intestine at which such injury was evident was often less than one-third that which caused the specimen to burst. So, clearly, the ultimate stress of these tissues is not a reasonable limit for benign interactions with an endoscopic robot. This research proposes three other measures for the prediction of injury.

Firstly, this analysis can predict the internal stresses that result from deformations produced by the robot. This biaxial stress state causes the aforementioned injuries. So, one simple approach to limiting the impact of the robot on the intestinal wall is to determine a measure of the biaxial stresses that causes injury and prevent the robot's effects from exceeding those levels. Although it is not well motivated by these circumstances, the *von Mises Stress* is often used to predict the failure of solid materials. This criterion was developed to predict the failure of linearly modeled materials as a limit of the allowable strain energy of deformation. It is slightly more conservative than the common, maximum shear stress criterion (the Tresca criterion for yielding) in linear analysis. Nevertheless, it is the following measure of the biaxial stress state in the membrane:

$$\sigma_{vonMises} = \sqrt{\sigma_m^2 - \sigma_m \sigma_c + \sigma_c^2} \, . \tag{4.36}$$

A second *ad hoc* limitation on the acceptable levels of loading could be the magnitude of the normal traction applied to the inner surface of the intestine. Villi line the intestine's inner surface, and large contact forces to these fragile structures can be injurious. So although this measure of the robot's impact on the intestine neglects the internal wall stresses within the membrane, care

must be taken to ensure that it remains at a benign level. Also, this interfacial contact loading could be measured directly using tactile sensors located on the robot's gripper segments. Since the experiments used only internal pressure to provide tractions on the intestine, the biaxial stress state that is produced in these experiments would be expected to differ significantly from that which results from action of robotic gripper segments. Nevertheless, the relative ease by which the normal traction is measured by a robot indicates that it should be considered in addition to more sophisticated measures of acceptable loading.

The last, proposed injury criterion for the small intestine actually was inspired by the biomechanics experiments on living intestines. Since the mechanical behavior of the pigs' intestines were observed while their blood supply was intact, their health could be monitored qualitatively as well. This was critical to provide insights into the mechanisms of injury for these fragile membranes. For loading conditions that seemed quite modest, that is, for internal pressures that measured at roughly one pound per square inch above atmospheric pressure (roughly 1.07 Atmospheres, absolute), the intestines' blood supply was constricted visibly. As may be expected, the larger vessels appeared to contain blood after the flow in the smaller ones was clearly nonexistent. This would suggest that a measure that predicts the collapse of smaller intestinal blood vessels may be a well motivated criterion for limiting the maximum loadings of the small intestine. In rubber elasticity theory (recall the assumption of incompressible material behavior), the stress state is typically reduced to the sum of two constituent tensors: the *isotropic stress tensor* and the *deviatoric stress tensor*. Since these materials exhibit zero dilatation, stresses that would otherwise tend to cause such volume changes can grow without impact on the deformation of the body. These stresses are often referred to as the isotropic

stress, or pressure, within the body. Generally, this term is removed from the stress tensor as it plays no role in the prediction of the deformations in rubber. However, in the case of the constriction of intestinal blood flow, this "hydrostatic" pressure seems to play a very significant role. This pressure builds in the membrane surrounding the intestinal blood vessels. When this isotropic stress exceeds the local blood pressure, the capillaries and relatively thin walled veins will collapse under their external loading. Once this happens, blood flow supplying the intestines is effectively shut down. By analogy, the external loading can "ring the blood out" of the membranes like water from a towel. This is evident as the pressure builds, and the natural color of the intestines vanish. ("Color" returns as soon as the loading is removed, but it is not a desirable color. At this point the delicate tissues are bruised and hemorrhaging.) The isotropic stress tensor is a scalar multiple of the identity tensor, and this scalar is calculated to be one-third of the trace of the Cauchy stress tensor. For this intestinal modeling, the pressure is merely one-third of the sum of the meridional and circumferential stresses.

$$\sigma_{iso} = \frac{1}{3}(\sigma_m + \sigma_c) \tag{4.37}$$

4.5 Elasticity Experiments of the Small Intestine

4.5.1 Experimental Goals and Issues

To conduct a complete study of the mechanical properties of a given material, especially when the material is expected to be anisotropic, one must conduct a

series of experiments to study the tensile and shear effects on various orientations of the material specimens. Of course, this is made less daunting if one can *a priori* anticipate the nature of the anisotropy (by insightful consideration of the material's internal structure) and thus reduce the number and complexity of the required experiments. As designed, the gripper segments of the robot expand uniformly to push against the intestinal walls and the extensor segments are laterally compliant to minimize local loading asymmetries. So the robot can be assumed to produce roughly axisymmetric radial expansion and axial stretching in the intestine. Under this assumption, segments of intestine can be considered to be membranes subjected to axisymmetric internal loadings. So, the significant stresses to be considered in this intestinal study are the so called "hoop stress" and the "meridional stress."[57] This simplification also allows experimentation on the intestines of living pigs; this is a critical advantage and an original contribution of this research. Because the intestines are loosely supported in the abdomen by a thin, vascularized membrane, the mesentery, one can excise a section of small intestine that is still connected to its blood supply. This is only true if the section of intestine is left in a "tubular" condition. Any attempt to produce strip-like, test specimens for uniaxial, tensile tests would transect its blood supply as its blood vessels circumscribe the intestine. In his text, Y.C. Fung argues for testing both dissected specimens and whole organs to better understand their biomechanics [17].

The primary objective of these experiments is to provide a tool for the design of an endoscopic robot; therefore, the whole organ behavior is of primary concern. And since the robot is to be introduced into the human GI tract, the geometry and mechanical behavior of *human* intestines are ultimately required. Of course, these measurements can only be performed on cadavers. It

is hoped, however, that if there are differences in the behavior of dead versus living human intestine, the pigs' intestines will reflect it qualitatively. In this research, the experiments included: *in vitro* pig intestine tests and *in vivo* pig intestine tests. All these tests utilized the same experimental apparatus which, in fact, could be employed in future studies on human cadavers. In each experiment, a segment of intestine, either living or dissected, is attached between two end plugs and inflated to carefully regulated internal pressures as its longitudinal, radial and thickness measurements are taken (the specimen is inflated like a balloon). Unfortunately, this technique simultaneously loads the intestines in both the radial and longitudinal (axial) directions which, in turn, produces a *biaxial* state of stress within the membranes. Of course, the proposed robot provides a similar influence on the intestinal wall, but ideally, one would prefer to measure the circumferential and axial material properties individually thereby minimizing the number of potentially invalid, simplifying assumptions made during data reduction and analysis.

4.5.2 Experimental Apparatus

For these experiments, the apparatus consisted of: an interal pressure regulation system, machined plugs to seal the ends of the intestinal segment while providing the desired boundary conditions, and instruments to measure the diameters, lengths and thicknesses of the intestines while they are being subjected to internal pressure.

The internal pressure is controlled manually by adjusting a precision, low-pressure regulator and observing the measured pressure on a 0 - 4.5 psi pressure gauge. The plugs for the ends of the segment of intestine must provide ad-

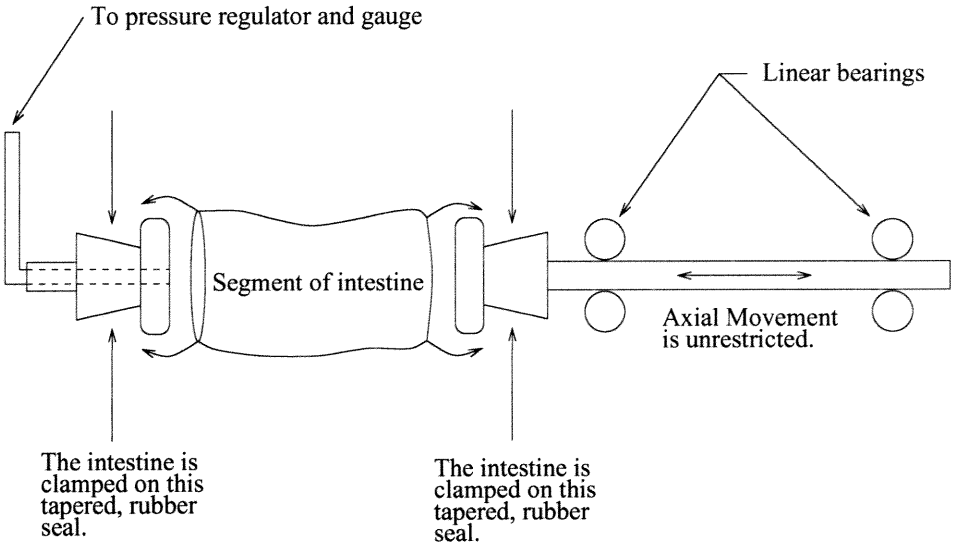

Figure 4.9: A close-up schematic of the test fixture.

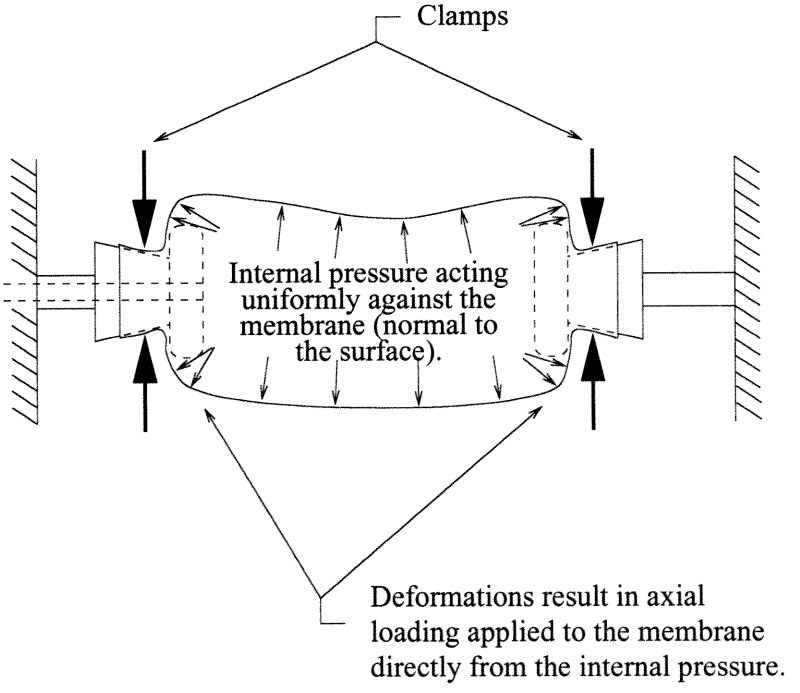

Figure 4.10: No experimental boundary conditions can prevent axial tension in the test specimen.

equate sealing and boundary conditions for the experimental specimen. To provide the necessary seals, as illustrated in Figure 4.9, the intestinal segment is clamped onto truncated rubber cones using hose clamps and lengths of string. Additionally, one plug must move longitudinally under small forces to guarantee that the expected axial loads are applied to the intestine. If the ends of the specimen were prevented from moving, there would be no method to determine the magnitude of the longitudinal loading on the membrane. One must recognize that these membranes expand tremendously in the radial direction. This ensures that there will be longitudinal/axial stressing (tension) in the membrane solely due to the internal pressure (see Figure 4.10). The clamping boundary condition dictates that one plug must move freely in the longitudinal direction to allow the axial tension forces to be calculated; this force is merely the internal pressure acting on the projected area of the specimen's cross section (this was discussed in Section 4.4). Reiterating, one cannot measure circumferential and longitudinal behavior independently using internal pressure as the input. If independent measurements of these orthogonal properties are required for intact intestinal lumens, then separate experimental systems must be created: one to expand radially without causing axial loading, and one which performs a uniaxial tensile test of the tube-like specimen. And guaranteeing that these orthogonal properties are actually *uncoupled* is quite suspect.

Exterior dimensional measurements were taken manually with machinists calipers. Although stainless steel calipers were used initially, the light weight of plastic, digital calipers (from Mitotoyo, Japan) provided increased tactile sensitivity and control of contact between the calipers and the specmen. Ink spots were placed on the specimens to locate these measurements consistently;

the measurements were taken near the middle of the specimens to minimize any end effects (St. Venant's Principle). Although this approach is straightforward, there are a few significant drawbacks. All sharp edges of these instruments were dulled for obvious reasons, but repeated abrasion of the calipers' jaws at the measurement locations could abrade the membrane (fortunately, this was not evident in the live animal experiments, only with the excised tissues). Also, at low internal pressures, the experimental uncertainty of these measurements increases due to the extreme compliance of the specimen. The difficulty of manually measuring the changes in length of these membranes is even greater than that of their diameters. This is because one must measure visually the distance between two ink dots on the surface of the intestinal segment. Typically, there is a slight curvature in each intestinal segment; hence, these dots must be placed as close as possible to each specimen's "neutral axis." Of course, there is additional imprecision introduced when one attempts to measure between these dots which expand and fade under the stretching of the membrane. In the surgical experiments, these marks were created using electrocautery. A very shallow burn mark was made on the outer membrane of the intestine which could be highlighted using a felt tip marking pen. Since these fiducial marks locally impact the membrane's mechanical properties, care was taken to minimize the burn region. Fortunately, with care, electrocautery pens can be used extremely precisely for this application.

Consistency of measurement was of high priority which led to the additional decision to measure exclusively the diameter or length changes during certain trials (7 trials measured both diameter and length changes, 10 trials studied diameter exclusively, and 11 trials observed the length changes exclusively). By concentrating on one dimension exclusively during a trial, its con-

sistent and timely measurement could be obtained (with each increase in the internal pressure). Because the possibility of these materials displaying time dependent stretching (creep), inconsistent and/or excessive time between the measurements would introduce an additional source of random error. Unfortunately, a reasonable argument in opposition to this approach is that it cannot provide data that manifests a correlation between the circumferential and longitudinal behavior of each experimental segment. In this light, seven trials were conducted in which both diameter and length measurements were obtained. (And to investigate the possible effects of creep on these measurements that required significantly more time to complete, several in vitro experiments were conducted to study the time dependent behavior of these materials.) And although there were impediments to accurate measurements of length and diameter using calipers, the measurement of internal pressure was relatively straightforward. The careful adjustment of the apparatus' precision regulator could establish the desired pressure loadings in increments of 0.1 psi with uncertainties of less than 0.01 psi (less than 0.005 psi was typical).

Lastly, in order to determine the stresses in the membrane, one needs to measure its wall thickness. This is not a trivial issue. Since intestinal tissue is extremely soft, using calipers to measure its "unstressed" thickness is virtually impossible. In addition, a more valuable experiment would measure the intestinal wall thickness as a function of loading. One possible experimental technique measures the delays between the echoes of ultrasound pulses impinging on the walls of the membrane. If the speed of sound within the material is known, then the membrane thickness can be determined. Such measurements could then validate the assumption of incompressible intestinal behavior. And if so, then all admissible, three-dimensional, kinematic behavior would be pre-

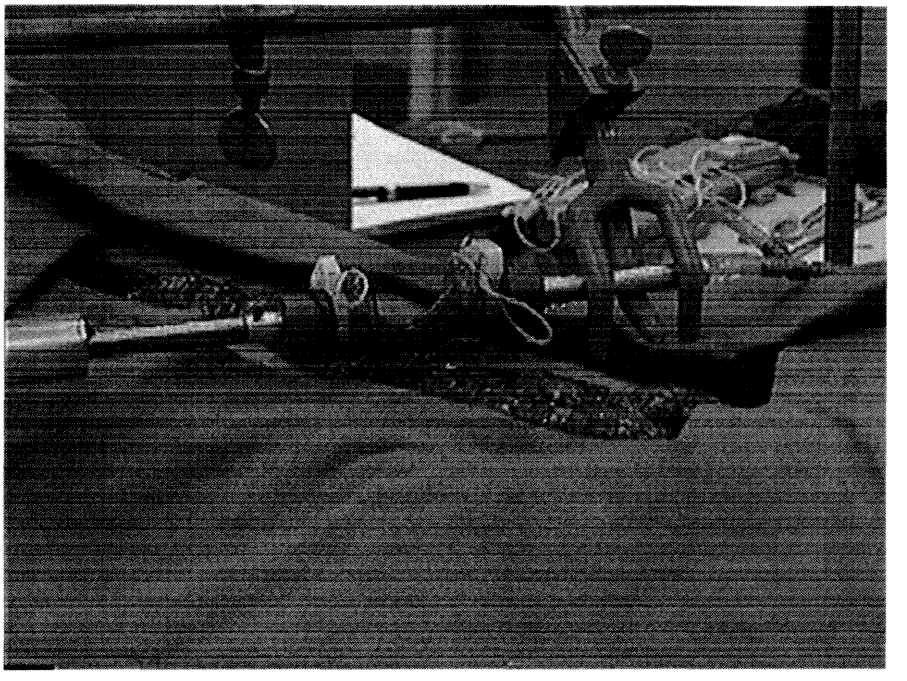

Figure 4.11: An intestinal specimen is prepared for testing.

scribed by two independent coordinate variables (any two of the following measurements: length, width and membrane thickness). To this end, several piezoelectric, ultrasonic transducers were evaluated for the measurement of the thickness of excised intestinal tissues. These initial trials supported the purchase of a custom, 25 MHz, focused, immersion transducer with a bubbler assembly (to couple the ultrasonic pulses into the intestinal membrane with minimum contact loading). The initial application of this measuring device has been promising; however, useful data has yet to be obtained.

4.5.3 *In Vivo* Biomechanics Experiments

These experiments were conducted in the Department of Comparative Medicine at Cedars-Sinai Medical Center (Los Angeles, CA). Experiments were performed on eight pigs ranging in weight from 65 to 150 pounds. The exper-

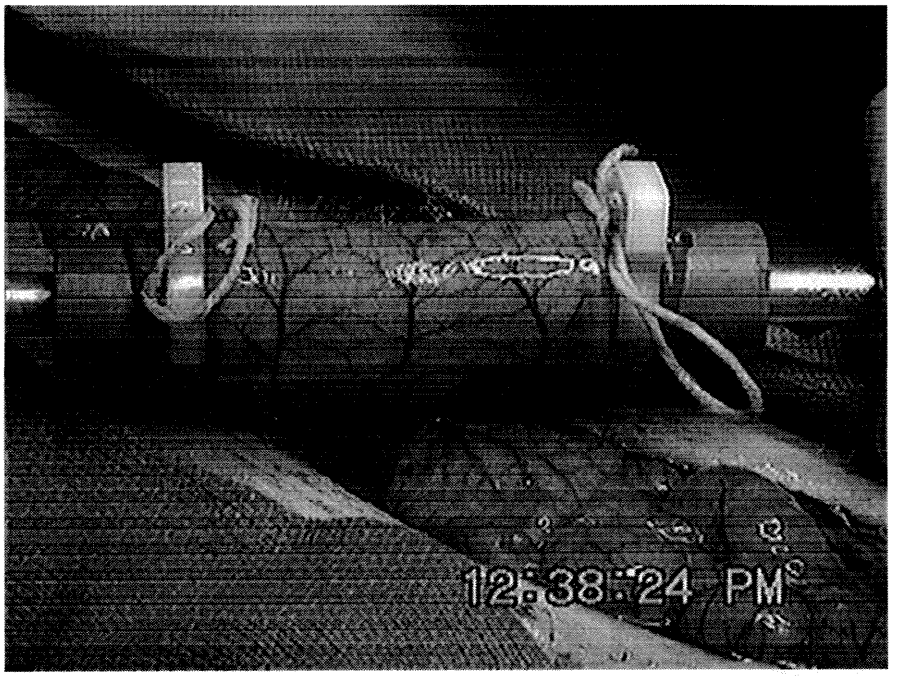

Figure 4.12: An intestinal specimen is inflated to a low internal pressure.

Figure 4.13: Blood flow has been visibly constricted in many vessels.

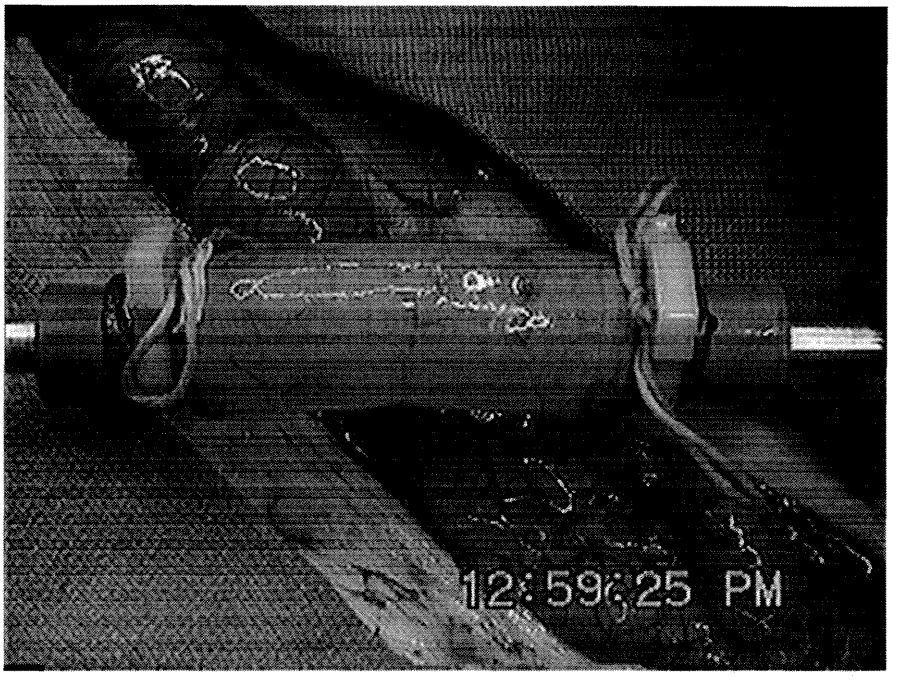

Figure 4.14: With increased internal loading, the intestinal specimen is substantially injured. Essentially, all its blood has been squeezed out.

imental procedure for the intestinal biomechanics will follow.

The pig is sedated, hooked to the anesthesia equipment, and then surgery commences to gain access to the small intestine. Once the abdominal incision is completed, the experimental apparatus is moved over the surgical field. The apparatus is lowered so that a segment of the intestine can be attached as shown in Figure 4.11. A region of the intact intestine is lifted from the abdomen and a short specimen is selected according to the locations of the "vertical" blood vessels in the local mesentery. The goal is to locate and dissect the desired specimen such that its center remains sufficiently connected to the animal's circulatory system. Additionally, the ends of the specimen must be cut from the mesetery to provide clamping regions; these cuts will be made through the mesentery near and along the ends of intestinal segment (not too closely, however). And to isolate the specimen from any loading transmitted

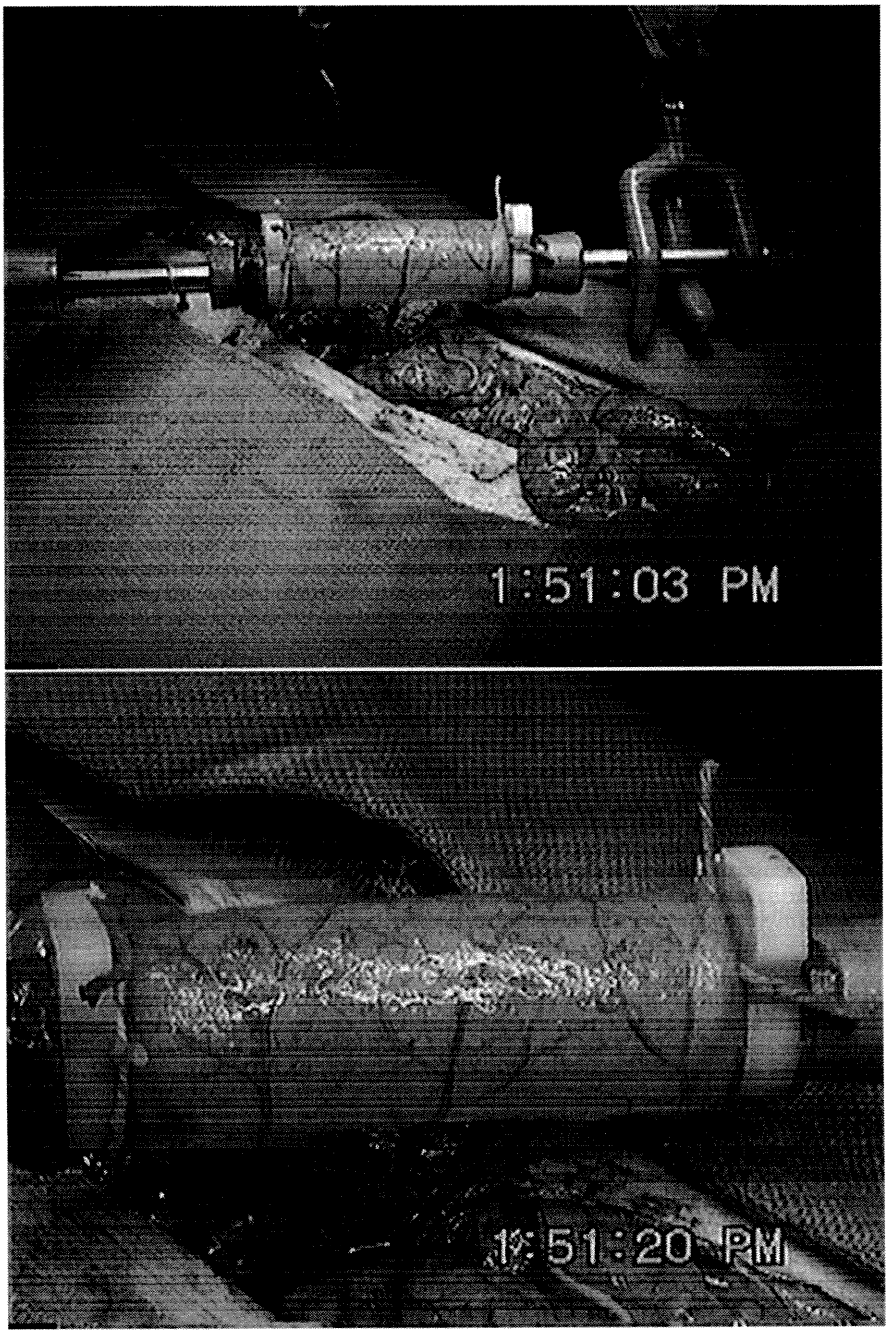

Figure 4.15: Injury is apparent by: the numerous dots of hemorrhage evident in the membrane and visibly constricted blood vessels. Stress relieving cuts between blood vessels in the mesentery are visible beneath the tubular segment.

through the mesentery, the mesentery is cut down away from the specimen (not too deeply as the blood vessels converge at the other end of this membrane). In order to prevent any of these incisions from bleeding, the blood vessels near the ends of the proposed segment must be sealed using electocautery (COAG) along each vessel "chasing the blood out." Once this blood supply near the ends is removed, the necessary incisions are made through the mesentery. Then, the two transections of the intestine are made. This basically completes the process of preparing a specimen, but depending on the circumstances of the trial, e.g., the length of the specimen, the mesentery can begin to be placed in tension. Although this additional stiffness would likely help a robot crawl, its asymmetric and unmodeled behavior may ruin the data. So, multiple methods were used, together and separately, to ensure that the mesentery would provide as little impact as possble. Firstly, the position of the experimental apparatus is adjustable, and it can also rotate about a vertical axis to remove any twisting in the lifted mesentery. The second approach was to produce vertical cuts parallel to and between the blood vessels in the mesentery. These holes in the supporting membrane would open up as the specimen's length increased. The ability of the blood vessels supplying the segment to move with it prevented tension in the mesentery from building. When viewed carefully, Figure 4.15 shows the effect of these cuts. The third method recognizes that all of the structural stiffness within the mesentery is located on its surface. Thus, very shallow incisions in the surface of this membrane can basically remove its ability to carry a load. This was the most time consuming method, and least applied.

As mentioned above, the apparatus is positioned horizontally as low to the animal as possible to relieve tension in the mesentery while permitting the

moving plug to slide freely in its linear bearings. Any tilt of this assembly impacts the experiment; specifically, the weight of the moving plug can either add to or oppose the pressure forces in the longitudinal direction (neither situation is acceptable). Once a segment is prepared in the manner above, its ends are pulled over the plugs and sealed in place mechanically with plastic clamps and knotted string. Figure 4.11 displays a prepared specimen mounted on the experimental apparatus. In this clamping process, one can induce or reduce the effective curvature of the specimen; to minimize unmodeled effects, clamp the segment such that when the specimen is gently tugged over the end plugs, its lateral contraction is coaxial with them. Also, it was observed that the intestinal curvature is concave toward the mesentery, so sliding the opposite side of the lumen slightly farther over each plug before clamping will tend to reduce the specimen's curvature. However, potential segments that exhibit obvious curvature should be passed over entirely as all the modeling assumes axisymmetry and this technique is, by definition, an eccentric loading condition. Nevertheless, measurements are taken near the center of each segment where St. Venant argued such uneven effects tend to equilibrate.

Since the animal is under general anesthesia, the time alloted for experimentation is limited. Constant monitoring of its vital signs is required in order to guarantee the experiment's longevity, but the number of trials that can be accomplished with each animal cannot be predicted a priori.

The process of data procurement was simply to increase the applied internal pressure loading in increments of 0.10 psig ($\pm$ 0.005 psig, typically). The confidence in these pressure measurements is considerably higher than that of the dimensional measurements. An estimate of the experimental uncertainty in the diameter measurement is 0.010 in. and for the length, about 0.020 in.

Lastly, exposure of the specimens to air could cause them to dry out, especially as their blood supply diminished at the higher internal pressures. Thus, when necessary, saline was sprayed to prevent surface dessication.

4.5.4 *In Vivo* Experimental Observations

- Figures 4.16 and 4.17 represent the raw data gathered for intestinal specimens investigated in vivo.
- Initially, the experiments were conducted on 150 pound pigs for pressures increasing toward catastrophic failure of the tissues. When two specimens burst at roughly 2.5 psig and all were seen to visually hemorrhage for pressures under 3.0 psig, the experimental procedure was amended to conclude after a pressure of 2.5 psig was reached. This decision was intended to maximize the amount of relevant data for robotic endoscopy that could be obtained for each animal under the given time constraints. Actually, the mechanical behavior of the intestines after they are injured has been considered to be of little importance at this stage of research as these robots are intended to locomote without applying such dangerously high loadings to the intestines.
- All reports in the biomechanics literature identify considerable dispersion as endemic to soft tissue studies. Thus, experimental samples sizes must be large enough to ensure a valid statistical analysis. Only eight pigs were used in these experiments producing data from twenty-eight intestinal segment specimens.
- Thirteen of the twenty-eight segments tested burst at internal pressures less than 2.6 psig, with one extremely fragile specimen failing at 0.8 psig (a 65 pound pig, none of whose segments survived beyond 2.5 psig). For compari-

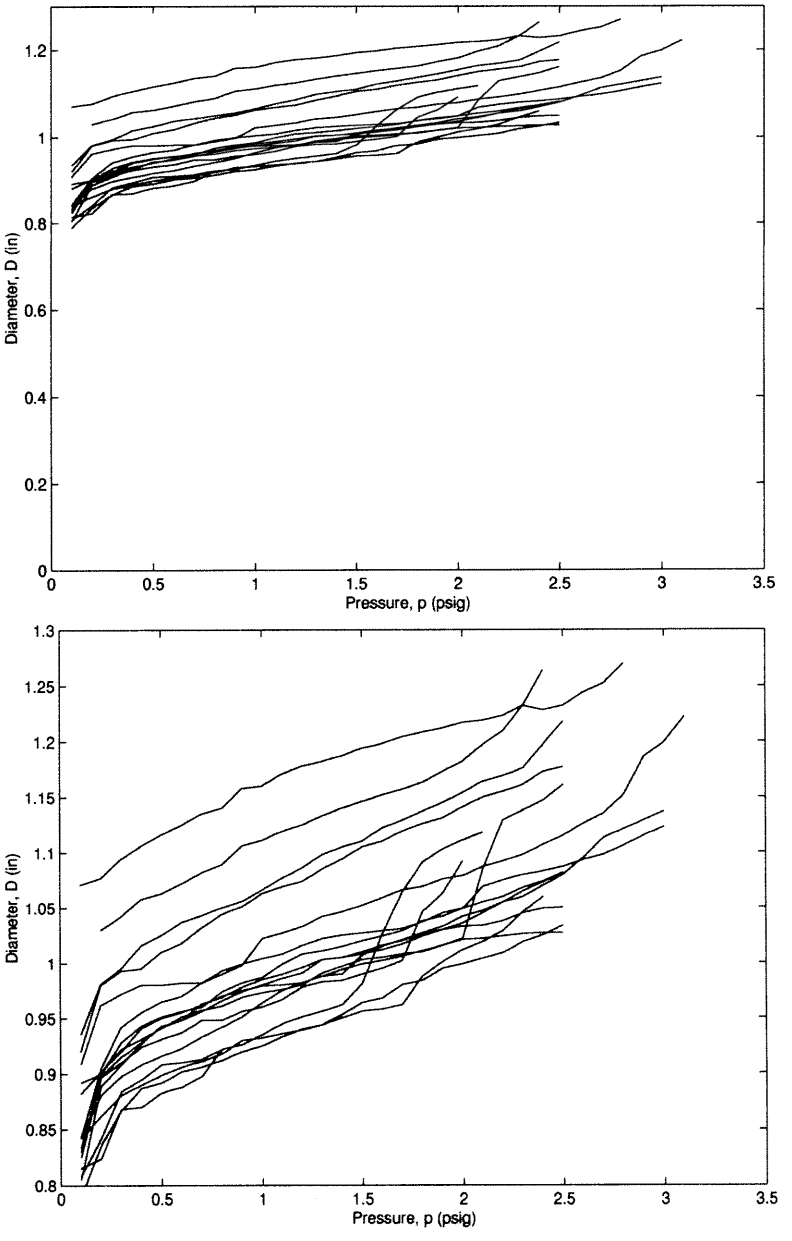

Figure 4.16: The *in vivo* measurements of intestinal diameter as a function of internal pressure.

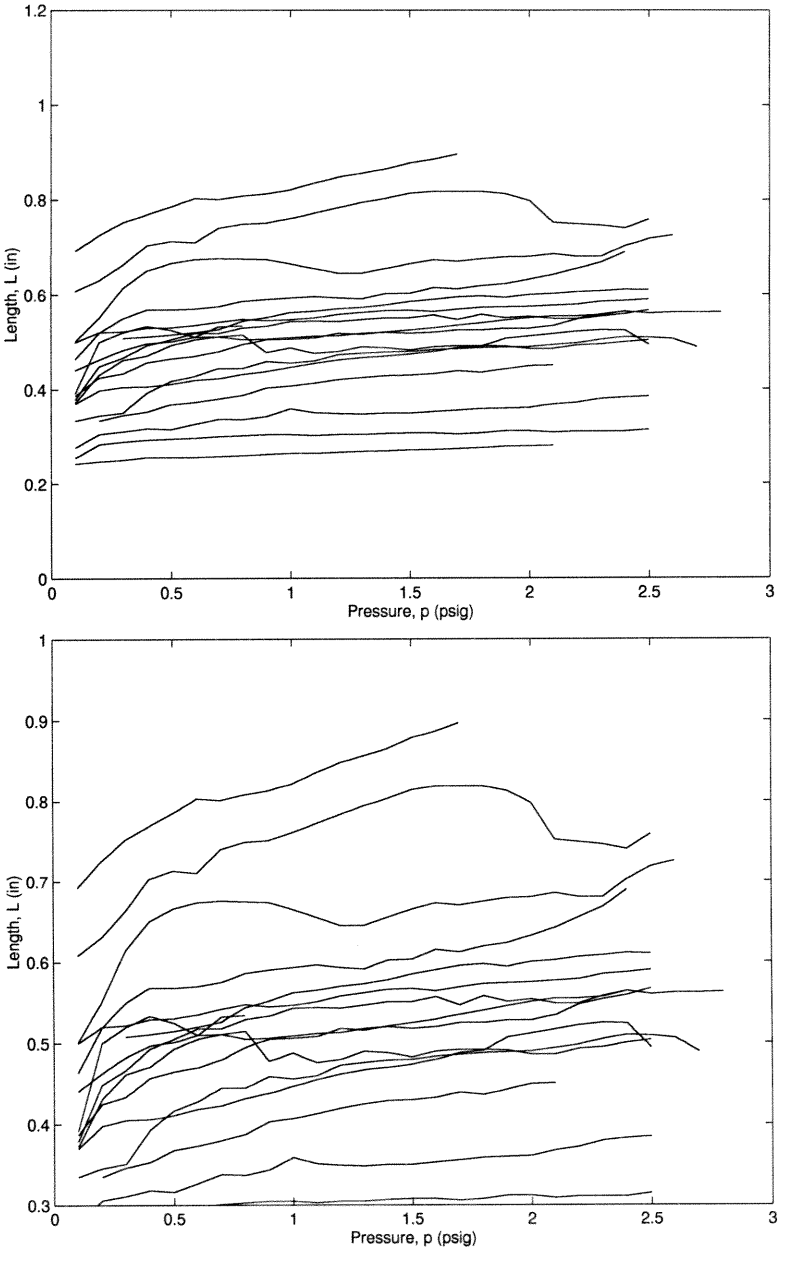

Figure 4.17: The *in vivo* measurements of length of an intestinal segment as a function of internal pressure.

son, of the eight specimens from 150 pound pigs, only one burst at a pressure below 2.5 psig (it failed at 2.4 psig). These details are only provided to demonstrate that for juvenile animals the soft tissues tend to strengthen with age; this phenomenon is documented in the literature (where stiffening is likewise affected).

- There were large variations in size/age of the animals available to this study; this was not anticipated when the experimental protocol was developed. This may be expected to introduce additional dispersion and systematic errors in the resulting data. Unfortunately, the following experimental procedure was followed. Perform the measurement of diameter versus pressure for several intestinal segments. Subsequently, measure the segment length versus pressure data for a different series of intestinal segments. This highly efficient approach assumes that the gathering of a larger data set is more important than attempting to maintain a correlation between the diametric and length data. Since there were three large pigs (weighing about 150 pounds) primarily involved in diameter versus pressure measurements, and three small pigs (two weighing roughly 65 pounds, one approximately 80 pounds) that were used exclusively in the length versus pressure measurements, a systematic error in the measured anisotropy may have occurred. This would likely be reflected as a stiffening of the circumferential behavior relative to the longitudinal behavior.
- For a low internal pressure of approximately 1.0 psig, numerous small and medium sized blood vessels in the intestinal membrane appeared occluded, i.e., the normally solid red curves/lines would appear as "dashed." Due to the challenges of gathering quantitative data for these segments, anecdotal reports of constricted blood vessels were noted whenever possible. But no attempt was

made to observe a minimum internal pressure that causes such constriction of blood flow as it appears to be dependent upon the diameter of the blood vessel. The smaller the blood vessel, the lower the pressure loading required to collapse it. And generally, the blood flow through even the largest vessels appeared to be nonexistent at pressures between 1.5 and 1.7 psig. Postulating that smaller vessels collapse at lower pressures leads to the conclusion that to investigate the minimum internal pressure which will constrict the blood flow will require microscopy of the intestinal capillaries. This optical complication was not pursued. Further discussion of this phenomenon will be provided in Section 4.6.

- Small hemorrhages were very common for even moderate levels of internal pressure, e.g., 1.8 psig. But truly dramatic bruising was evident as soon as the internal pressure was reduced for every specimen that had remained intact at 2.5 psig. The injuries sustained would often cause these specimens to bleed excessively from their ends. To prevent this, sutures were used at the other end of the mesentery to tie off their blood supply.
- Without a means to measure the intestinal thickness as a function of internal pressure, i.e., thickness measurements using ultrasound were not successfully implemented, the wall thickness data for "unloaded" specimens were gathered using calipers. The membrane was squeezed between the jaws of the instrument as little as possible during these measurements. Eight segments were measured yielding the following data set: $t_0 = (0.020, 0.035, 0.032, 0.035, 0.037, 0.032, 0.031, 0.031)$ in inches.

4.5.5 *In Vitro* Biomechanics Experiments

Additional experiments were performed on small intestines that had been excised from pigs that weighed between 120 and 200 pounds. These specimens were procured from The Farmer John Company (Los Angeles/Vernon, CA). Over the course of experimentation, five small intestines were studied. When these specimens were received, they had been freshly dissectly, closely trimmed from the mesentery, rinsed thoroughly, and packaged in ice. Their cleaning process was described as follows: each length of intestine (in its entirety) was slid over a stainless steel tube spraying water. This process could provide an uncorrelated *preconditioning* of these specimens. These experiments were performed to investigate the viability of testing dissected tissues in lieu of specimens in vivo. As it was described, the rinsing process for these particular intestines may have imposed them to excessive preconditioning; therefore, the results of these experiments should be evaluated primarily for the qualitative behavior of dead intestines.

The following experiments were conducted: (1) specimen diameter versus internal pressure and (2) the intestinal diameter versus time for an internal pressure of 0.6 psig, i.e., the diametric creep.

The process of measurement of these intestinal segments was generally identical to those described above. But for these trials the tissues tended to dessicate considerably faster, necessitating more frequent applications of saline spray. Unfortunately, they also appeared to exhibit significantly more porosity than their living counterparts, and their pores seemed to close as the applied saline solution bathed the intestinal surface. With each spraying of saline, the internal pressure would momentarily increase which was followed by a decrease

as the liquid dripped off. Thus, additional care was taken to anticipate this phenomenon and stabilize the applied internal pressures before, during, and after each dimensional measurement was obtained.

It was mentioned that possible creep of these tissues could introduce errors in the earlier data, so experiments were conducted to investigate that potential. These trials subjected individual intestinal segments to an internal pressure loading of 0.6 psig for a period in excess of one hour (trials lasted from 60 to 110 minutes). Unfortunately, such protracted experimentation is prohibitively expensive for tissues in vivo; therefore, this initial study was conducted solely on excised intestines. The specimens' diameters were measured in five minute intervals, and between measurements, a saline solution spray was regularly applied.

4.5.6 *In Vitro* Experimental Observations

- Figure 4.18 displays diameter versus internal pressure data for the in vitro experimental trials. These results will be compiled with the in vivo data in the next section.

- The "creep" experiments observed the increase in the intestinal segment diameter for constant internal pressure, 0.6 psi, as a function of time. The data obtained for all these trials is shown in Figures 4.19 and 4.20. Detailed modeling of this time dependent behavior was not considered necessary for this preliminary investigation. The value of these plots is that they demonstrate that every specimen's circumferential strain over time was smaller than the dispersion found in the ensemble of circumferential strain trials. In other words, the variations in behavior from one specimen to the next is greater

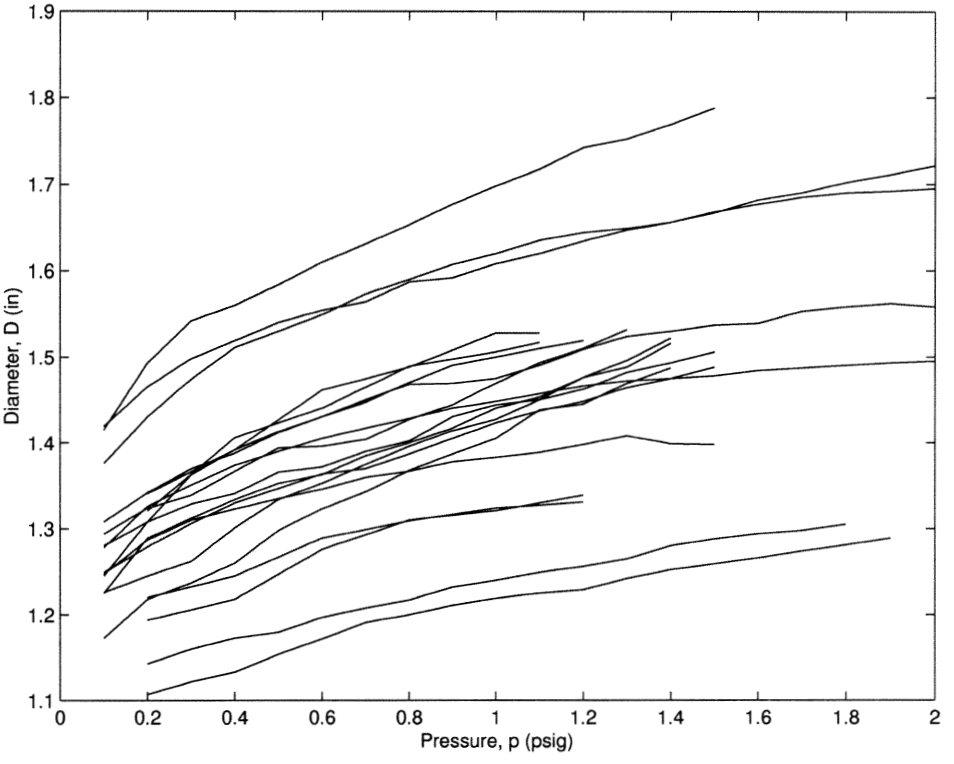

Figure 4.18: The *in vitro* measurements of intestinal diameter as a function of internal pressure.

than the time varying elongation of any particular individual. So if the robot is capable of locomotion within a variety of intestines, then it will likely tolerate smaller changes that occur over time at each location. (As an aside, the aforementioned "quasilinear" modeling suggested by Fung [21] may be valid for intestines as the data appear quite linear when plotted on linear v. logarithmic axes, as shown in Figure 4.20.)

4.6 Biomechanics Results

This section will report the findings from the elasticity experiments that were performed on pigs' small intestine. The first subsection utilizes the data that was obtained experimentally to develop an anisotropic constitutive relationship for pigs' intestines. Furthermore, it provides a comparison between the elastic behavior of the living intestines with that from dissected specimens. The second subsection provides a brief discussion of the experimental results. The final subsection uses the derived constitutive relationships and equations from Section 4.4 to produce an animated model of the elastic response of the intestines to the expansion of an enveloped robotic gripper segment.

4.6.1 Data Reduction for Modeling

The method to determine ensemble material properties for pig's intestines began by studying the data from each trial individually to infer its "unstressed" reference configuration. This may have introduced error from extrapolation of each trial's *nonlinear* data to estimate the dimensions of its unloaded configuration. However, since each specimen had unique geometry and material properties (and therefore a unique unstressed reference configuration), it was

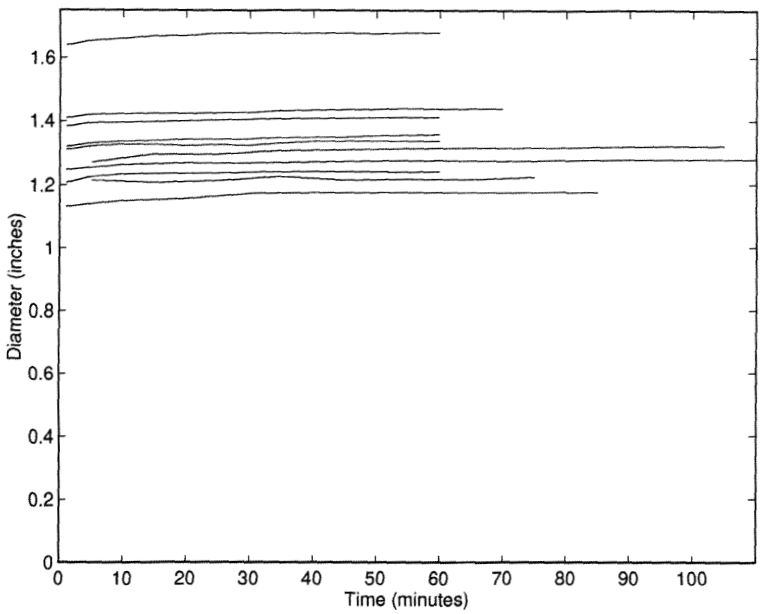

Figure 4.19: Raw creep data (lin-lin): all *in vitro* trials.

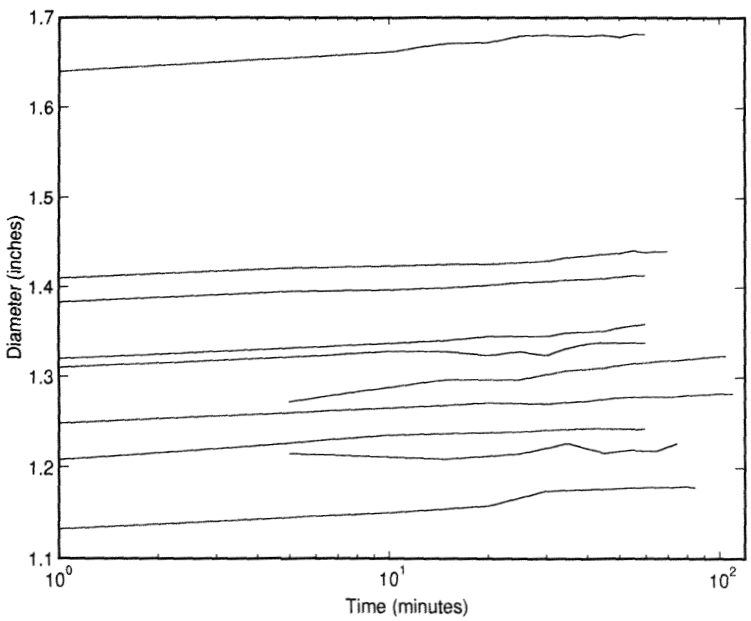

Figure 4.20: Raw creep data (lin-log): all *in vitro* trials.

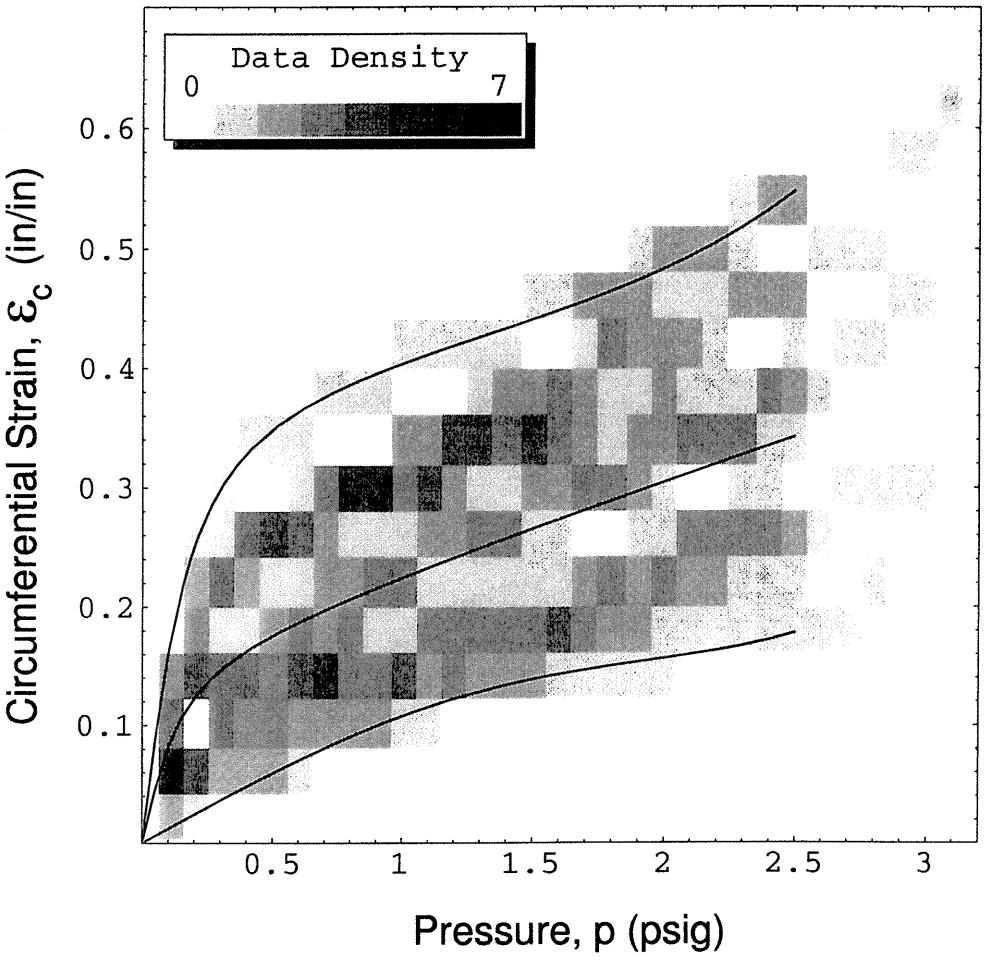

Figure 4.21: Circumferential (OD) strain versus pressure for 17 *in vivo* trials.

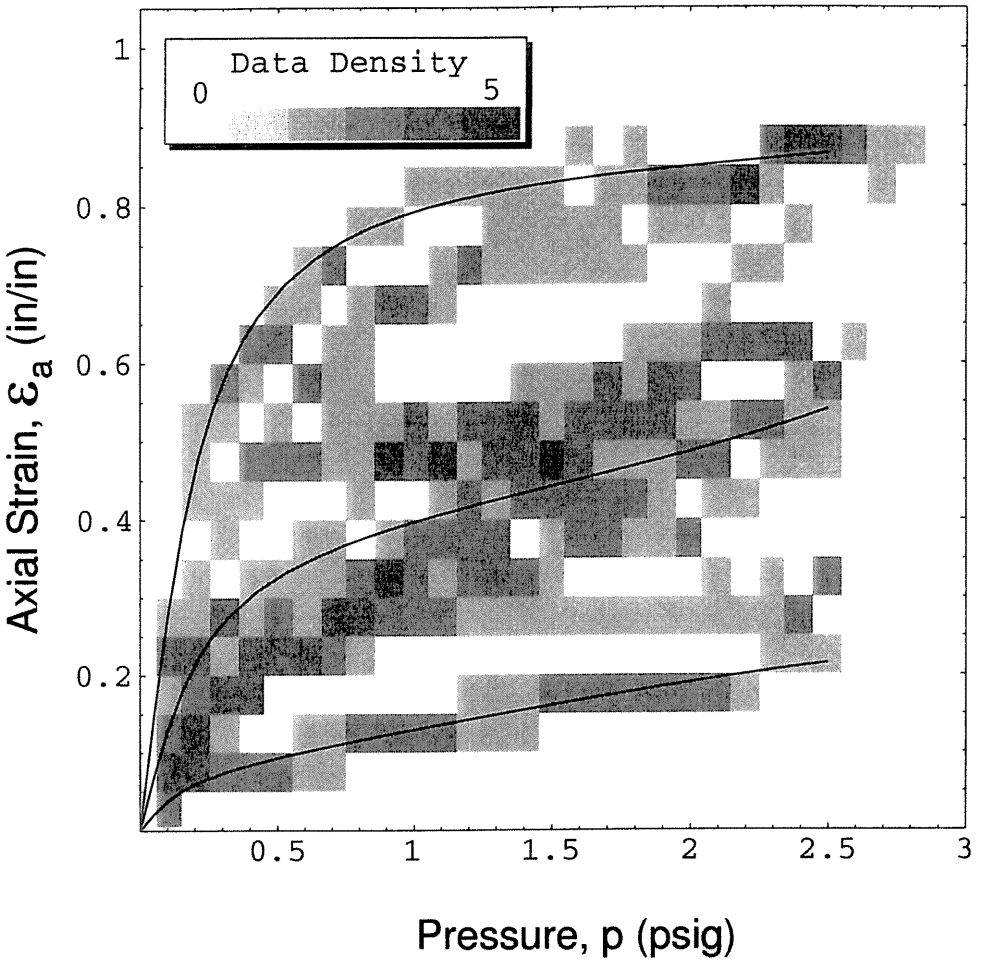

Figure 4.22: Axial/meridional strain versus pressure for 17 *in vivo* trials.

decided that the data from each trial be "normalized" prior to any averaging process over the various trials. Thus, each trial was plotted individually and the zero pressure intercept (on the diameter or length axis) was estimated. With the additional assumption that any residual stresses in the membrane are negligible, then the *unloaded reference configuration* would approximate the *unstressed reference configuration.* This process was performed for every trial of diameter versus pressure and length versus pressure. As discussed in Section 4.1, the following kinematic relations were used to define the strains: $\varepsilon_m = \lambda_m - 1$, $\varepsilon_c = \lambda_c - 1$, $\varepsilon_t = \lambda_t - 1$, where m, c and t are "meridional," "circumferential," and "thickness," respectively.

So, using its unique zero pressure intercept, each trial of the *in vivo* experimental data was mapped pointwise to plot the strain versus internally applied pressure. To provide a representation of the distribution of these data points, two-dimensional histograms of the ensemble strain versus internal pressure are provided in Figures 4.21 and 4.22. In these plots, the "data density" refers to the number of data points within each respective rectangular region. The dimensional measurements using the calipers were significantly less precise than the pressure measurements which were consistently taken at 0.1 pound per square inch intervals. Thus, at each level of pressure, the ensemble data was averaged. This average strain versus pressure behavior was fitted by the middle curves shown in Figures 4.21 and 4.22. The upper and lower curves represent numerical fits of the upper and lower bounds of the measured strains versus pressure behavior. These upper and lower bound curves represent direct fits of the data at the extremes of each ensemble of experimental trials. All of the curves share a familial foundation of the following four parameter

nonlinear functions:

$$\varepsilon_i \;=\; A_i \arctan(B_i\, p) \;+\; C_i\, p \;+\; D_i\, p^5 \quad \text{for} \;\; i \in \{c, m\}\,.$$

The fits of strain versus pressure that are presented graphically in Figures 4.21 and 4.22 are provided below:

$$\varepsilon_c \;\Big|_{\text{upper bound}} = \; 0.04325\, p \;+\; 6.016 \cdot 10^{-4}\, p^5 + 0.2512 \arctan(7.227\, p) \tag{4.38}$$

$$\varepsilon_c \;\Big|_{\text{mean}} = \; 0.07418\, p \;-\; 5.286 \cdot 10^{-6}\, p^5 + 0.1031 \arctan(8.737\, p) \tag{4.39}$$

$$\varepsilon_c \;\Big|_{\text{lower bound}} = \; -1.244\, p \;+\; 1.006 \cdot 10^{-3}\, p^5 + 7.188 \arctan(0.1901\, p) \tag{4.40}$$

$$\varepsilon_m \;\Big|_{\text{upper bound}} = \; -5.706 \cdot 10^{-4}\, p \;+\; 8.087 \cdot 10^{-5}\, p^5 + 0.5752 \arctan(5.190\, p) \tag{4.41}$$

$$\varepsilon_m \;\Big|_{\text{mean}} = \; 0.05731\, p \;+\; 3.209 \cdot 10^{-4}\, p^5 + 0.2441 \arctan(5.455\, p) \tag{4.42}$$

$$\varepsilon_m \;\Big|_{\text{lower bound}} = \; 0.06045\, p \;-\; 9.346 \cdot 10^{-5}\, p^5$$

$$+ 0.04795 \arctan(7.459\,p) \qquad (4.43)$$

Recalling Equations 4.13 and 4.17:

$$\sigma_c = \frac{pr}{t} = \frac{r^2}{t_0 r_0}\frac{\Delta s}{\Delta s_0}$$

and

$$\sigma_m = \frac{r}{2t}p = \frac{r^2}{2t_0 r_0}\frac{\Delta s}{\Delta s_0}p\,,$$

and proposing that the constitutive relationships be modeled by Equations 4.22 and 4.23:

$$\sigma_c = \sigma_c(\varepsilon_c + \nu\varepsilon_m) \quad \text{and} \quad \sigma_m = \sigma_m(\varepsilon_m + \nu\varepsilon_c)\,,$$

experimental, biaxial material properties are derived. In this derivation, the material stresses and strains are related for incremental increases in the internal pressure, p, which is the only independent parameter. This yields the curves given in Figure 4.23 which represent the anisotropic, nonlinear, biaxial constitutive laws for these tissues. As mentioned in the experimental observations, Section 4.5.4, the smaller and larger blood vessels were observed to collapse at roughly 1.0 psig. and 1.6 psig., respectively, so the corresponding stresses/strains are plotted as circles and asterisks in this figure. These marks demonstrate where the loading was considered excessive.

The circumferential stretching behavior for the *in vitro* specimens was compared to that of living tissue as well. The extrapolation process that was used to estimate the unloaded circumference of the living intestines was applied to the experimental data for 19 experimental trials utilizing dead tissue. In the

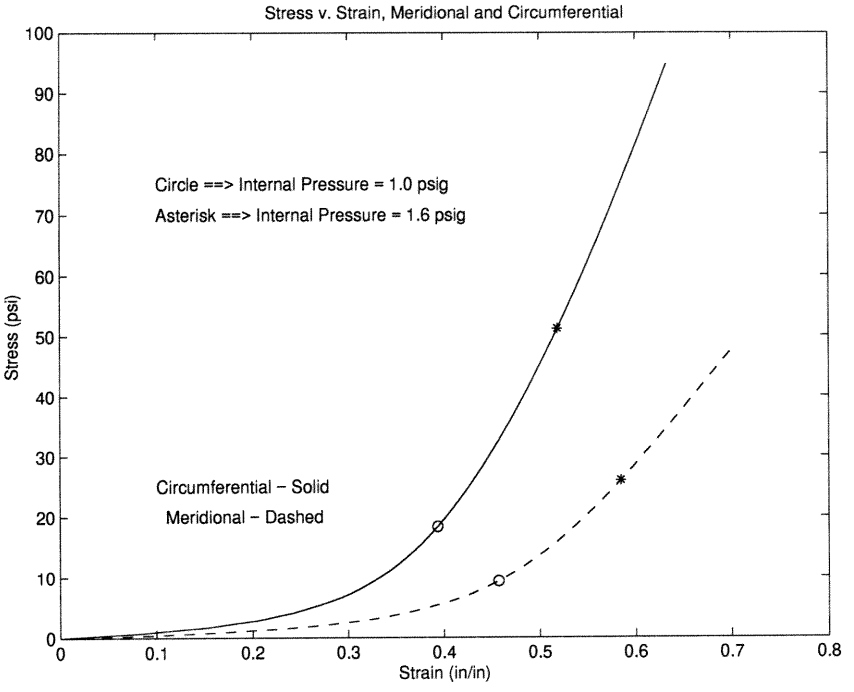

Figure 4.23: The anisotropic constitutive relations for intestines, specifically: $\sigma_m = \sigma_m(\varepsilon_m + \nu\varepsilon_c)$ and $\sigma_c = \sigma_c(\varepsilon_c + \nu\varepsilon_m)$.

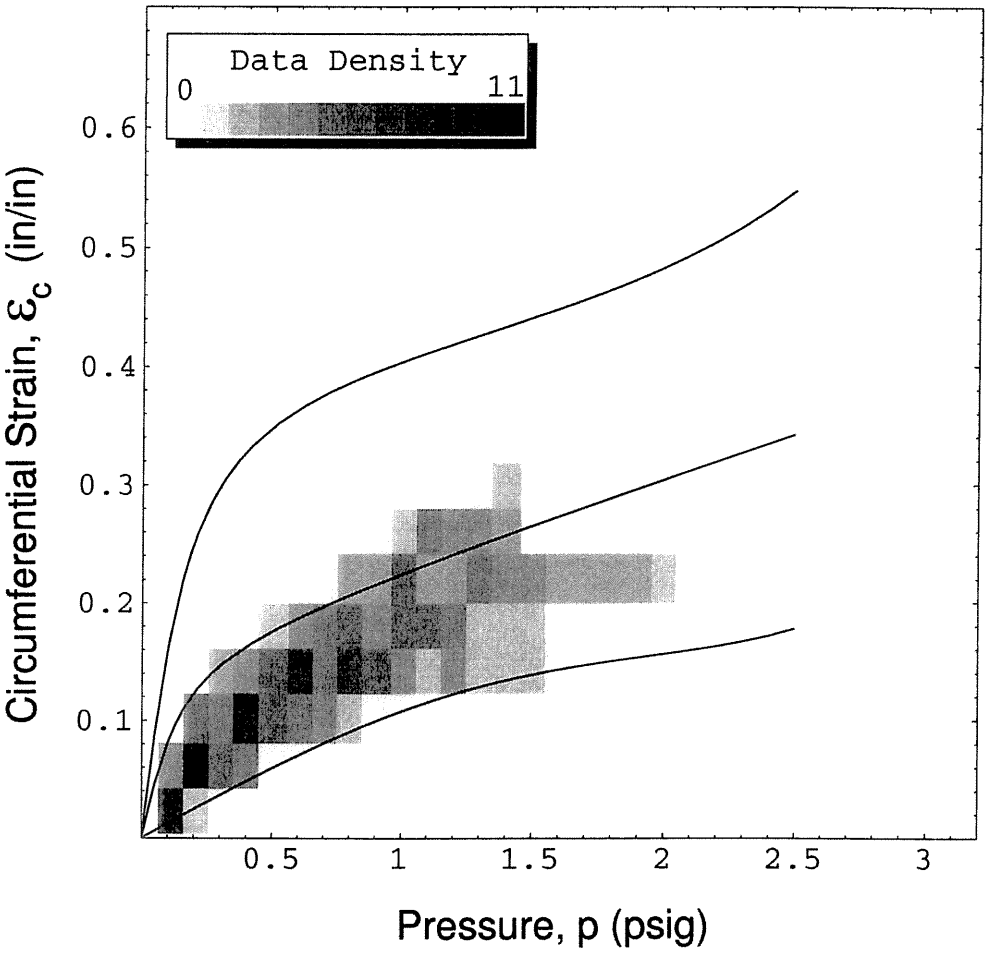

Figure 4.24: Circumferential (OD) strain versus pressure for 19 *in vitro* trials.

manner described above for the *in vivo* data, the resulting distribution of circumferential strain versus internal pressure was plotted as a two-dimensional histogram in Figure 4.24. In this figure, the solid curves of strain as functions of internal pressure are those that were generated for the living specimens. Thus, comparisons between the data from living and dead intestines can be deduced.

Discussions of Figures 4.21, 4.22 and 4.24 follow in the next section.

4.6.2 Discussion of the Experimental Results

As mentioned earlier, the measurements were conducted on pigs of different sizes (and therefore ages). Tested were the intestines of three pigs weighing 150 pounds, of one that weighed 80 pounds, and of four that weighed roughly 65 pounds. As expected from descriptions of age related changes (Yamada [60]), such variations would increase the observed dispersion in the data. Exacerbating this problem is that measurements in only one dimension, either diameter or length, were taken during many trials in order to reduce the experimental uncertainty of each measurement. It was noted in the last section that, on average, the diameter versus pressure data was generated for intestines from larger pigs than the length versus pressure data. This would likely appear as a systematic "stiffening" of the constitutive law for the circumferential behavior relative to that for the meridional behavior. Similarly, the intestines procured from Farmer John were taken from animals weighing between 120 to 200 pounds. Thus, their intestines would likewise be expected to be on average stiffer than those from 65 to 80 pound pigs. These effects are reflected in Figures 4.23 and 4.24. In former figure, the experimentally

derived constitutive relationship for the circumferential direction is shown to be significantly stiffer than that for the meridional direction. This behavior is contrary to many reports in the literature regarding the anisotropy for intestines, but the inconsistency in the sizes of the subject animals could explain this anomaly. Figure 4.24 plots the in vitro circumferential strain versus pressure data against the deduced strain curves from the in vivo trials. As seen in this figure, the tendency for the in vitro strain results to fall in the lower half of the in vivo ensemble strains could be explained by the relative ages/sizes of the pigs from which this data was obtained. In this plot, the lower the data point, the stiffer the specimen (less strain for the same internal pressure); therefore, the in vitro specimens from larger/older pigs would be expected to produce data that falls into the lower regions of this plot. And this result is born out experimentally. However, it should be noted that the in vitro data falls entirely within the envelope created by the dispersion of the in vivo data; thus, one could argue for consistency between the constitutive behavior of the dead and living intestines. If valid, this assertion implies that future experiments on dead, excised intestinal segments can produce useful biomechanics results.

However, in vitro experiments can never provide a valid measure for excessive loading of the intestinal tissues. In contrast, the observations of constriction of blood flow seem to provide a substantially better measure for overstress than those used by previous researchers, e.g., tearing, breakage and bursting. Biomechanics experimentation on living tissues is necessary to determine useful criteria to predict injury due to excessive stresses. In Figure 4.15, one can observe both pinpoint hemorrhages and significantly collapsed blood vessels, both of which are considered harbingers of injury for an otherwise structurally

sound membrane (macroscopically). Thus, the collapse of the blood vessels by the pressure loading surrounding them can be argued to be a reasonable threshold value of excessive loading. From the observations, the collapse of larger diameter blood vessels occurs at higher levels of internal pressure. Specifically, 1.0 psig. will cause occlusion of small to medium vessels and 1.6 psig. for almost all vessels; thus, a reasonable minimum threshold seems to be that which collapses the capillaries in the tissue. In fact, once they collapse, all blood flow will stop. So microscopy can be used to investigate the loading that collapses the capillaries. Alternatively, if the blood pressure within the capillaries is approximately the diastolic blood pressure, then they will collapse when the "hydrostatic pressure" within the membrane (but outside of the capillaries themselves) exceeds the venous or diastolic blood pressure. This membrane pressure is the isotropic portion of the local state of stress, Equation 4.37, as described in Subsection 4.4.5. Under this supposition, the membrane's blood flow will stop when one-third of the sum of the circumferential and meridional stresses is greater than the capillary blood pressure.

4.6.3 Quasistatic Model of the Gripper-Intestine Interaction

The modeling of the intestinal behavior culminated with the development of a computer simulation of intestinal response to the actions of a hypothetical gripper segment. This numerical modeling utilized the mean, biaxial stress-strain relationships described in the previous subsection (and shown in Figure 4.23). The algorithm that forms the foundation of this simulation follows.

This numerical approach models the behavior solely in an Eulerian frame-

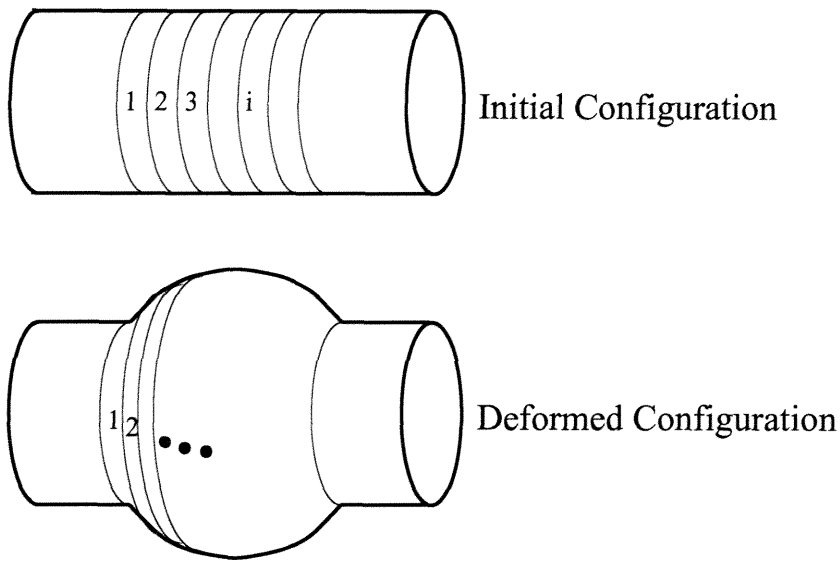

Figure 4.25: The unstressed reference configuration and the deformed configuration of the simulated intestinal segment.

work because the relevant constitutive laws were formulated using the Cauchy stresses (true stresses). The model assumes that a gripper has been inserted into an intestine whose unstressed diameter is given. It assumes further that the gripper's shape grows and deforms the intestine in a given manner (illustrated in Figure 4.25). The shape of the gripper is assumed to change slowly enough that any membrane dynamics can be ignored; as such, this simulation is considered to be *quasistatic*. In spatial terms, the circumferential stretching of the surrounding intestine is dictated by the shape of the encompassed gripper. Thus, at all points surrounding the gripper, the circumferential stretch ratio (the *principal stretch*, λ_c) can be calculated.

Unknown, however, is the meridional stretch ratio, the other *principal stretch*, which is required for calculation of the circumferential and meridional stresses via the constitutive laws. Observations described in Section 3.6.1 (and

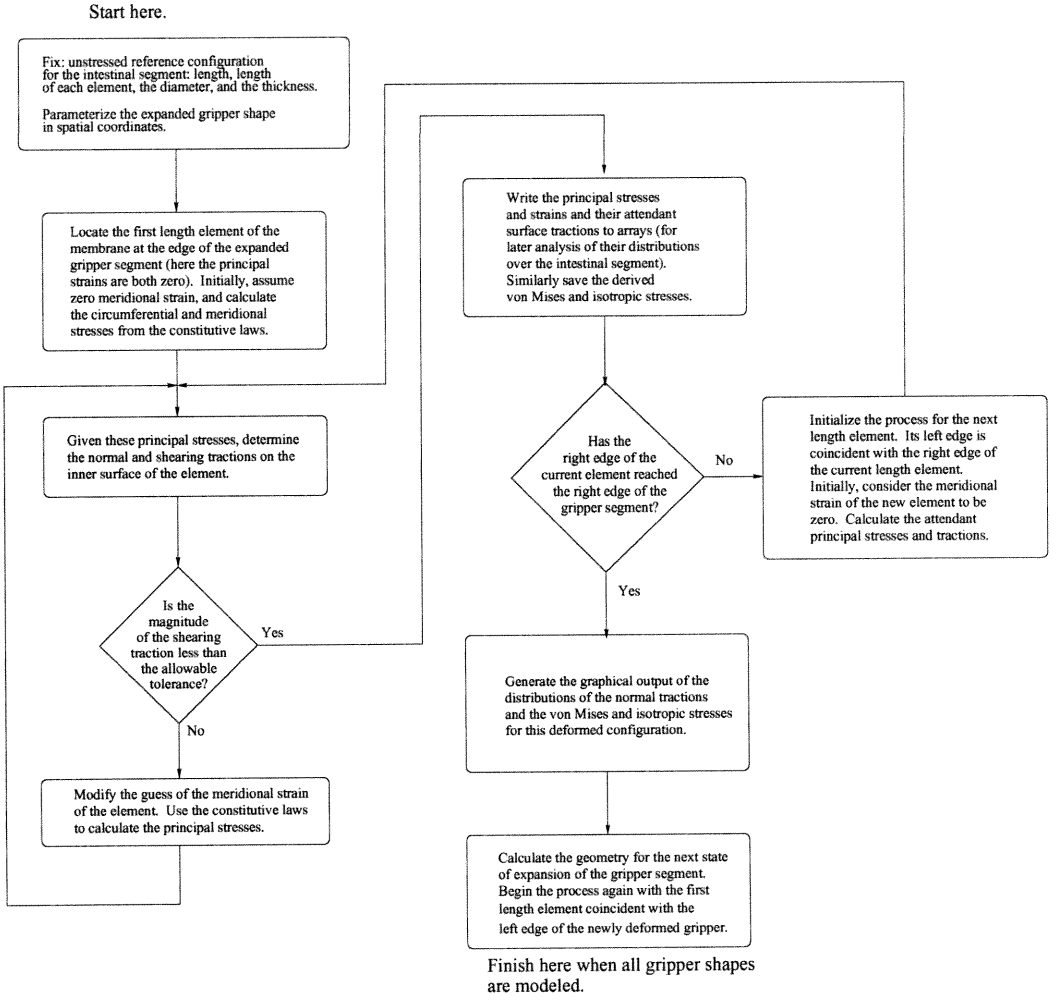

Figure 4.26: The flow chart for the numerical simulation of the intestinal reactions of an expanding gripper segment.

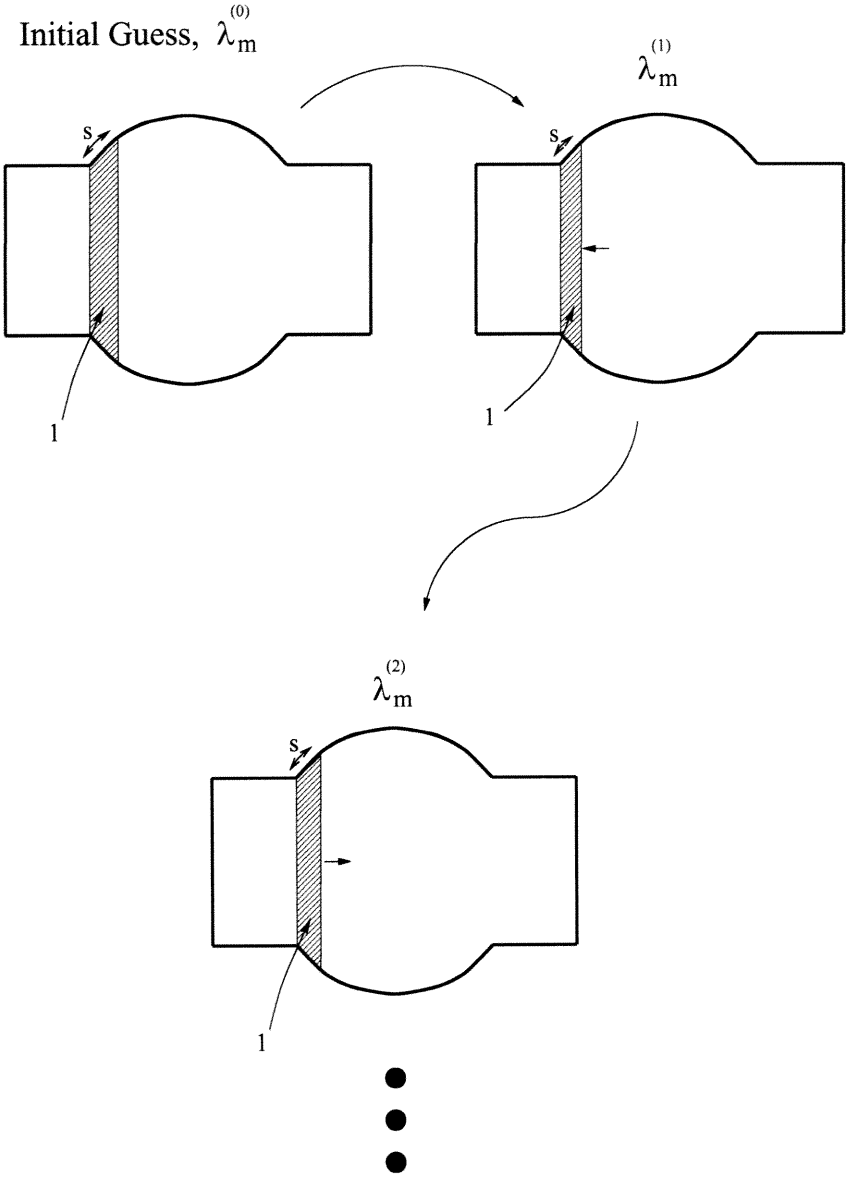

Figure 4.27: A graphical representation of the iterative process converging toward the zero traction configuration of the first length element of the intestinal segment.

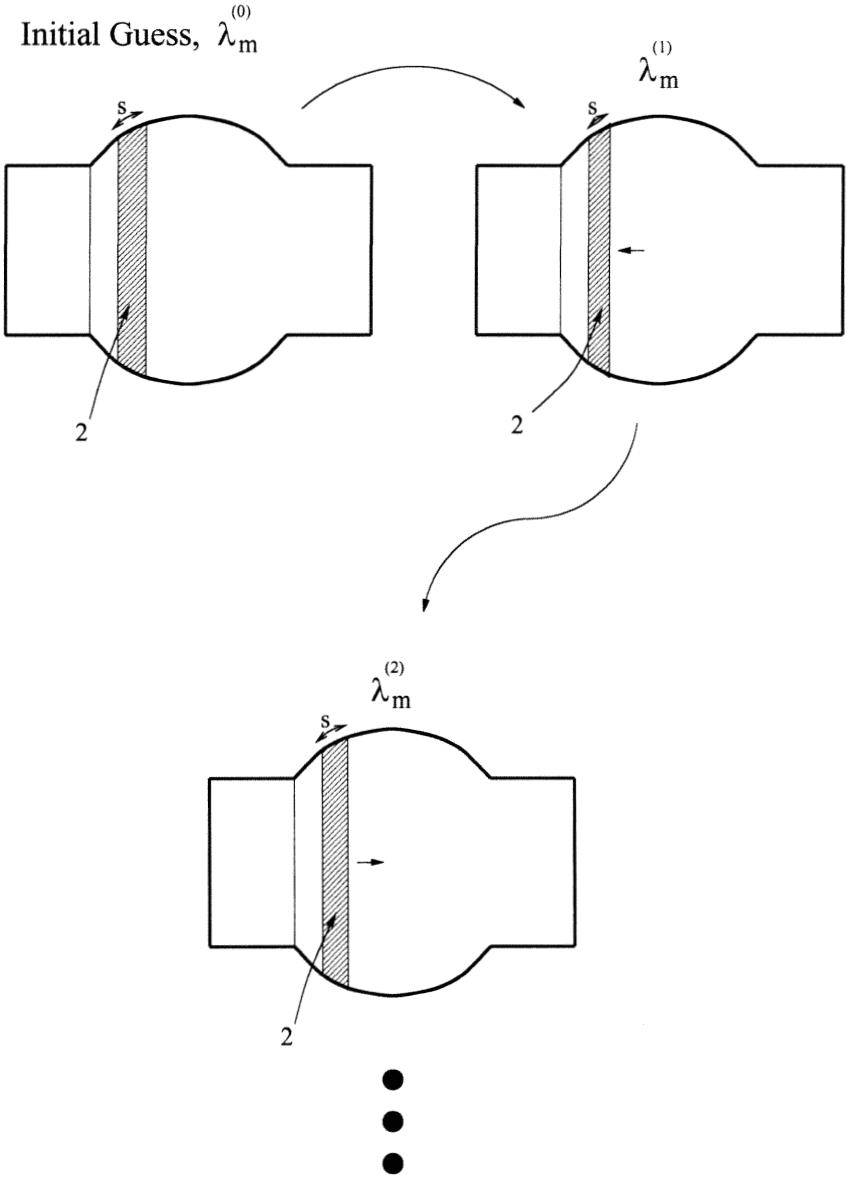

Figure 4.28: A graphical representation of the iterative process converging toward the zero traction configuration of the second length element of the intestinal segment.

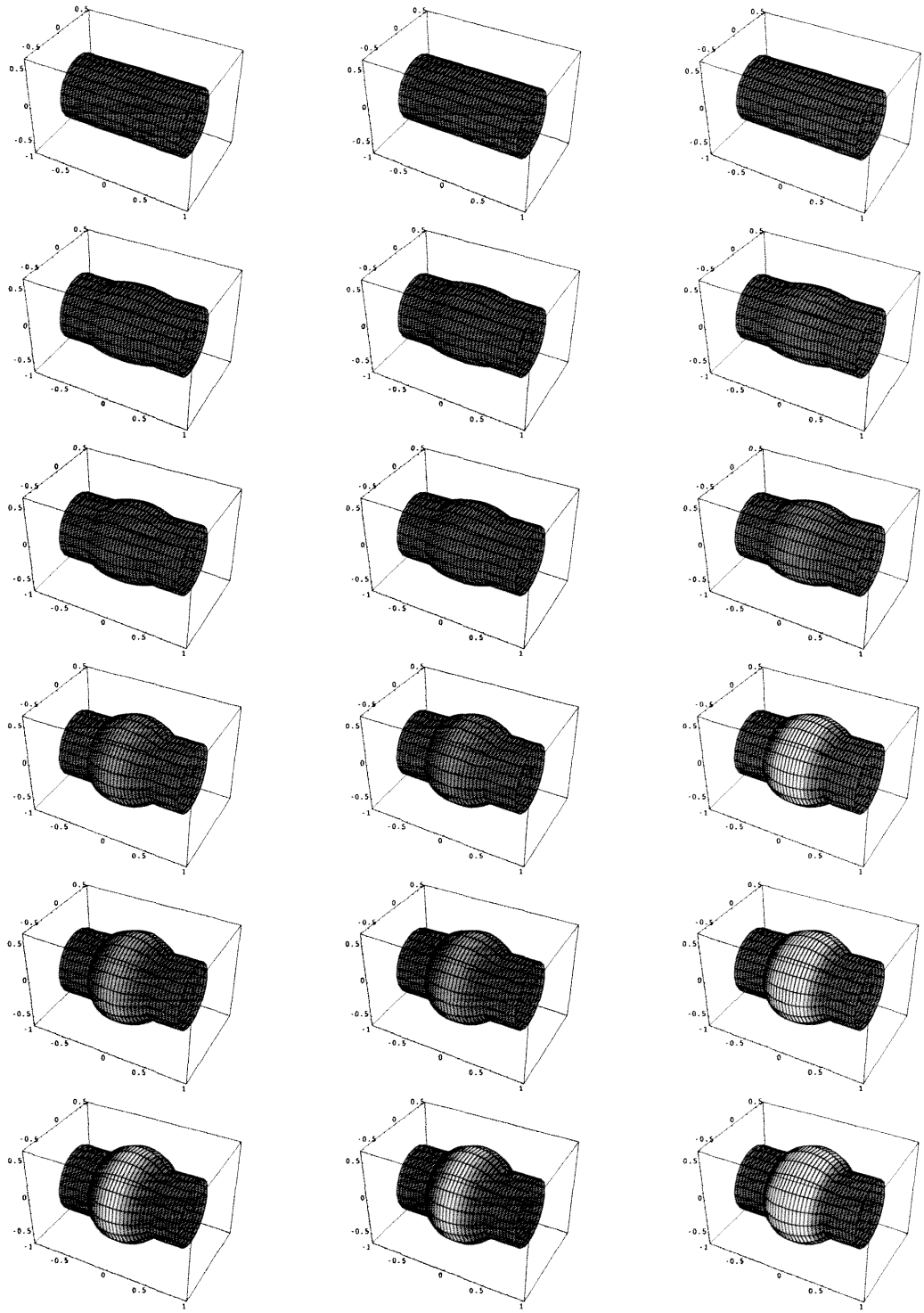

Figure 4.29: Animation of gripper-intestine modeling. The grayscale reflects relative impact of the loading (white = danger). Left (contact pressure), Center (von Mises stress), Right (isotropic stress).

illustrated in Figure 3.20) provide a means to model the meridional stretching. In those experiments, the intestinal membrane appeared to slip longitudinally over the enlarging gripper with very little friction. To a first order approximation, the observed intestines slid on the inflating gripper such that the frictional/shearing contact traction appeared to vanish. Under this condition, the lateral boundary conditions applied to this axisymmetric membrane are "mixed." That is, the circumferential stretching at all points of the membrane is given merely by the shape of the gripper (a purely kinematic statement), and the meridional stretching is the consequence of minimzing the shearing traction in the meridional direction (a statement involving kinetics). So in this simulation, the degree of meridional stretching in the deformed intestine will correspond to the vanishing of the meridional shear tractions (to be calculated using Equation 4.35).

In the initial configuration of the gripper segment, the intestine is unloaded and assumed to be unstressed. For simplicity, the contracted diameter of this prototypical gripper segment equals the unstretched diameter of this intestine. The gripper is then expanded to a specified shape.

The algorithm proceeds as illustrated in the flow chart provided in Figure 4.26. In the unloaded reference configuration, the intestinal segment is divided longitudinally into short length elements. The first such element is located with one end coincident with the edge of the gripper (see Figures 4.25 and 4.27). This implies that this "left" edge of the first element is not subjected to any circumferential stretching; similarly, all points of the intestine lying to the left of this edge are completely unstretched (and assumed to be unloaded and, therefore, unstressed). Initially assuming zero meridional strain, i.e., $\lambda_m = 1$, locates the "right" edge of this element at a point on the expanded

gripper segment. Then using the constitutive relations and these kinematics, the circumferential and meridional stresses within this element are calculated. From this geometry and these stresses, the normal and shearing tractions are calculated according to the equation of equilibrium, Equation 4.5, and the shear traction equation, Equation 4.35. If the calculated shearing traction is not negligible, then the assumed meridional stretch is modified accordingly, i.e., the right edge of the element is moved along the expanded gripper, and the process is repeated (as shown in Figure 4.27). These new kinematics generate new stresses and consequently new tractions. This process of guessing the meridional stretch and calculating the shear traction on the deformed element continues until the shear traction vanishes to within a given tolerance. At this point, the circumferential and meridional stresses and stretches are determined for the first element (the normal traction is also calculated using Equation 4.5). The program now advances to focus on the second length element.

Naturally, the second element begins where the first element ends. Thus, the circumferential stretching of the left edge of the second element is given. In the same iterative manner as for the first length element, the program converges to the meridional stretch associated with zero shearing traction on the second element (illustrated in Figure 4.28). The derived location of the right edge of the second element locates the left edge of the third length element, and so on. The length elements are progressively modeled until the right side of the expanded gripper segment is reached. At this point, the intestinal reaction to this current state of the gripper is completely predicted, i.e., the stresses, strains and normal tractions (locally applied, internal pressure) are determined for all points along the membrane. These distributions of the

stress state and the applied loading will be used to predict the onset of injury to the modeled intestine.

The gripper shape can now be changed, and the modeling of the surrounding intestine begins anew. The number of intestinal length elements required to surround the expanded gripper is not dictated a priori in this process. And as the gripper expands quasistatically, the number of length elements that are required to surround the gripper will increase. This is a consequence of modeling these biomechanics within an Eulerian framework.

Three criteria for the prediction of the onset of injury have been proposed. They are: the applied normal or pressure loading on the inner surface of the intestine, the local von Mises stress, and the local isotropic stress. Distributions of these measures are calculated in this computer simulation and presented in Figure 4.29. In this figure, the danger of injury is reflected in the color of the membrane surface with white representing excessively high loading/deformation. In these renderings, across each row is a given deformation (and state of internal stress) of the intestine caused by the expansion of the gripper. Down the left column, the grayscale reflects the distribution of the locally applied pressure loading compared to 1 psig., the internal pressure under which multiple blood vessels were observed to be occluded. In the center column, the grayscale reflects the distribution of the von Mises stress in the modeled intestine compared to the von Mises stress corresponding to an internally applied pressure of 1 psig. Lastly, the grayscale mapping on the membrane surface in the right column of renderings demonstrates a comparison of the distribution of local isotropic stress with a normal pig's diastolic blood pressure, 108 mm Hg. The normal blood pressure for pigs has been reported to be 170/108 mm Hg for pigs weighing 200 kg (Green [23]). Thus, in

these renderings, a white surface indicates istropic stresses equal to or greater than 108 mm Hg.

Closer observation of Figure 4.29 identifies one additional characteristic. With these measures of excessive loading, the right column, i.e., the isotropic stress criterion, appears to be the most conservative choice. One may expect this result as the limiting value of 1.0 psig. was determined by unaided visual observations of the occlusion of intestinal blood vessels. Conceivably, using optical microscopy, lower limiting values of applied pressure loading and von Mises stresses could be measured; these would correspond to observations of occlusion of smaller intestinal blood vessels. Such results may provide a correlation between the three criteria.

Chapter 5

Conclusions and Recommendations for Future Work

This thesis reviewed current state of medical endoscopy and minimally invasive surgical practice. The ongoing efforts to apply advanced technology to many facets of the medical art were examined. Societal benefits of the increased use of minimally invasive medicine were discussed (for both improved provision of health care as well as potentially reduced fiscal healthcare spending). And minimally invasive small intestinal endosopy was identified as a field particularly ripe for technological improvement.

5.1 The Problem Revisited

Inflammatory bowel diseases of the small intestine afflict hundreds of thousands of individuals annually in the United States alone. At present, diagnosis is performed primarily by evaluation of external symptoms (aided by an upper GI barium x-ray), and typical therapy involves the use of strong anti-inflammatory medications given systemically (corticosteroids are common).

In extreme cases, surgery is indicated but generally only when necessary as it does not seem to prevent the recurrence of the disease processes. In contrast, gastroenterologists use endoscopes to perform minimally invasive surgeries within the stomach and colon without external incisions. Unfortunately, such access to deep within the small intestine is impossible using current endoscopic technology. Many researchers are attempting to develop advanced endoscopic devices. However, most of these designs are ultimately limited in their ability to reach deeply into the body as they are advanced by forces generated at their proximal ends. This is consistent with conventional flexible endoscopy. One notable exception is the concept for a"tracked vehicle" (similar in concept to an army tank) type of endoscopic robot proposed by researchers at MIT and Columbia University Medical School. This machine has been envisioned to propel itself into the colon, an environment currently within reach of commonly available endoscopes.

Since they are pushed from their proximal ends, existing flexible endoscopes represent a design compromise between stiffness to prevent buckling and lateral compliance to negotiate internal curvature of the lumen. All of the proposed advancements, including the design concepts described herein, attempt to overcome this inherent limitation in minimally invasive technology.

5.2 Significant Results of This Research

This research covered two distinct areas of endeavor: the development of a concept for a self-propelled robotic endoscope with several proof-of-concept prototypes and an investigation into the elastic behavior of its intended environment, the small intestine. In the design efforts, the robotic devices evolved

over five generations culminating with a machine for ongoing experiments within the intestines of living pigs. In the biomechanics study, a nonlinear, anisotropic, finite deformation, analysis was performed for segments of an axisymmetric membrane (a simplified construction for the small intestine). Experiments on living and excised pig bowel furnished this model of the small intestine with the necessary data to develop a numerical simulation of its quasistatic elastic response to the actuation of a robotic gripper component.

5.2.1 The Robotic Endoscope System Design

In an effort to provide a means for minimally invasive access throughout the small intestine, a self propelled robotic endoscope has been conceived and patented. Initial theories of locomotion were developed in an effort to increase the dependability of such a device, i.e., the ability to crawl within a lubricious, flexible and curved environment safely (including, for example, redundancy against mechanical failure). Several series of prototype robots were fabricated to investigate this design morphology. Such devices demonstrated computer controlled locomotion within irregularly curved tubes, provided video images from within such environments, and crawled within the small intestines of a pig (pigs are often used as biological models of humans). These efforts highlighted unanticipated issues that substantially impacted the design of the fifth generation prototype. As an example, the extreme compliance of the intestinal membrane and its buckling forced a reassessment of the fundamental concepts of intestinal locomotion.

As the early experiments with pig's intestines suggested, an increased understanding of these organs' mechanical behavior was necessary for any real-

istic possibility of developing a successful robotic endoscope. In addition, the literature contained only the results of intestinal tissue studies performed with dissected tissues in uniaxial tension. Such results did not fundamentally answer questions of the nonlinear material behavior when subjected to complex loading conditions. And of critical importance, none of these investigations could identify a limit loading above which the tissue will be injured (as no evidence of non-catastrophic injury exists for "dead" tissue, only tearing or bursting). Thus, a "whole organ" experiment was developed which measured the mechanical properties of an intact small intestinal specimen. An analysis of idealized, anisotropic, nonlinear, axisymmetric membranes was performed to model these experimental specimens. Soft tissue biomechanics data was obtained for vital specimens surgically accessed from anesthetized pigs as well as for excised intestines (for comparison between living and dead tissue). From these experiments, average constitutive relations were produced. And subsequently a numerical model was developed to predict the interaction between a generic robotic component and the intestinal membrane. This modeling can estimate the potential for injury as a function of the robot's actions. Criteria for this prediction of injury are both empirically generated heuristics (applied normal traction, and the membrane's von Mises stress) as well as biologically and experimentally motivated (the membrane isotropic stress versus the capillary or venous blood pressure).

The proposed locomotion concept appears viable for safe and reliable endoscopic traversal of the small intestine. Modeling of the robot's mechanical traction against the inner surface of the small intestine falls outside the realm of conventional robotic grasping theory and concepts (that tend to study reasonably solid objects in contact). Thus, questions of the robot's immobiliza-

tion within the intestine, or the requisite numbers of gripper contacts between the robot and the intestinal wall to provide a stable "footing" will likely not be answered by conventional grasping or fixturing analysis. The first tool to investigate these questions for small intestinal locomotion is the biomechanics modeling of Subsection 4.6.3 which can be used to predict: the effects of gripper balloon shape and size on its traction, intestinal loading, and injury potential, the relative values of multiple grippers expanding for gently/safely applied traction, etc. This software permits refinement of the mechanism design with fewer live animal experiments.

In vivo experimentation provided insights into the significant differences between pipe crawling and intestinal locomotion. Additionally, these studies provided a biologically inspired limitation on the acceptable stresses generated within the intestinal membrane.

As an added benefit, this modeling can further impact the analysis of other surgical tools, for example, radially expanding interluminal anastomotic staplers can injure the bowel as they are used. Also, balloon devices are commonly inserted rectally for a variety of applications including: lower GI barium x-rays [42] and colonic distension/probing for assessment of functional diseases and neuropathy [12]. In both of these cases, similar modeling with constitutive relations measured for the sigmoid colon could increase their relative safety.

5.3 Future Work

As these efforts represent an initial foray into robotic endoscopy of the small intestine, innumerable areas for engineering and scientific research remain unexplored. The following list identifies several possible directions for further

study.

- A detailed study into the use of the magnitude of the membrane's isotropic stress as a viable predictor of injury would be very valuable to correctly model these living tissues.

- Although care was taken in gathering the experimental biomechanics data, a possible systematic error was introduced by the inconsistent sizes/ages of the animals that were available. It would be beneficial to compile additional data that permits improved correlation between the meridional and circumferential elastic behavior of the small intestine for the animals studied.

- All of the biomechanics analysis and experiments depended upon an assumption of "locally volume preserving" deformations, i.e., incompressible behavior. This simplification should be verified by experiments that measure the wall thickness of the intestinal specimen concurrently with its length and diameter.

- Using both numerical modeling and experimental trials, investigation of the relationship between the numbers of robotic segments and locomotion performance should commence. This would involve, in addition to the testing of advanced robotic prototypes, the quasistatic computer simulation to be expanded to model the intestinal response from multiple robotic segments, i.e., a complete mechanism.

- Given a successful demonstration of robotic locomotion of a derivative prototype, the biomechanics experiments and modeling should be repeated for human cadavers. Obviously, one cannot perform these investigations with living human intestines. But, the pig intestine studies that were performed on both living and dead tissue showed that dissected tissue behaves similarly to vital tissue. So, it may be reasonable to expect the mechanical behavior

of cadaver human intestines to mirror that of their living counterparts. Thus, the experiments and computer modeling should be repeated for intestines that have been disected from recently deceased, human cadavers.

- If it is possible, the relaxation of the assumption of axis symmetry for the intestinal modeling would be potentially valuable for the prediction of the effects of a variety of gastrointestinal medical devices.

Bibliography

[1] J.R. Adler, A. Schweikard, R. Tombropoulos, and J.-C. Latombe. Image-guided robotic radiosurgery. In *Proc. First Int. Symp. on Medical Robotics and Computer Assisted Surgery*, pages 291–7, 1994.

[2] D.H. Bergel. The static elastic properties of the arterial wall. *J. Physiology*, 156:445–57, 1961.

[3] S. Berman, M. Hashizume, Y. Yang, J. DuPree, and T. Matsumoto. Intraoperative hemostasis and wound healing in intestinal anastomoses using the ila stapling device. *The American Journal of Surgery*, 155:520–5, 1988.

[4] M.K. Bluett, D.A. Healy, G.C. Kalmeris, and J.P. O'Leary. Comparison of automatic staplers in small bowel anastomoses. *Southern Medical Journal*, 79:712–6, 1986.

[5] T.E. Carew, R.N. Vaishnav, and D.J. Patel. Compressibility of the arterial wall. *Circulation Research*, 23:61–8, 1968.

[6] S. Charles. Dexterity enhancement for surgery. In *Proc. First Int. Symp. on Medical Robotics and Computer Assisted Surgery*, pages 145–60, 1994.

[7] G.S. Chirikjian and J.W. Burdick. The kinematics of hyper-redundant locomotion. *IEEE Trans. on Robotics and Automation*, 10:343–54, 1994.

[8] C.J. Chuong and Y.C. Fung. Three dimensional stress distribution in arteries. *J. Biomech. Eng.*, 105:268–74, 1983.

[9] C.J. Chuong and Y.C. Fung. *Residual Stress in Arteries*, pages 117–29. Springer-Verlag, New York, 1986.

[10] K. Cronin, D.S. Jackson, and J.E. Dunphy. Changing bursting strength and collagen content of the healing colon. *Surgery, Gynecology and Obstetrics*, 123:747–53, 1968.

[11] J.S. Duffy and M. Shuter. Evaluation of soft-tissue properties under controlled expansion for reconstructive surgical use. *Med. Eng. Phys.*, 16:304–9, 1994.

[12] L.-P. Erasmus, P. Pull, M. Kratzmair, and R. Holzl. Method and apparatus for pressure-controlled distension of the lower gastrointestinal tract. *Med. Eng. Phys.*, 16:338–47, 1994.

[13] K. Fackler, L. Klein, and A. Hiltner. Polarizing light microscopy of intestine and its relationship to mechanical behaviour. *Journal of Microscopy*, 124:305–11, 1981.

[14] T. Fukuda, S. Guo, K. Kosuge, F. Arai, M. Negoro, and K. Nakabayashi. Micro active catheter system with multi degrees of freedom. In *Proc. IEEE Int. Conf. on Robotics and Automation*, pages 2290–5, 1994.

[15] T. Fukuda, H. Hosokai, and M. Uemura. Rubber gas actuator driven by hydrogen storage alloy for in-pipe inspection mobile robot with flexible

structure. In *Proc. IEEE Int. Conf. on Robotics and Automation*, pages 1847–1852, 1989.

[16] J. Funda, R. Taylor, S. Gomory, B. Eldridge, K. Gruben, and M. Talamini. An experimental user interface for an interactive surgical robot. In *Proc. First Int. Symp. on Medical Robotics and Computer Assisted Surgery*, pages 196–203, 1994.

[17] Y.C. Fung. *Biomechanics: Motion, Flow, Stress, and Growth*, pages 382–446. Springer-Verlag, New York, 1990.

[18] Y.C. Fung. *Biomechanics: Mechanical Properties of Living Tissues*, pages 298–300. Springer-Verlag, New York, second edition, 1993.

[19] Y.C. Fung. *Biomechanics: Mechanical Properties of Living Tissues*, page 141. Springer-Verlag, New York, second edition, 1993.

[20] Y.C. Fung and S.Q. Liu. Strain distribution in small blood vessels with zero stress state taken into consideration. *Am. J. Physiol.*, 262:H544–52, 1992.

[21] Y.C.B. Fung. Elasticity of soft tissue in simple elongation. *Am. J. Physiol.*, 213:1532–44, 1967.

[22] T. Gibson, H. Stark, and J.H. Evans. Directional variation in extensibility of human skin *in vivo*. *J. Biomechanics*, 2:201–4, 1969.

[23] C.J. Green. *Animal Anaesthesia*, page 196. Laboratory Animals, LTD., London, 1979.

[24] W. Grundfest and L. Daykovski. *Personal communication.* Cedars-Sinai Medical Center, Los Angeles, California, 1992.

[25] W.S. Grundfest, J.W. Burdick, and A.B. Slatkin. Robotic endoscopy. *U.S. Patent No. 5337732*, August 16, 1994.

[26] W.S. Grundfest, J.W. Burdick, and A.B. Slatkin. Robotic endoscopy continuation-in-part. *U.S. Patent No. 5662587*, September 2, 1997.

[27] T. Hendriks and W.J.B. Mastboom. Healing of experimental intestinal anastomoses: Parameters for repair. *Diseases of the Colon and Rectum*, 33:891–901, 1990.

[28] F.L.E.M. Hesp, T. Hendriks, E.-J.C. Lubbers, and H.H.M. deBoer. Wound healing in the intestinal wall. *Diseases of the Colon and Rectum*, 27:99–104, 1984.

[29] E.L Howes, J.W. Sooy, and S.C. Harvey. The healing of wounds as determined by their tensile strength. *Journal of the A.M.A.*, 92:42–5, 1929.

[30] K. Ikuta, M. Nokata, and S. Aritomi. Hyper-redundant active endoscope for minimum invasive surgery. In *Proc. First Int. Symp. on Medical Robotics and Computer Assisted Surgery*, pages 230–7, 1994.

[31] K. Ikuta, M. Tsukamoto, and S. Hirose. Shape memory alloy servo acuator system with electric resistance feedback and application for active endoscope. In *Proc. IEEE Int. Conf. on Robotics and Automation*, pages 427–430, 1988.

[32] T. Iwasaki. Study on the strength of the human intestinal walls. *J. Kyoto Pref. Med. Univ.*, 52:673–702, 1953.

[33] T. Iwasaki and T. Okamoto. Tension and bursting tests upon the intestinal walls of human fetus. *J. Kyoto Pref. Med. Univ.*, 52:879–87, 1953.

[34] R.M. Kenedi, T. Gibson, J.H. Evans, and J.C. Barbenel. Tissue mechanics. *Phys. Med. Biol.*, 20:699–717, 1975.

[35] H. Kimura and M. Tokuda. Studies on the bursting test tried on the intestinal canal of the rabbit. *J. Kyoto Pref. Med. Univ.*, 51:508–10, 1952.

[36] A.N. Kingsnorth, R. Vowles, and J.R.G. Nash. Epidermal growth factor increases tensile strength in intestinal wounds in pigs. *British Journal of Surgery*, 77:409–12, 1990.

[37] K. Kubo. Investiation on the development in mechanical strength of various organs. *J. Kyoto Pref. Med. Univ.*, 66:433–56, 1959.

[38] Y. Lanir and Y.C. Fung. Two-dimensional mechanical properties of rabbit skin–ii. experimental results. *J. Biomechanics*, 7:171–82, 1974.

[39] C.D. Mercer, P. Minich, and B. Pauli. Sutureless bowel anastomosis using nd:yag laser. *Lasers in Surgery and Medicine*, 7:503–6, 1987.

[40] B. D. Mittelstadt, P.H. Kazanzides, J. Zuhars, B. Williamson, P. Cain, F. Smith, and W.L. Bargar. The evolution of a surgical robot from prototype to human clinical use. In *Proc. First Int. Symp. on Medical Robotics and Computer Assisted Surgery*, pages 36–41, 1994.

[41] T.S. Nelsen and C.J. Anders. Dynamic aspects of small intestinal rupture with special consideration of anastomotic strength. *Arch Surg*, 93:93, 1966.

[42] J.A. Nelson, A.U. Daniels, and W.J. Dodds. Rectal balloons: Complications, causes, and recommendations. *Investigative Radiology*, 14:48–59, 1979.

[43] K. Oda. Study on the bursting test of a rabbit's viscera and tissues. *J. Kyoto Pref. Med. Univ.*, 50:447–64, 1952.

[44] Y. Ogawa and S. Narumiya. Examination of the shearing strength of various organs and tissues. *J. Kyoto Pref. Med. Univ.*, 66:801–5, 1959.

[45] T. Ohara. On the comparison of strengths of the various organ-tissues. *J. Kyoto Pref. Med. Univ.*, 53:577–97, 1953.

[46] Y. Okudaira, A.M. Kholoussy, H. Sharf, Y. Yang, and T. Matsumoto. Experimental study of singly placed staples for an everted intestinal anastomosis. *The American Journal of Surgery*, 147(2):234–6, 1984.

[47] J. Omens and Y.C. Fung. Residual strain in the rat left ventricle. *Circ. Res.*, 66:37–45, 1989.

[48] R. Reihsner, B. Balogh, and E.J. Menzel. Two-dimensional elastic properties of human skin in terms of an incremental model at the *in vivo* configuration. *Med. Eng. Phys*, 17:304–13, 1995.

[49] R. Rohling, P. Munger, J.M. Hollerbach, and T. Peters. Comparison of relative accuracy between a mechanical and an optical position tracker for image-guided neurosurgery. In *Proc. First Int. Symp. on Medical Robotics and Computer Assisted Surgery*, pages 277–82, 1994.

[50] T.J. Saclarides, D.A. Rohrer, A.K. Bhattacharyya, and M.S. Bapna. Effect of intraoperative radiation on the tensile strength of small bowel anastomoses. *Diseases of the Colon and Rectum*, 35:151–7, 1990.

[51] T.J. Saclarides, D.O. Woodard, M.S. Bapna, and S.G. Economou. Fibrin glue improves the healing of irradiated bowel anastomoses. *Diseases of the Colon and Rectum*, 35:249–52, 1992.

[52] H.J. Schulz, T. Lutze, and H.P. Trummler. Requirements of a planning and navigation device used in neuro-, ent-,and maxillocraniofacial surgery. In *Proc. First Int. Symp. on Medical Robotics and Computer Assisted Surgery*, pages 272–6, 1994.

[53] Y. Shishido, H. Adachi, H. Hibino, H. Miyanaga T. Yamamoto, S. Takayama, Y. Ueda, Y. Aoki, and S. Yamaguchi. Pipe-inspecting apparatus having a self propelled unit. *U.S. Patent No. 5090259*, February 25, 1992.

[54] M.L. Shuter, C.M. Malata, J.S. Duffy, and D.T. Sharpe. Determination of relative contributions of 'mechanical' and 'biological' creep in tissue expansion using *in vivo* pressure monitoring: A preliminary report. *Med. Eng. Phys.*, 16:24–8, 1994.

[55] R.H. Sturges and S. Laowattana. A flexible, tendon-controlled device for endoscopy. In *Proc. IEEE Int. Conf. on Robotics and Automation*, pages 2582–91, 1991.

[56] M. Takigawa. The tension and bursting tests upon a dog's intestinal walls. *J. Kyoto Pref. Med. Univ.*, 53:390–4, 1953.

[57] S. Timoshenko and D.H. Young. *Elements of Strength of Materials*, chapter 3. D. Van Nostrand Reinhold Company, New York, New York, fifth edition, 1968.

[58] D.R. Uecker, C.L. Lee, Y.F. Wang, and Y. Wang. A speech-directed multi-modal man-machine interface for robotically enhanced surgery. In *Proc. First Int. Symp. on Medical Robotics and Computer Assisted Surgery*, pages 176–83, 1994.

[59] *New Developments in Medical Technology.* The Wilkerson Group, 1991.

[60] H. Yamada and E.G. Evans (ed.). *Strength of Biological Materials.* Williams and Wilkins Company, Baltimore, Maryland, 1970.

[61] J. Yan and S.E. Salcudean. Design and control of a motion scaling system for microsurgery experiments. In *Proc. First Int. Symp. on Medical Robotics and Computer Assisted Surgery*, pages 211–6, 1994.

[62] T. Yoshida. Study on the bursting strength of the hollow organs. *J. Kyoto Pref. Med. Univ.*, 66:809–35, 1959.

[63] K. Yoshikawa, K. Takezono, and H. Yasuda. The bursting strength of the digestive canal in birds. *J. Kyoto Pref. Med. Univ.*, 72:669–75, 1963.